Dynamics and Control of a Ground Vehicle Subjected to a Tire Blowout

by

Mahdi Jamil Awad Al-Quran

A Dissertation Presented in Partial Fulfillment
of the Requirements for the Degree
Doctor of Philosophy

Approved March 2021 by the
Graduate Supervisory Committee:

Abdel Ra'ouf Mayyas, Chair
Abdelrahman Shuaib
Yan Chen
Sze Zheng Yong
Yi Ren

ARIZONA STATE UNIVERSITY

May 2021

ABSTRACT

The tire blowout is potentially one of the most critical accidents that may occur on the road. Following a tire blowout, the mechanical behavior of the tire is extremely affected and the forces generating from the interaction of the tire and the ground are redistributed. This severe change in the mechanism of tire force generation influences the dynamic characteristics of the vehicle significantly. Thus, the vehicle loses its directional stability and has a risk of departing its lane and colliding with other vehicles or the guardrail. This work aims to further broaden our current knowledge of the vehicle dynamic response to a blowout scenario during both rectilinear and curvilinear motions. To that end, a fourteen degrees of freedom full vehicle model combined with the well-grounded Dugoff's tire models is developed and validated using the high fidelity MSC Adams package. To examine the effect of the tire blowout on the dynamic behavior of the vehicle, a series of tests incorporating a tire blowout is conducted in both rectilinear and curvilinear maneuvers with different tire burst locations. It is observed that the reconstruction of the tire forces resulting from blowout leads to a substantial change in the dynamics of the vehicle as well as a severe directional instability and possibly a rollover accident. Consequently, a corrective safety control system utilizing a braking/traction torque actuation mechanism is designed.

The basic idea of the stability controller is to produce a regulated amount of input torque on one or more wheels apart from the blown tire. The proposed novel control-oriented model eliminates the simplifying assumptions used in the design of such controllers.

Furthermore, a double integrator was augmented to enhance the steady-state performance of the sliding mode closed-loop system. The chattering problem stemmed by the switching nature of the controller is diminished through tuning the slope of saturation function. Different apparatuses are used in terms of actuation, using an individual front actuator, utilizing multi-actuator, and using two-wheel braking torques successively. It is found that the proposed controllers are perfectly capable of stabilizing the vehicle and robustly track the desired trajectory in straight-line and cornering maneuvers.

DEDICATION

I dedicate my dissertation work to my parents Huda and Jamil, my beloved wife Amena, my daughters Salma and Sara, and my sisters and brothers.

ACKNOWLEDGMENT

I would like primarily to dedicate my sincere gratitude and appreciation to Professor Abdel Ra'ouf Mayyas for the continuous guidance and motivation throughout my Ph.D. His immense and outstanding experience, enthusiasm, and knowledge in the subject matter have guided me during the research.

In addition, I would like to thank my dissertation committee, Dr. Abdelrahman Shuaib, Dr. Yan Chen, Dr. Yi Ren, and Dr. Sze Zheng Yong, for their willingness to provide support and guidance in the different disciplines of my research. Their feedbacks and valuable discussions have significantly enhanced the research work.

I am also deeply grateful to my mother, father, wife, and daughters for their love, support, prayers, and encouragement to complete this work. Furthermore, I would like to thank Ms. Christine Quintero for her assistance and guidance throughout my graduate study.

Finally, I gratefully acknowledge the generous funding and support received from the Hashemite University to pursue my Ph.D. In addition, I would like to sincerely thank the Jordan Design and Development Bureau (JODDB) for the assistance and guidance in using MSC Adams package in my research.

TABLE OF CONTENTS

Page

CHAPTER Page

APPENDIX Page

LIST OF TABLES

LIST OF FIGURES

NOMENCLATURE

α_{ij}	Slip angle of the ij tire
A_s	Projected surface area
a_V	Acceleration vector of the vehicle body center of mass
β	Side slip angle of the vehicle
C_a	Tire longitudinal stiffness
C_b	Tire cornering stiffness
C_D	Dimensionless drag coefficient
C_{rij}	Rolling resistance coefficient of the ij tire
c_{sij}	Suspension damper coefficient
c_{tij}	Tire vertical damping
d_{aero}	Offset from aerodynamic force application point to vehicle center of mass
δ	Front steering angle
δ_W	Steering wheel angle
e	The error variable
F_{aero}	Aerodynamics force
F_{aij}	Longitudinal force of the ij tire observed from the tire body-fixed frame

F_{Aij}	Longitudinal force of the ij tire observed from the tire body-fixed frame (planar model)
F_{arbij}	Anti-roll bar force vector
F_{bij}	Lateral force of the ij tire observed from the tire body-fixed frame
F_{Bij}	Lateral force of the ij tire observed from the tire body-fixed frame (planar model)
F_{cl}	Climbing resistance force
F_{dij}	Suspension damping force
F_{rij}	Rolling resistance force of the ij tire
F_{sij}	Suspension spring force
F_{tij}	Tire forces vector
F_{xij}	Longitudinal force of the ij tire observed from the vehicle body-fixed frame
F_{yij}	Lateral force of the ij tire observed from the vehicle body-fixed frame
F_{zij}	Normal force of the ij tire
g	Gravitational acceleration
h	Distance from the ground to vehicle center of mass
η	The width of the boundary layer
I_x	Vehicle mass moment of inertial abut its *x*-axis

I_y	Vehicle mass moment of inertial abut its y-axis
I_z	Vehicle mass moment of inertial abut its z-axis
k_{arb}	Anti-roll bar torsional stiffness
k_{sij}	Suspension spring stiffness
k_{tij}	Tire vertical stiffness
K, a_i, α	Tuning parameters
λ_{ij}	Dummy variable of the ij tire
l_f	Distance from vehicle center of gravity to the vehicle front axle
l_r	Distance from vehicle center of gravity to the vehicle rear axle
l_{sij}	Instantaneous length of the suspension spring
l_{sij}	Static length of the suspension spring
l_{wf}	Front track width
l_{wr}	Rear track width
l_z	Vertical offset of the pivot point from vehicle body center of mass
m	Vehicle mass
M_{aero}	Aerodynamic moment
M_{arbij}	Anti-roll bar moment vector

μ	Coefficient of friction
n	The order of the sliding surface
ω_{ij}	Rotational spin speed of the ij wheel
ω_V	Rotational speed vector of the vehicle body
ϕ	Vehicle body roll angle
ψ	Vehicle yaw angle
Q	Q matrix in the LQR controller
R	R matrix in the LQR controller
r_{aij}	Position vector of the pivot point
r_{uij}	Position vector of the unsprung mass
ρ_a	Air density
ρ_{ij}	Spin angle of the ij wheel
${}^{V}R_{Uij}$	Transformation matrix of wheel body-fixed frame to the vehicle body frame
${}^{I}R_V$	Transformation matrix of vehicle body-fixed frame to inertial frame
R_w	Wheel radius
s	The switching surface
sat	Saturation function

σ_{ij}	Longitudinal slip ratio of the ij tire
SR	Steering ratio
s_{uij}	Road displacement excitations
T_{bij}	ij braking torque
T_{dij}	ij wheel traction torque
θ	Vehicle body pitch angle
θ_g	Road slope angle
V	Lyapunov function
V	Vehicle traveling velocity
v_{aij}	Longitudinal velocity of the center of the contact patch of the ij tire
v_{bij}	Lateral velocity of the center of the contact patch of the ij tire
v_{uij}	Velocity vector of the unsprung mass
v_w	Airstream velocity
v_x	Longitudinal vehicle velocity
v_y	Lateral vehicle velocity
v_V	Velocity vector of the vehicle body center of mass
x, y, z	Body center of mass translations
ξ	A positive constant

$x_{aij}, y_{aij}, z_{aij}$	Body-suspension attachment point translations
$x_{uij}, y_{uij},$ z_{uij}	Unsprung mass translations

Abbreviations

4WS	Four-wheel steering
ABS	Antilock braking system
ACC	Adaptive cruise control
AFS	Active front steering
ARC	Active roll control
ARS	Active rear steering
BO	Blowout
CACE	Computer-aided control engineering
CAD	Computer-aided design
CFD	Computational fluid dynamics
DISMC	Double integral sliding model control
DLC	Double lane change
DOF	Degrees of freedom
DYC	Direct yaw control
ECU	Electronic control unit

ESP	Electronic stability program
FEM	Finite element model
HIL	Hardware in the loop
IMU	Inertial measurement unit
ISO	International Organization for Standardization
LTI	Linear time-invariant
LTV	Linear time-variant
LQR	Linear quadratic regulator
MBD	Multibody dynamics
MPC	Model predictive control
ODE	Ordinary differential equation
PID	Proportional-integral-derivative
SMC	Sliding mode control
TBO	Tire Blowout
TCS	Traction control system
TPMS	Tire pressure monitoring system

CHAPTER 1

INTRODUCTION

The study of ground vehicle dynamics involves the interactions among the vehicle, the driver, and the environment. From a conceptual engineering perspective, the driver can be regarded as a controller, sensor, and actuator. Inputs from this controller are through the steering wheel, braking/accelerating pedals, and the engaged gear. The environment interferes with the dynamics through aerodynamic forces, road bumps, inclination and bank angles, etc.

The vehicle itself is considered a system within which many subsystems are mutually interconnected. It can be subdivided into chassis, suspensions, powertrain, tires, brakes, and steering. The dynamics of the vehicle can typically be categorized by longitudinal, lateral, and vertical dynamics. Longitudinal dynamics analyze the vehicle performance in acceleration and braking under varied conditions. Lateral dynamics is chiefly concerned with the vehicle response and handling stability against driver input and external disturbances. The main focus of the vertical dynamics is the tuning of the suspension system to provide comfort to the passengers in the presence of the vibrations induced by road irregularities.

1.1 Vehicle System Interactions

Apart from the inertial and aerodynamic loads, all forces and moments acting on the vehicle are generated at the contact region between the tire and the ground. These forces and moments are manipulated to effectively control traction, braking, cornering, and

vibrations from road surface irregularities. Therefore, it is a crucial concern to have an accurate description of the mechanics of the interaction of the tire and the road for vehicle dynamics and control studies purposes. The tire exhibits both steady-state and time-dependent behaviors resulting from numerous input parameters in a highly nonlinear fashion. To be able to capture the physics of the tire, many models are used in the literature, and these models are ranging from simple mathematical representations to complex nonlinear finite element models depending on the required degree of accuracy and the phenomena to be investigated.

The vehicle motion cannot maintain the required trajectory unless actively controlled through the driver, who observes the traffic motion and carries out suitable actions accordingly. This man-machine mutual interaction is advisable to be treated as a fully integrated control system for vehicle stability and control system design studies. In the hypothetical level, the driver acts as a controller, sensor, and actuator with assistance from some automatic systems in certain circumstances. Therefore, the design, build, and validation of the driver sub-model, which mimics the human-driver and can be integrated with the vehicle model, is essential.

The vehicle is not isolated in the road; it exchanges information with other vehicles and reacts to different extraneous perturbations from the environment. These perturbations might be excited by aerodynamics loads, slopes, bumps, road roughness, obstacles, pedestrians, weather, and traffic flow nature. Such disturbances can significantly affect the dynamics of the vehicle system.

Vehicle automatic control systems also interact with the driver by providing sensory information from the vehicle and the environment. Such systems help reduce driver burden by automating some low-level driving control tasks. Furthermore, they are designed to intervene with the vehicle dynamics to enhance its performance and stability characteristics.

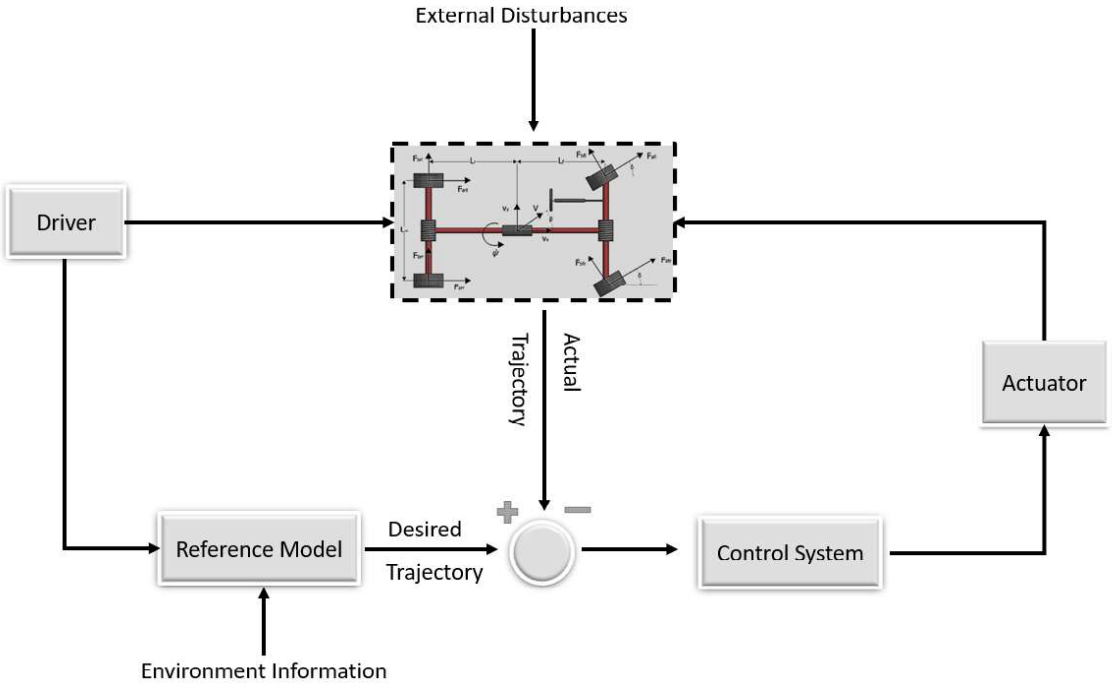

Figure 1.1. Vehicle System Interactions

The interdisciplinary nature of the vehicle dynamics requires a thorough understanding of the driver's behavior, the dynamics of the vehicle, the mechanics of the tire-road interaction, and their interdependencies with the environment, as illustrated in Figure 1.1. This intrinsic complexity makes an accurate mathematical representation of the real system a strenuous task. Nevertheless, vehicle control system strategies are predominantly formulated according to simplified but comprehensive versions of the model that capture the key characteristics of the system. Such simplified models can be

analyzed and utilized to design and evaluate vehicle control systems through mathematical simulation models.

1.2 Vehicle Simulation Models

A vehicle simulation model is a mathematical representation of the real vehicle that is derived from physical laws and captures its attributes within an adequate degree of accuracy. The necessity of being able to deduce the behavior of a vehicle system and subsystems prior to the actual implementation of the physical prototypes is increasing in the automotive industry. In the preliminary stages of the design, when the automobile is merely a concept, the engineers have wide freedom to perform significant modifications at low cost and high speed. However, when the project proceeds toward launching the physical prototype, the design flexibility is diminished, and the costs linked to modifications and real track tests start soaring. Besides predicting the dynamic behavior of the vehicle, vehicle dynamics simulation has a broad range of applications in the development of active driver assistance systems and driving simulators.

In many circumstances, it is needed to analyze certain driving scenarios that are dramatically affected by externally generated working conditions because it would be too much dangerous to conduct repetitive maneuvers by test human-drivers on the track. For instance, a moving vehicle subjected to external disturbances that are significantly affecting the dynamics of the vehicle and lead to severe instabilities falls under this category. Having a numerical experimentation model, such a risk, as well as time and cost demands, could be avoided, while the simulation model can reproduce the same results as the real tests. Moreover, through the investigation of the effect of numerous

system parameters, the effect of new changes can be examined, and some particular required system characteristics can be optimized.

1.2.1 Vehicle Body Models

From a vehicle body dynamics and control viewpoint, the vehicle mainly consists of chassis, suspension, drivetrain, steering, and braking subsystems. The inputs to the vehicle integrated system are the steering, brake pedal, and accelerator pedal. The questions of whether to model each subsystem and how much detailed these models are, depending on the objective of the study. The complexity of the solution, the interpretations of the results, and the computational burden increase as the details of the model increase. Such detailed models are suitable when accurate quantitative analyses are required or when simplified models are unable to capture the physics of the phenomenon under study. On the other hand, simplified models require lower computational effort and can be integrated with real-time studies. Furthermore, simplified models are extensively used to develop vehicle control systems as well as in cases where only qualitative or descriptive results are needed.

Many models adequately compromise between accuracy and the computational load have been developed in the literature. These models are detailed enough to reflect the system's major characteristics without going further beyond that. In general, vehicle models are extracted from full three-dimensional models through decoupling the modes of motion and proceeding with an isolated sub-model. For instance, to develop a vehicle handling stability controller like direct yaw controller (DYC), a simplified seven degrees of freedom (sometimes two degrees of freedom) handling model is utilized without any

contribution for the roll or bounce motions. Similarly, seven degrees of freedom (sometimes a quarter car one degree of freedom) ride model is utilized to develop a rollover prevention control system.

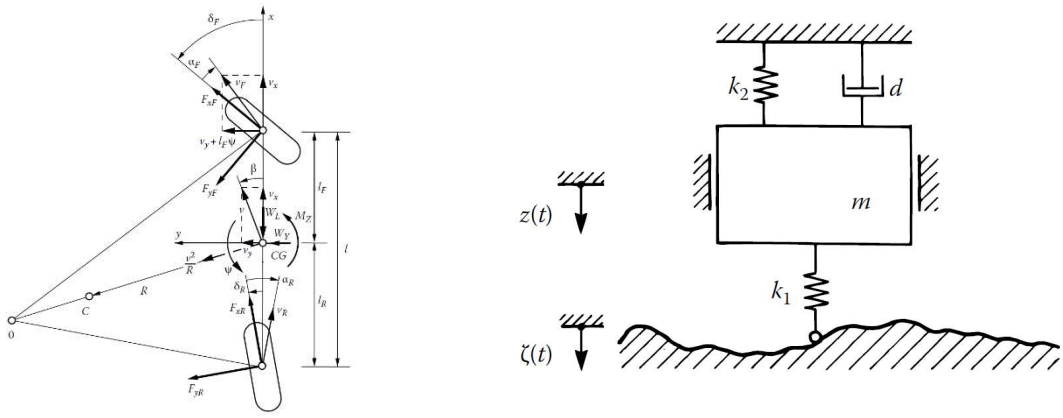

(a) (b)

Figure 1.2. Simplified Models [1] (A) Single Track Model (B) Quarter Car Model

Vehicle models can be categorized into three major groups according to their level of complexity: simplified linear models, lumped-parameter nonlinear models, and rigid or flexible multibody dynamics models. Examples of the first type include the linear single-track model and the quarter car model shown in Figure 1.2. The former is usually used in the preliminary handling studies to gain some conceptual understanding of the qualitative behavior of the system, while the latter is used as the first step in ride comfort analysis. The range validity of such models is narrow and usually limited to steady-state motion regimes and small tire slips.

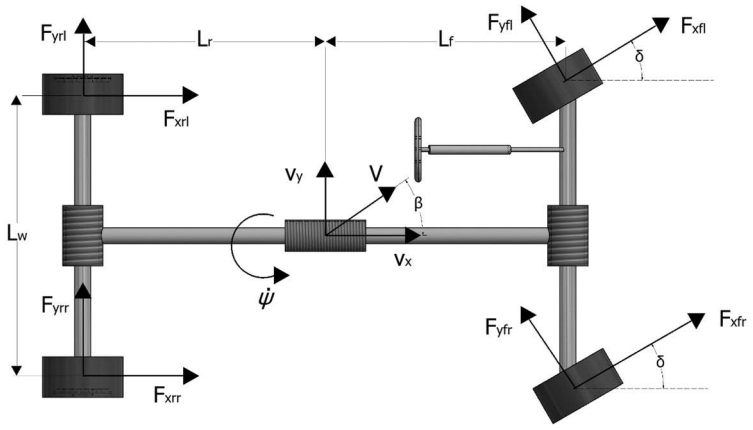

(a)

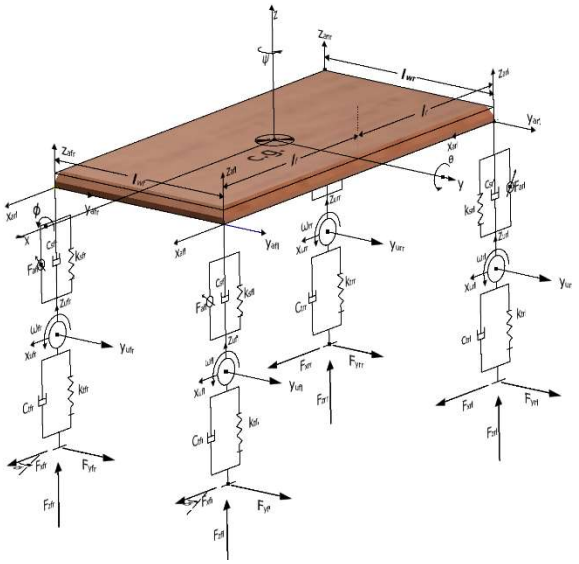

(b)

Figure 1.3. Lumped Parameter Model Example (A) 7 DOF Nonlinear Model (B) 14 DOF Coupled Model

The higher-order lumped parameter models are the most well-established and widely-used models. These models account for kinematic nonlinearities as well as tire nonlinear behavior. They are predominantly expressed in terms of a set of coupled nonlinear differential equations that are hand-coded. Moreover, in certain circumstances, these models account for the coupling among the modes of motion and the transient behavior

of the tires. Examples of models of this type are shown in Figure 1.3 where the number of degrees of freedom varies with reference to the aim of the study.

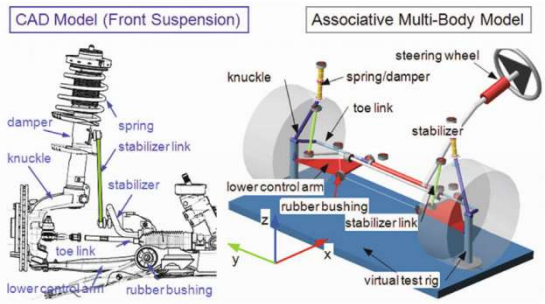

(a)

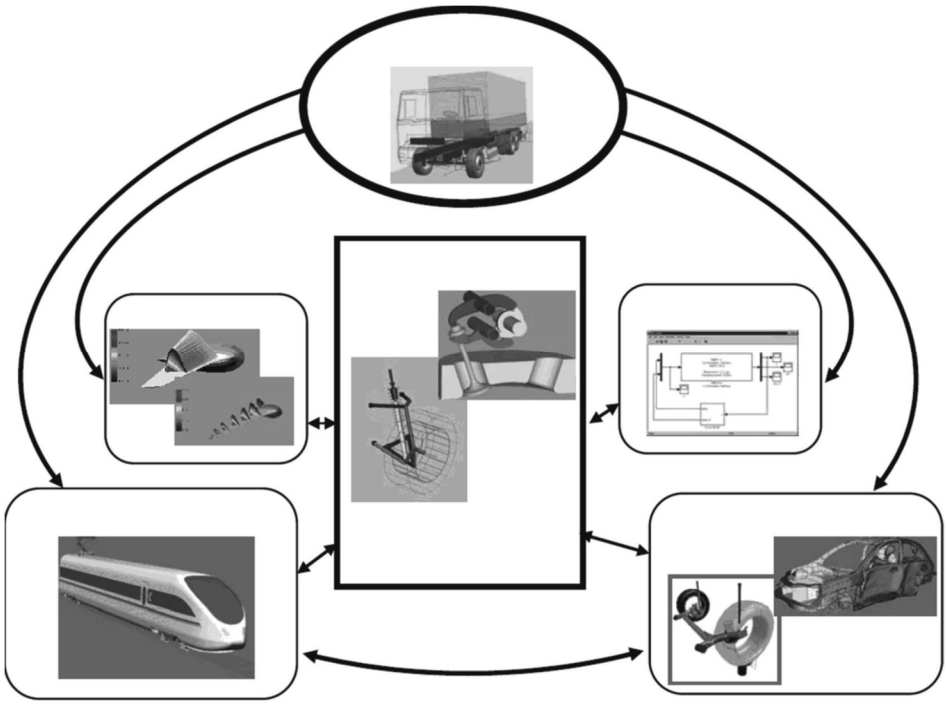

(b)

Figure 1.4. Interdisciplinary Analysis (A) MBD Vehicle Model [2] (B) Integrated Virtual Design Using Multi-Body System Simulation Software and its Bidirectional Interfaces [1]

Finally, multibody dynamic simulation (MBD) packages like MSC Adams (Figure 1.4-a), Simpack, and Altair Motionview, among others, treat each component of the vehicle and account for the dynamics of the connected bodies and with their bearings and joints in either rigid or flexible body assumptions. These tools can be linked to CAD models, computer-aided control engineering (CACE), and computational fluid dynamics (CFD) as well finite element solvers for further interdisciplinary analysis (see Figure 1.4-b). The monodisciplinary MBD model may consist of hundreds of degrees of freedom, not to mention the additional complexity when large-scale spatial flexible body motion studies are performed or when a multidisciplinary co-simulation is conducted. Therefore, the computational demand is relatively very high, and robust numerical solvers are needed for such complex simulations.

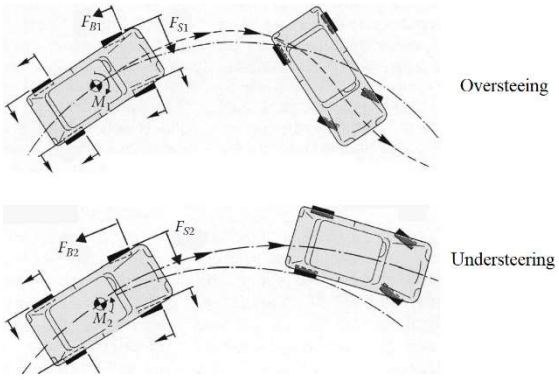

Figure 1.5. Steer Characteristics [1]

Some important terminologies are required to be introduced in the context of vehicle handling stability evaluation. As illustrated in Figure 1.5, If the vehicle is moving on a trajectory of decreasing radius, the vehicle is said to be under over-steer characteristics. The vehicle's tendency to move in an increasing radius, on the other hand, has under-steer characteristics.

1.2.2 Tire Models

The tire is a very complicated composite component consisting of different materials with varying mechanical, chemical, and thermal properties. The rubbery toroidal shape mounted in a metallic rim forms a chamber that can be inflated by air. The construction of the tire plays an important role in the performance of the vehicle. The outer surface of the tire in contact with the ground is supported by steel plies and radially arranged enforcement wires and has a complex geometry is called the tread, as shown in Figure 1.6 . The material behavior of such a construction is not only highly nonlinear but also time-dependent.

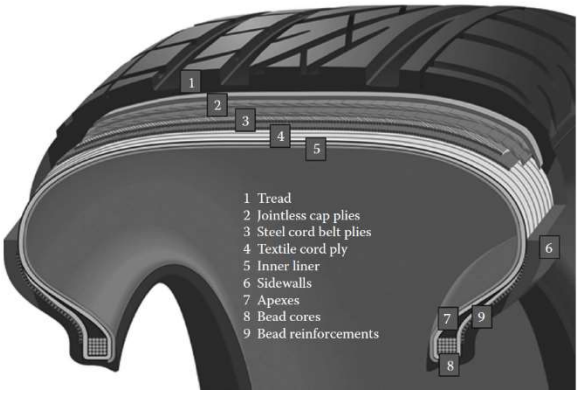

Figure 1.6. Tire Structure [1]

Apart from crash circumstances, the external forces and moments exerted on the vehicle are from aerodynamic, gravitational, and tire forces. By far, tire forces have more contribution on the dynamics of the vehicle compared with the aerodynamic loads (except in high-speed race vehicles). Accurate modeling of this primary source of external loads governs the overall accuracy of the vehicle coupled system. Unfortunately, modeling the dynamics of the intricate composite rolling tire is a very challenging task. Tire force transfer characteristics are highly complicated, nonlinear, and

dependent on a large number of parameters and variables. Tire strong nonlinearity arises from the nonlinear material behavior, nonlinear geometry, and nonlinear contact loadings.

To overcome the difficulty of modeling the dynamics of the tire, several tire models have been developed and experimentally validated in the literature. The principal role of such models is to predict the forces and moments generated in the contact area between the tire and the ground. In Figure 1.7, (a) presents the inputs and outputs channels through which the tire model exchanges the information with the vehicle, while (b) presents some examples of tire models.

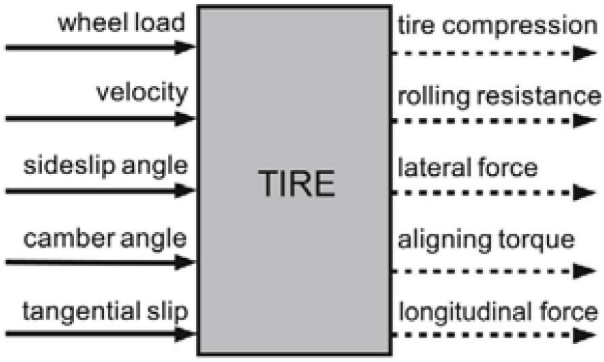

(a)

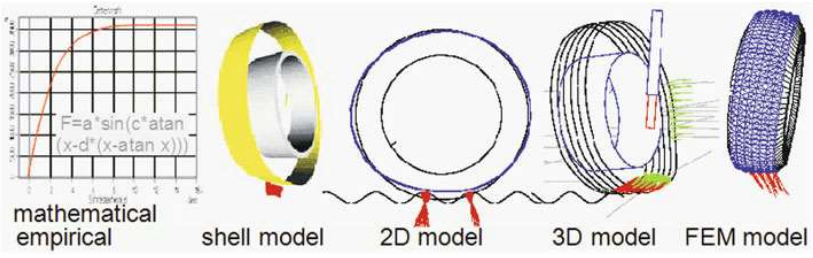

(b)

Figure 1.7. (a) Tire Model Input/Output Channels [2] (b) Different Tire Models [2]

Tire models vary in their level of detail, degree of complexity, and computational speed. The simplest tire model is the linear tire model, in which the tire is treated as a spring element. Extensions of the linear tire models are the tire models that utilize analytical, empirical, or semi-empirical approaches. The parameterization process of such models relies on experimental measurements. Tire parameters linked with these models are predominantly abstract in nature and do not reflect physical interpretations. Tire models of this kind are preferred in the context of vehicle control systems development because of their real-time capabilities. Nevertheless, the range of applicability as well as the accuracy of the semiempirical-based tire models are limited in comparison to the physics-based tire models.

More detailed tire models account for the structural properties of tire components like its stiffness, damping, and inertia. Physical models are either high fidelity finite element (FE) models or physical models with reduced accuracy used in dedicated software packages. Although FE models are capable of carrying out complex nonlinear transient simulations, they are computationally expensive and do not suit multibody dynamics context or control-oriented models. Therefore, FE modeling is generally used in the tire model development phase to verify experimental or analytical results. On the other side, physical models with reduced complexity compared to FE models can still simulate the physics of advanced tire behaviors and working conditions. In addition, their ad hoc approach allows more computationally efficient simulations, yet not real-time capable.

A key terminology that is extensively used in terramechanics literature is the slip (Figure 1.8). Slip quantities are the primary parameters in understanding the mechanism of tire force generation. The following discussion represents a brief description of the origination of tire slips and forces. For a further detailed discussion, the reader can refer to tire dynamics dedicated textbooks like in [4].

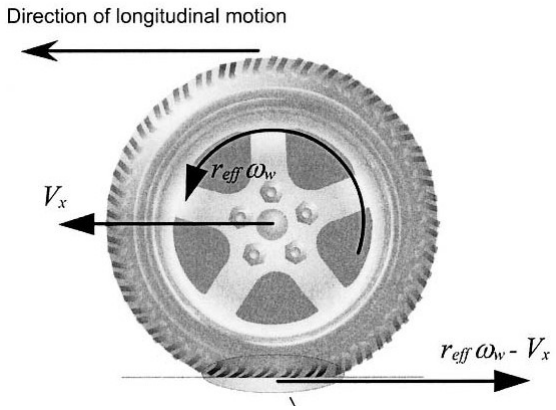

(a)

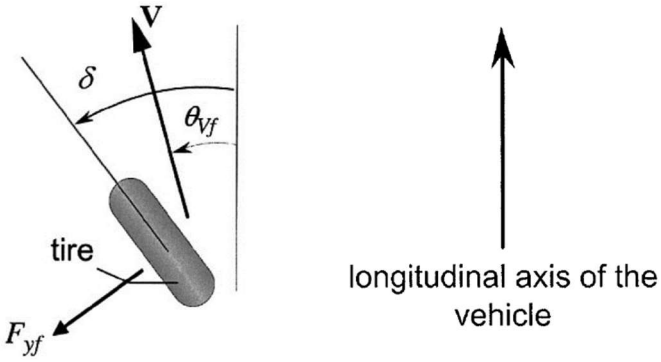

(b)

Figure 1.8. Tire slips [3] (a) Longitudinal (b) Lateral

With reference to Figure 1.8-a, when the tire is in free-rolling, the longitudinal velocity of the wheel center equals its rolling velocity (the rotational speed multiplied by tire effective radius). However, if braking or driving torque is applied, the rotational speed of the wheel decreases or increases, respectively. Therefore, this difference in velocity

deforms the tread of the tire in contact with the ground to generate the longitudinal tire force.

Another force acting on the tire's longitudinal direction and opposes the direction of motion is the rolling resistance force. The mechanism of rolling resistance force generation is quite complicated. Nonetheless, as the name implies, it can be treated qualitatively as the dissipative force generated from the contact of the viscoelastic tire and the ground.

When the orientation is changed or steering is applied to negotiate a curve, the tire treads are typically transversely deformed. The lateral tire force is essentially dependent on this deformation which is represented in terms of the slip angle. As demonstrated in Figure 1.8-b, slip angle is the angle α is the difference between the steering angle δ and the wheel translational velocity orientation θ_{VF}.

1.2.3 Driver Models

The human driver is an integral subsystem of the coupled vehicle/driver closed-loop system and must, in consequence, be incorporated in the loop in dynamic stability analysis. In addition, the possible interference and coordination between the driver and the control system are essential in the development of driver assistance systems. The driver applies inputs as steering angle, accelerator or brake pedal, and gear to follow a prescribed route and maintain a desired velocity according to the perceived signals regarding vehicle status and the environment. Consequently, a model for a driver that emulates the human driver tasks of actuation and sensing is crucial.

To quantify these tasks in a mathematical representation, a wide spectrum of driver models has been developed and evaluated. In fact, modeling the driver is more challenging than modeling the vehicle because drivers vary in their skills and in the way they respond to unexpected situations. Nonetheless, modeling the driver as a controller with the assistance of the well-developed control theory has been extensively used in the literature. For instance, the driver can be simply injected into the loop as a Proportional-Integral-Derivative (PID) controller.

1.3 Vehicle Control Systems

With the assistance of the progressive and rapid development of electronics, computers, sensors, and actuators, control systems have been broadly utilized in different automotive applications. Vehicle control systems can be loosely classified into either passive systems or active systems. The former is concerned about the safety of the vehicle occupants following an accident, like the safety belts and airbags. Active systems, on the other hand, use the information exchanged with the vehicle or acquired from the environment to help in preventing the occurrence of the accidents or at least reduce their impact.

In general, active vehicle control systems receive the dynamic status of the vehicle (like translational and rotational velocities and accelerations, forces and moments, etc.) as well as the driver inputs like the steering angle and traction/braking torque. Furthermore, some active systems are capable of performing advanced measurements like the position with respect to the road center of the lane and the other vehicles, road surface condition, and the road path. According to this information, the controller interferes with the dynamics of the vehicle to achieve certain goals like improving stability, ride comfort, or drivability

to match prescribed desired characteristics. Moreover, the control system enables the vehicle to be invariant against environmental disturbances as well as wrong driver reactions in severe circumstances.

The actuation methodology used in vehicle dynamic control systems is predominantly through influencing the characteristic behavior of the contact forces between the tire and ground, the steering system, or a combination of both. Thus, the motion of the vehicle can be manipulated in longitudinal, lateral, and vertical directions. One way of classifying vehicle dynamic control systems is according to the direction of motion they are acting on. For instance, antilock braking (ABS) is used to control the longitudinal motion of the vehicle, while the electronic stability program (ESP) is utilized to stabilize the transversal motion.

A brief description of each of the major vehicle dynamic control systems used in commercial vehicles is given in the following sections.

1.3.1 Longitudinal Motion Controllers

The objective of the longitudinal vehicle dynamics controllers is to control longitudinal characteristics of the vehicle, such as its distance from the preceding vehicle, braking and traction performance, and vehicle forward velocity and acceleration. Longitudinal motion control is typically achieved using throttle and brake actuators. Examples of longitudinal active control systems in production and under development are:

1- Antilock Braking (ABS)

One of the most commonly used active control systems in modern vehicles is the ABS. Its objective is to improve vehicle stability and prevent excessive tire slips during heavy braking. It is essential in the cases of hard braking where the wheels may experience locking, the braking distance is increased, and vehicle steerability is difficult.

The sensors mounted on the wheel hub measure the angular speed and acceleration of the tire. The ABS algorithm in the electronic control unit (ECU) processes these measurements and compares them with some threshold values. If a wheel locking is detected, a signal will be transmitted to the hydraulic pressure modulator unit to reduce the braking pressure in the wheel. In fact, the ABS does not directly set a desired value of the braking pressure; instead, it controls the rate of change of the braking pressure.

2- Traction Control Systems (TCS)

Similar to ABS, TCS was developed to improve the longitudinal performance and stability of the vehicle but now during acceleration. In a low-adhesion coefficient road, the driving wheels may slip or spin in a slippery road resulting in poor vehicle handling and performance.

TCS utilizes the same sensors as ABS to maintain the traction slip lower than a predetermined threshold value. If excessive slips are detected during acceleration, TCS reduces the power supplied by the engine to keep the slip in the optimum range.

3- Adaptive Cruise Control (ACC)

In the absence of leading vehicles, the ACC performs indistinguishable from the conventional cruise control in which the vehicle is tracking a required speed. However, if a preceding vehicle is detected by means of a “looking forward” sensor which is likely radar or laser, the ACC tries to maintain offset from that vehicle. With reference to the distance from the preceding vehicle, the ACC accelerates or decelerates the vehicle to maintain a safe distance.

1.3.2 Lateral Motion Controllers

The lateral motion of the vehicle in normal operating conditions is usually controlled by the driver through the steering wheel. However, if the motion of the vehicle is disturbed and the driver loses control of the vehicle, stabilizing the vehicle will be challenging. In fact, a situation of this kind may occur for various reasons such as poor traction, low friction road, or problems with tire operating conditions. In order to stabilize the vehicle in such situations, an active-controlled torque can be applied to the vehicle to track desired performance measures. This torque can be produced either by steering-based systems, braking/traction-based systems, or active differentials.

1- Steering-based control

With reference to a certain speed and input steering angle from the driver, the steering-based controller algorithm calculates the vehicle target states and compares them with the actual ones. Subsequently, the steering angle is corrected such that the desired states are achieved. The steering input is possible to be commanded to the front wheels (active front-wheel steering AFS), rear wheels (active rear-wheel steering ARS), or four wheels

(active four-wheel steering 4WS). The active steering system intervenes with the driver steering command using either “steer-by-wire” systems or by integrating the controller with the traditional steering mechanism.

2- Braking/Traction-based Controllers

Based on a reference desired model, the controller applies braking or traction torques that are optimally distributed among the vehicle wheels. To generate a clockwise yaw moment, for instance, a larger braking torque is applied to the left wheels compared to the right wheels using a hydraulic pressure modulator. This strategy is called the electronic stability program (ESP) and is used to mitigate the swerving and drifting of the vehicle. Also, using variable torque distribution systems based on active differentials, independent drive torque can be distributed among the four wheels without decelerating the vehicle. Moreover, the concrete idea of torque biasing is also implemented in electric vehicles using independent in-wheel motors.

3- Integrated Systems

Each of the steering and braking/traction active controllers has its own advantages and disadvantages related to the response and performance. To compensate for the shortcomings of these systems, an integrated control technique can be utilized such that the vehicle follows the nominal motion in the linear regime expected by the driver. The coordination between the two actuation systems is crucial and requires authority switching and optimization strategies. Thus, due to the complexity and computational burden, such systems are still in the early development phases.

1.3.3 Vertical Motion Controllers

Vertical dynamics is mainly concerned with the comfort of the driver and passengers by means of a suspension system. The suspension system transmits the forces and moments from the tires to the vehicle body, suppresses the vibrations induced from the road surface, and plays an important role in vehicle handling. The objective of vertical motion controllers is to match road irregularities and vertical excitations as well as enhancing handling stability by proper adjustment of the stiffness and damping properties of the suspension system. According to the level of automation used, suspension control can be classified into semi-active and active suspensions.

1- Semi-active Suspension

In a semi-active suspension system, the force induced by the damper can be adjusted according to the continuously varying driving conditions to achieve maximum ride comfort without degrading handling quality. In this system, the vertical displacement is actively sensed, and the damping force is regulated accordingly in full energy storage and dissipation framework, and without any active force supplied to the vehicle chassis. The adjustment of the damping coefficient is usually attained using an electronically controlled valve to achieve quick responses.

2- Active suspension

In contrast to the semi-active suspension system, active suspension systems employ an external electric or hydraulic power source to manipulate the stiffness and damping characteristics of the suspension according to active measurements. Active suspensions provide the vehicle body with external energy to enhance the ride quality and handling performance. Nevertheless, the active suspension system is bulky and expensive because

it replaces the springs and dampers with hydraulic and electric actuators aside from the pumps and valves as well as electronics and sensors.

3- Active Roll Control (ARC)

The vehicle roll motion has relatively low damping which is problematic in extreme maneuvering where excessive roll moments are generated with the risk of vehicle rollover. Active roll control magnifies the overall roll damping capacity and eliminates the excessive roll angles provoked in curvilinear maneuvers. The active anti-roll torques induced by the ARC system are usually produced by hydraulic actuators.

1.4 Motivation

The sudden deflation and loss of pneumatic pressure is known as a tire blowout. It may severely affect the vehicle's dynamic characteristics, particularly at high speeds on the highway. In general, tire blowout is caused by overloading, overheating, manufacturing defects, and road hazards. After rapid deflation of the tire, severe damage to the tire structure occurs, and the dynamic behavior of the vehicle is tremendously affected due to the non-uniformity of the tire rotational speed. The motion of the vehicle is disturbed by the yaw moment induced as a result of the blown tire. Hence, the vehicle loses its directional stability and has a risk of departing its lane. Unfortunately, the result of this unsteadiness is sometimes colliding with the guardrail or other vehicles. This also leads hypothetically to additional consequences in cooperative systems like a platoon of driverless vehicles. The multivehicle coordination task among the participating vehicles that is performed through vehicle-to-vehicle communication is very sensitive to

longitudinal and lateral relative motions. Hence, the tire blowout consequences will even be amplified in the upcoming “connected and automated vehicles” technology.

In fact, according to statistics reported by the National Highway Traffic Safety Administration, 23000 accidents involve flat tire or tire blowout occur annually, from which 535 are catastrophic and fatal [5]. A more recent report recorded 738 deaths in the United States from tire-related crashes in 2017 [6]. In 2016, 8 people were killed, 150 seriously injured, and 1044 slightly injured in road accidents in the UK because of defective or deflated tires [7]. In the period from 1996 to 2002, it was found by a French motorway network [8] that 3.5% of all truck accidents were reported with blown-out tires. In China, it was observed that more than 70% of vehicle accidents on the highway involve tire failure and caused severe structural property damage and fatal injuries [9]. Finally, in the Middle East region, statistics show that extreme heat is responsible for 39% of all accidents due to tire blowout [10].

Finally, there are no multibody dynamics solvers or tire models (except FEA and FEA-based solvers) that are capable to capture the physics of the tire blowout and its effect on vehicle motion.

1.5 Problem Statement

Despite the existence of vehicle stability control systems such as differential braking, active torque distribution, etc., tire blow is still considered a significant reason for many fatal

accidents. Nonetheless, maintaining vehicle stability in both longitudinal and curvilinear motions is critical for all vehicle active safety systems in order to function properly. Therefore, there is a need for a safety control system to assist in maintaining vehicle stability during and after the blowout. Moreover, the upcoming driverless vehicle technology requires effective control to operate safely since it relies solely on the tire-road interaction, which significantly undergoes different transients when the blowout event takes place. Such a transient is even more problematic to the stability of such cooperative systems. This study introduces an accurate higher-order model that is capable of predicting the motion of the vehicle during and after a tire blowout, besides being able to account for the couplings among the critical degrees of freedom. Accordingly, a sequence of tire blowout simulations is carried out to analyze the handling/roll coupled dynamics of the vehicle. In addition, the study presents a control-oriented model that captures a wide range the vehicle dynamics without the simplifying assumptions used extensively in the literature. Correspondingly, a safety control system that stabilizes the vehicle suffering from tire blowout is developed. Moreover, different actuation techniques are introduced to suit different vehicle platforms like conventional and electric vehicles. This current simulation study is essential at the virtual development stage. The proposed controller will be next implemented and tested in a hardware-in-the-loop (HIL) experimentation. The hardware bench test system serves as a first step for the actual controller implementation on a real vehicle.

1.6 Research Objectives

Despite this hazardous event, the blowout problem, to the best of the author's knowledge, cannot be completely avoided until now, and building an automatic safety control system to alleviate the consequences of this phenomenon is indispensable. Subsequently, the aim of the current study is to examine the behavior of the vehicle experiencing a tire blowout and how to mitigate its impact. The following listed research objectives would holistically facilitate the accomplishment of this aim.

- Develop and validate a full vehicle model to be used in the analysis and control of vehicle dynamical systems in general as well as in this study specifically. This model accounts for different tire models, driver models, steering mechanism, and driveline dynamics.
- Extensively analyze the vehicle dynamic response to a tire blowout under rectilinear and curvilinear motions. Moreover, to carry out in-depth parametric studies to examine the effect of different system parameters on the vehicle dynamic characteristics. Such analysis serves as a stimulus for building tire blowout safety control systems in commercial vehicles.
- Extract and build nonlinear as well as linearized vehicle handling control-oriented models to be used in the control design phase.
- Design, evaluate, and compare active control systems aiming to stabilize the vehicle subjected to a tire blowout using different control methodologies.
- Apply the proposed controller to the conventional as well as electric vehicles with different individual and integrated actuation techniques.

1.7 Literature Review

Tires are the primary source of the external forces and moment exerted on the vehicle. Modeling these forces is a challenging task and dependent on many parameters. One of the important parameters affecting tire forces and moments is the inflation pressure. Qualitatively, the major effects of the reduction of the operating inflation pressure on the key tire parameters are listed in Table 1.1 [11,12].

Table 1.1. Effect of Inflation Pressure Reduction on Tire Parameters

Tire rolling resistance	increase
Tire cornering stiffness	decrease
Tire radial stiffness	decrease
Tire camber stiffness	decrease
Self-aligning moment	increase

Conventional tire models like the magic formula, Fiala, and Dugoff tire models among others, don't incorporate the effect of inflation pressure in their formulations. Therefore, these models have been extended to allow for variations in inflation pressure. Besselink, et. al. [13], enhanced the magic formula by including the effect of inflation pressure, followed by enlarging the range of inflation pressure variations in [14]. Physical tire models derived from high fidelity finite element analysis models like Cosin FTire [15] and CDTire [16] are also capable to simulate the effect of different inflation pressure values. The reduction of the inflation pressure increases the contact area between the tire and the ground as well as the rolling resistance force. Tripathi, et. al. quantified the

increase of rolling resistance force by means of the rolling resistance coefficient [17]. This increase in rolling resistance force was found to be diversely affecting the fuel economy because of the dissipating nature of this force [18].

Due to the interdisciplinary nature of the vehicle/tire integrated system, the dynamics of the vehicle are affected by the inflation pressure of the tire. Several studies have been conducted to investigate the effect of inflation pressure on the dynamics of the vehicle. Larocca et. al. [19] carried out experimental and simulation studies to examine the effect of the tire inflation pressure on the forces and moments applied to a commercial vehicle's steering system. The study showed that the forces and moments exerted on the steering mechanism are significantly influenced by the inflation pressure reading. Moreover, numerous studies have been conducted to analyze the consequences of changing the inflation pressure on the braking performance [20,21] as well as its implications on the antilock braking system [22,23].

Moreover, despite being insignificant, the variation inflation pressure has an influence on the suspension system and the ride quality [24,25]. Even with a complete loss of inflation, tire burst was found to has a slight to no impact on the comfort of vehicle passengers [26]. On the other hand, comprehensive studies have been executed to examine the handling stability sensitivity to the tire inflation pressure [27-29]. Depending on the amount and rate of deflation and the location of the deflated tire/tires, it has been concluded that the inflation pressure has an enormous effect on the handling stability of the passenger cars. Cossalter et., al., applied the aforementioned handling studies on a

moving motorcycle [30,31] while in [32], the effect of the inflation pressure on the handling of a bus was assessed. Rabhi et. al [33] estimated the shift in the vehicle center of gravity as a result of inflation pressure variation. Using a planar bicycle model, Brown et al. [34] analyzed the vehicle dynamic behavior undergoing a gradual tire inflation pressure reduction. Parczewski [35] investigated the impact of pressure change on the weight redistribution and dynamics of the vehicle during a braking maneuver. Stryjek et al. [36] carried out experimental tests to examine the effect of partial and complete loss of pressure on the steerability of the vehicle.

An unanticipated and complete rapid loss of the tire inflation pressure intuitively has a more significant impact on the vehicle motion than partial or gradual reduction. A large number of crashes occurs annually as a result of blowout [5-10]. Various studies for analyzing the mechanics of blowout and its impact on vehicle transient response have been proposed by many researchers. Simulation models were developed and implemented in commercial vehicle dynamics simulation platforms. Furthermore, well-instrumented experiments were carried out for different blowout scenarios. Based on these studies, safety control techniques have been established.

Blyth [37] used user input multipliers for these parameters to decrease (stiffness values) or increase (rolling resistance values) a value of a parameter. A linear change for these parameters throughout the blowout duration was assumed. This approach was implemented in a new tire blowout module in EDVSM software. To validate the results from simulations, four distinct well-instrumented maneuvers were carried out involving a

rear tire blowout scenario. By conducting several blowout and delamination tests under different operating conditions, Robinette and Fay [38-40] presented three papers in which the dynamic characteristics associated with the disablement event including a zero-pressure case were analyzed. Lozia [41] then applied the simplified model proposed by Blyth to a biaxial vehicle model to investigate the response of the vehicle to a tire blowout and provided a qualitative description of the change in dynamic characteristics as a result of blowout event. Both studies concluded that the blowout problem itself does not lead to the remarkable loss of stability provided no driver steering or braking actions. However, neither study considered any contribution from the driver as a reaction to the blowout.

Wang and Guo [42] undertook a series of inflation-deflation experiments to examine the effect of pressure change in cornering, longitudinal, camber, and radial stiffnesses as well as longitudinal friction coefficient and rolling resistance. Again, a linear behavior is assumed for these parameters based on a 0.1 seconds blowout duration. Using the simple linear tire model, Guo [43] examined the vehicle dynamic response with normal and zero inflation pressure using Carsim. The variations in mechanical properties of the tire were obtained using experiments at a low-speed bench. Under zero tire inflation pressure, it was found that the tire longitudinal stiffness reduces to 34.28% of the normal value, the tire lateral stiffness reduces to 37.63% of its normal value, and the friction coefficient increases 20 times its normal value.

Cornetto et. al [44] investigated the stability of tractor-semitrailer following a steer axle tire blowout. Full-scale well-instrumented tire blowout tests were made, and the results were compared to computer simulation models. The first simulation model is SIMON which has a tire blowout add-in based on [37]. The second model is Trucksim. Trucksim was modified to implement the blowout scenario. Han [45] thoroughly analyzed the results of [37] and [41] to estimate the correction factors for tire stiffnesses, rolling resistance, friction coefficients. He incorporated these factors in his modified bilinear tire model to study the dynamics of a vehicle subjected to a tire blowout. To verify the simulation results, he analyzed the results of recorded scenes for a passenger car exposed to a tire blowout. Vichare and Palanivelu [46] calibrated Blyth's multipliers to accommodate a vehicle semi-trailer vehicle tires. They used Trucksim to simulate various rear axle super single tire blowout scenarios. To investigate the effect of the heavy vehicle scrub radius in tire blowout situations, 20 drivers of different ages were exposed to repeated front tire blowout tests, it was observed that the reducing the scrub radius from 12 cm to 0 cm by means of configurable power steering system reduces the average lateral deviation from 23 cm to 16 cm [47]. Larson and Cuadrado [48] carried out several tests to investigate the stability of a heavy-duty truck with a trailing axle tire blowout. Utility vehicles, pickups, and vans were also tested extensively to analyze their sensitivities when a tire airs out [49].

It has been concluded by many researchers that the dominant factor in vehicle accidents due to a tire blowout is the wrong driver reaction [50, 51]. Hence, investigating the variations among the motorists' behaviors when they experience a blowout problem is

inevitable. Tagesson et. al [47] developed a driver model based on driving tests carried out for different drivers. Using a driving simulator, Horak and shane [52] combined a human driver model to analyze and control the dynamics of a pickup experiencing tire blowout. Yu et. al [53] implemented a steering model and a braking model to represent the driver model mathematically.

Finite element analysis was also employed to study the rapid tire inflation pressure loss variation in the mechanics of the pneumatic tire. Bolarinwa and Olatunbosun [54] used ABAQUS to conduct stress-strain type structural analysis to estimate the tire weakest point as a result of high inflation pressures. A study with the same objective was performed for a truck tire in [55, 56] and for a motorcycle by Barbani et. al [57] in which the tire burst phenomenon was investigated. Cai et. al [58, 59] established a tire blowout generator to carry out a tire burst experiment from which he can validate the LSDYNA simulation results. The simplified models in these studies cannot accurately capture the tire mechanics during and after the tire blowout. Alternatively, a more complicated nonlinear anisotropic model including the major tire components and different material characterization should be used.

In order to enhance the safety of the vehicle, Tire Pressure Monitoring System (TPMS) has been equipped on the vehicle. TPMS reports real-time pressure information inside the pneumatic tire to the driver of the vehicle [62]. Afterward, in September 2007, NHTSA stipulated that TPMSs must be installed in all new imported or manufactured passenger cars [63]. Nevertheless, since the tire blow-out predominantly occurs suddenly due to

nails or severe sharp cornering [64], TPMS can't completely prevent the occurrence of tire burst. Likewise, the automatic system proposed for maintaining the operating tire pressure around its optimal value in [65] can improve tire life but can't handle the blowout problem.

The dramatic loss of vehicle stability directly after the tire blowout encourages researchers to investigate this vital subject during the past two decades. Consequently, a need for an emergency controller to reduce the impact of a tire blow-out is critical. According to many researchers, the striking feature in the tire blowout problem is the degraded stability is in the yaw direction. In general, the most well-documented yaw stability control techniques that have been proposed and developed are steer by wire, differential braking, and independent all-wheel drive distribution [3]. These control techniques can be further modified to facilitate the problem of the blowout and its implications.

The proposed control strategies for vehicle safety improvement in a tire blow-out situation can be divided into three main categories: steering-only control, braking-only control, and integrated control. The first published endeavor to tackle the problem was developed by S. Patwardhan [60, 66] in which a steering-only control approach is introduced. However, their experiments were conducted at a vehicle speed of 20 miles/hour which is a low speed compared with the high speeds on highways where a quick turn of the steering right after a blow-out is dangerous; indeed, it can lead to a rollover accident [42]. The steering-only control strategy was strengthened later by

incorporating the driver behavior [52] and under expressway circumstances [80, 104]. Guo et. al [67, 68] and Yue [104] utilized a three degrees of freedom bicycle model and veDYNA simulation software to design a nonlinear model predictive controller based on steering-only actuation. Wand [105] incorporated their model predictive control in the context of a triple-step nonlinear controller to solve the path following problem of an autonomous vehicle with a flat tire. Nonetheless, the control scheme is tedious and computationally demanding. Hence, a new approach to control the lateral stability of the vehicle using a brake-only controller was implemented.

A tire blow-out automatic braking system selectively uses a controlled braking force to generate the yaw rate required to stabilize the vehicle. This principle along with different control apparatuses and optimization techniques has been examined broadly [69, 70, 81, 82]. Yet, none of these studies accounted for the possible random steering actions from the driver. Instead of using pressure measurements, Liu et. al [70] developed a tire blowout sensing algorithm using wheel speed measurements. In their study, the variation of the pressure with time was approximated using Bernoulli's equation and validated by experiment. Carsim-Simulink co-simulation was used in conjunction with an active braking system to slow down and stabilize the vehicle at a medium-high speed regime. Aki [106] used a driving simulator to investigate the behavior of the driver reacting to tire blowout. Yu et. al [53] augmented the driver behavior model in an electrohydraulic brake-based brake-by-wire control scheme. Output feedback inclusive of a torque allocation algorithm was implemented to stabilize an electric vehicle exposed to tire blowout [83]. Yang et. al [107] stabilized an electric vehicle suffering from tire blowout

using reconfiguration of torque distribution and vertical load. Li, et. al. [108] enhanced the tire blowout model through explicit considerations of the tire vertical load redistribution and self-alignment torque. A two-stage vertical force redistribution model is employed for the vertical load variations instead of the one-stage model used in Blyth's study. Subsequently, the driver behavior model was injected into the control loop to design a shared control scheme using a bicycle model [109].

Recently, a combination of the two controllers to further improve the dynamic stability of the vehicle as well as maintain the lane of travel has been presented. Wang et. al [71] comprehensively applied this idea through a sequence of studies for a straight driving condition while in [72, 73] the approach was enhanced and further extended to the turning driving condition followed by the improvement of the optimization algorithm in [74]. However, since the vehicle response time should not exceed a few seconds after a tire blow-out, the time-delay is a crucial problem and was not considered in these studies.

Other researchers developed some safety and safety-assisted systems for the blowout problem without considering the dynamics of the vehicle. Xulina, Xuejianfeng, and Sunjinhao [75] utilized pressure and temperature sensors to evolve sound-light tire burst warning system. In his study, [76] established a fuzzy control algorithm to maintain the vehicle's original trajectory when exhibits a blowout problem. The system is provoked as soon as the vehicle tends to depart the lane. The stabilization actuation process is activated by means of differential braking. Chen, et. al [77] proposed an indirect real-time identification methodology that activates braking and stability control systems. The

system relies solely on tire vibrations and effective radius analyses to activate the warning and safety system. Based on the rate of change of the inflation pressure and steering rack force measurements, Li et. al [78] developed a control strategy to reduce the moment generated in the steering wheel as a result of tire burst in the speeding vehicle. Chen et. al [79] developed a test set that activates an emergency braking system to slow down and stop the vehicle during tire blowout occasions.

Previous work has only focused on the sensitivity of the tire blowout on the handling dynamics of the vehicle using simplified vehicle models. Additionally, an accurate higher-order model that is capable of predicting the motion of the vehicle during and after a tire blowout besides being able to account for the couplings among the critical degrees of freedom has not been established. For instance, previous studies have failed to address the question of whether it is conceivable for the vehicle to rollover following a tire blowout.

The objective of the present study is to carry out an in-depth three-dimensional dynamic analysis for a vehicle subjected to a tire blowout. To that end, the study introduces an accurate vehicle model that is capable to reflect the dynamic behavior of the vehicle including the couplings among its essential degrees of freedom. The accuracy of the proposed model is then validated by comparing its response to the response of the high-fidelity MSC Adams/Car state-of-the-art package to the same prespecified inputs. This model can be used to predict the dynamics of the vehicle as well as to evaluate the performance of safety control strategies for arbitrary vehicle maneuvers, including the

tire blowout. Such a platform does not only provide a reliable vehicle motion behavior, but it also requires short computational time which is advantageous for the development of hard-real-time automatic safety control systems. Another advantage of the proposed tire blowout-oriented simulation platform is that it enables the exchange of the time-dependent tire properties among the vehicle, tire, and environment coupled system. Moreover, such a platform provides a custom environment in which the vehicle/tire mechanical properties can be modified to achieve a required user-input behavior easily through hand-coding.

Furthermore, Previous stability controllers of a vehicle subjected to a tire blowout are predominantly based upon over-simplistic models that do not reflect the highly-nonlinear dynamics of such a complicated event. This work presents a novel approach for controlling the vehicle without neglecting the nonlinear vehicle dynamics nor the nonlinear tire behavior. Indeed, the simplifying assumptions of small steering and slip angles as well as neglecting the longitudinal motion (constant velocity assumption) are eliminated. Accordingly, a planar nonlinear seven degrees of freedom vehicle model is derived and validated with the high-fidelity vehicle dynamics package MSC Adams. Furthermore, the robustness property built in the paradigm of the variable structure controller as well as its ability to control the dynamical system outside the linear region are exploited to widen the range of applicability of the blowout safety controller in the literature. A nonlinear traction torque input on the basis of the sliding mode controller is proposed to stabilize and slow down the vehicle experiencing tire blowout. The chattering problem stemmed by the switching nature of the controller is diminished

through reducing the slope of saturation function. Moreover, a double integral sliding surface is utilized in the control strategy to improve the steady-state performance.

The remaining part of the dissertation is divided into three chapters. Chapter two introduces the derivation and validation of the high-fidelity vehicle model as well as the tire blowout dynamic analysis[1], while chapter three discusses the development and evaluation of the safety control system. Two different approaches are introduced: single actuator[2] and multi-actuators[3]. Finally, chapter four summarizes the study and discusses several further research extensions.

---

[1] Submitted to the SAE International Journal of Vehicle Dynamics, Stability, and NVH. as:

M., Al-Quran, A., Mayyas, "Three-dimensional in-depth dynamic analysis of a ground vehicle experiencing a tire blowout", **Submitted**, *SAE International Journal of Vehicle Dynamics, Stability, and NVH*., 2021.

[2] Accepted in SAE International Journal of Vehicle Dynamics, Stability, and NVH. as:

M., Al-Quran, A., Mayyas, "The Design of a Nonlinear Controller for Ground Vehicles Subjected to a Tire Blowout Using Double Integral Sliding Mode Controller", **Accepted** , *SAE International Journal of Vehicle Dynamics, Stability, and NVH.*, 2021.

[3] Accepted in the IEEE Access as:

M., Al-Quran, A., Mayyas, "A Nonlinear Tire Blowout Stabilizer Based on a Novel Integral Terminal Sliding Mode Controller", **Accepted**, *IEEE Access*, 2021.

CHAPTER 2

VEHICLE MODELING AND TIRE BLOWOUT ANALYSIS

To investigate the dynamics of the vehicle in the context of multibody system dynamic, four interacting subsystems are considered for traditional ground vehicles, the sprung mass (the main body of the vehicle), the wheels (unsprung masses), the suspension system, and tire-road contact description. Hence, it is essential to build a mathematical representation that accounts for three dimensional kinematic and inertial couplings between the sprung and the unsprung masses as well as the forces and moments transmitted from the suspensions and the ground.

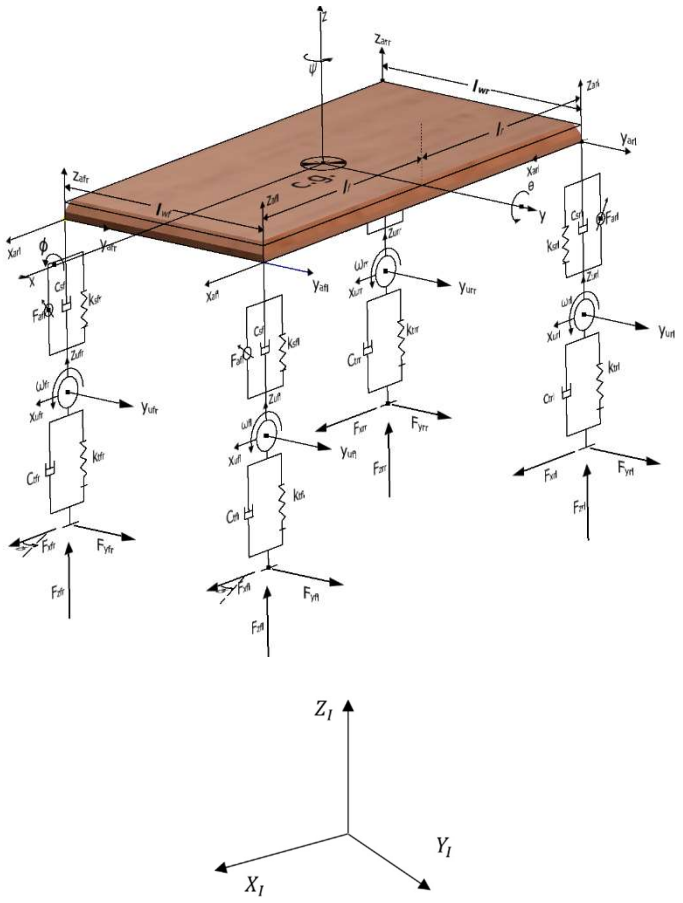

Figure 2.1. Vehicle Full 14 DOF Model

2.1 Vehicle System Modeling

The current study introduces the development, simulation, and validation of a 14 degrees of freedom full vehicle model according to the following assumptions:

1- The vehicle chassis is assumed to be a rigid body, and the sprung and unsprung masses are treated as lumped masses.

2- A front-wheel steering vehicle is considered with the outer and inner steering angles being the same.

3- The wheels are connected to the vehicle body through suspension springs and dampers. In other words, the kinematic description by which this connection is implemented in a real vehicle, as well as the effect of camber, are ignored.

The schematic in Figure 2.1 represents the vehicle model used in this study. The dynamics of the vehicle body are characterized by six degrees of freedom; namely, x, y, z, ϕ, θ, and ψ corresponding to the translations and rotations about the chassis principal axes and measured from the body-fixed frame which is coincident with the body center of mass. The motion of the vehicle can be observed from an inertial frame $X_I Y_I Z_I$ aligned with the mutual perpendicular principal directions through consecutive rotational transformations of the angles ϕ, θ, and ψ. Similarly, the motion of the wheel is predicted by the body-fixed frame $x_u y_u z_u$ attached at the wheel center. The motion of each corner of the chassis is described by the coordinate $x_a y_a z_a$ attached to the pivot point connecting the suspensions and the vehicle body. The wheel is grounded in the transverse direction and cannot move independently in the longitudinal direction. Each wheel is free to move independently in the vertical direction and spin around the axis aligned with the axle and passing through the wheel center. The forces transmitted to the vehicle from the tire

contact patch generated by the tire-ground interaction are denoted by F_{xij}, F_{yij}, and F_{zij}, where the subscript i refers to front and rear, while the subscript j denotes left and right. k_{tij}, c_{tij} and k_{sij}, c_{sij} represent the stiffness and damping of the tire and the suspension, respectively. F_{aij} accounts for the forces exerted by the suspension actuators, if any. l_f and l_r are the distances from the vehicle center of gravity to the front and rear axles while l_{wf} and l_{wr} are the front and rear track widths, respectively. The steering angle is assumed to be equal for the left and right front wheels and denoted by δ. Hence, the vehicle has 14 degrees of freedom with the generalized coordinate summarized as the state vector $\begin{bmatrix} x & y & z & \phi & \theta & \psi & z_{ufl} & z_{ufr} & z_{url} & z_{urr} & \rho_{fl} & \rho_{fr} & \rho_{rl} & \rho_{rr} \end{bmatrix}^T$, where ρ_{ij} is the spin angle of the ij[th] wheel rotating at a speed of ω_{ij}.

The governing equations of motion are derived using Newton-Euler equations. It is a good practice in 3D multibody dynamics problems to start with the kinematics of the system followed by the dynamics. The reader is enormously encouraged to refer to the references [84-88] to further understand and explore three-dimensional mathematical vehicle models.

2.1.1 Vehicle Kinematics

To describe the motion of the vehicle body with respect to the reference ground frame, three elementary sequential rotations in terms of CARDAN angles are executed to generate the transformation matrix

$$ {}^{I}R_V = R_3(\psi)R_2(\theta)R_1(\phi) = \begin{bmatrix} c\psi & -s\psi & 0 \\ s\psi & c\psi & 0 \\ 0 & 0 & 1 \end{bmatrix} \begin{bmatrix} c\theta & 0 & s\theta \\ 0 & 1 & 0 \\ -s\theta & 0 & c\theta \end{bmatrix} \begin{bmatrix} 1 & 0 & 0 \\ 0 & c\phi & -s\phi \\ 0 & s\phi & c\phi \end{bmatrix} $$

$$= \begin{bmatrix} c\theta c\psi & c\psi s\theta s\phi - s\psi c\phi & s\psi s\phi + c\psi s\theta c\phi \\ s\psi c\theta & c\psi c\phi + s\psi s\theta s\phi & s\psi s\theta c\phi - c\psi s\phi \\ -s\theta & c\theta s\phi & c\theta c\phi \end{bmatrix} \tag{2.1}$$

In the aforementioned quantities, $c\psi$ is a short form for $cos\psi$, $s\psi$ for $sin\psi$, and so on. In addition, the description of the tire motion with respect to the vehicle coordinate system is required to express the velocities of the tire origin as well as tire forces with respect to the vehicle fixed frame. For the steered axle, the transformation matrix is

$$^{V}R_{U_{fl,fr}} = \begin{bmatrix} c\theta c\delta & -s\delta c\theta & -s\theta \\ c\delta s\theta s\phi - s\delta c\phi & c\phi c\delta - s\phi s\theta s\delta & c\theta s\phi \\ -s\delta s\phi + c\delta s\theta c\phi & -s\delta s\theta c\phi - c\delta s\phi & c\theta c\phi \end{bmatrix} \tag{2.2}$$

For front left (FL) and front right (FR) tires, while for rear tires

$$^{V}R_{U_{rl,rr}} = \begin{bmatrix} c\theta & 0 & -s\theta \\ s\theta s\phi & c\phi & c\theta s\phi \\ s\theta c\phi & -s\phi & c\theta c\phi \end{bmatrix} \tag{2.3}$$

The angular velocity of the chassis relative to the inertial system and represented in the coordinates of the vehicle fixed coordinate system is calculated as [98]

$$^{I}\omega_V = R_1(\phi)\begin{bmatrix} \dot{\phi} \\ 0 \\ 0 \end{bmatrix} + R_1(\phi)R_2(\theta)\begin{bmatrix} 0 \\ \dot{\theta} \\ 0 \end{bmatrix} + R_1(\phi)R_2(\theta)R_3(\psi)\begin{bmatrix} 0 \\ 0 \\ \dot{\psi} \end{bmatrix}$$

$$\xrightarrow{yields} \; ^{I}\omega_V = \begin{bmatrix} \dot{\phi} - \dot{\psi}s\theta \\ \dot{\theta}c\phi + \dot{\psi}c\theta s\phi \\ -\dot{\theta}s\phi + \dot{\psi}c\theta c\phi \end{bmatrix} \tag{2.4}$$

Subsequently, the rate of change of angular velocity is

$$^{I}\dot{\omega}_V = \begin{bmatrix} \ddot{\phi} - \ddot{\psi}s\theta - \dot{\psi}\dot{\theta}c\theta \\ \ddot{\theta}c\phi - \dot{\theta}\dot{\phi}s\phi + \ddot{\psi}c\theta s\phi - \dot{\psi}\dot{\theta}s\theta s\phi + \dot{\psi}\dot{\phi}c\theta c\phi \\ -\ddot{\theta}s\phi - \dot{\theta}\dot{\phi}c\phi + \ddot{\psi}c\theta c\phi - \dot{\psi}\dot{\theta}s\theta c\phi - \dot{\psi}\dot{\phi}c\theta s\phi \end{bmatrix} \tag{2.5}$$

If the position vector of the center of mass of the vehicle body relative to the inertial reference frame is expressed by $\begin{bmatrix} x \\ y \\ z \end{bmatrix}$, the velocity vector of the vehicle body center of mass relative to the reference inertial frame is ${}^{I}v_V = \begin{bmatrix} \dot{x} \\ \dot{y} \\ \dot{z} \end{bmatrix}$. The current velocity vector can be transformed to the vehicle body-fixed frame as

$$ {}^{V}v_V = \begin{bmatrix} v_x \\ v_y \\ v_z \end{bmatrix} = {}^{I}R_V^{-1}. \begin{bmatrix} \dot{x} \\ \dot{y} \\ \dot{z} \end{bmatrix} \tag{2.6} $$

The translational acceleration of the vehicle center of mass is promptly obtained using the following equation

$$ {}^{V}a_V = {}^{V}\dot{v}_V + {}^{I}\omega_V \times {}^{V}v_V \tag{2.7} $$

The vertical motion of the pivot point connecting the suspension and the vehicle body with respect to the inertial frame is needed to calculate the forces in the suspension springs and dampers. This can be achieved by the relation

$$ {}^{I}r_{aij} = \begin{bmatrix} 0 \\ 0 \\ z \end{bmatrix} + {}^{I}R_V.{}^{V}r_{aij} \tag{2.8} $$

where ${}^{V}r_{aij}$ is the position vector of the pivot point relative to the vehicle body-fixed frame, given by

$$ {}^{V}r_{afl} = \begin{bmatrix} l_f \\ \frac{l_{wf}}{2} \\ -l_z \end{bmatrix}, {}^{V}r_{afr} = \begin{bmatrix} l_f \\ \frac{-l_{wf}}{2} \\ -l_z \end{bmatrix}, {}^{V}r_{arl} = \begin{bmatrix} -l_r \\ \frac{l_{wr}}{2} \\ -l_z \end{bmatrix}, {}^{V}r_{arr} = \begin{bmatrix} -l_r \\ \frac{-l_{wr}}{2} \\ -l_z \end{bmatrix} $$

l_z is the vertical offset between the vehicle center of mass and the attachment point a. A kinematical relation between the vehicle body center of mass velocity and the velocity of the attachment point of the suspension is needed as well

$$^{I}v_{aij} = {}^{I}v_V + {}^{I}\omega_V \times {}^{V}r_{aij} \tag{2.9}$$

Furthermore, the computations of the tire slip quantities require the current position and the absolute speed of the wheel center relative to the vehicle body as well as the circumferential speed expressed in the tire reference frame. These equations are given through equations 2.10-2.12

$$^{V}r_{uij} = {}^{V}r_{aij} - {}^{I}R_V^{-1}.\begin{bmatrix} 0 \\ 0 \\ l_{sij} \end{bmatrix} \tag{2.10}$$

$$^{V}v_{uij} = {}^{V}v_V + {}^{I}\omega_V \times {}^{V}r_{uij} - {}^{I}R_V^{-1}\begin{bmatrix} 0 \\ 0 \\ \dot{z}_{aij} - \dot{z}_{uij} \end{bmatrix} \tag{2.11}$$

$$^{U}v_{uij} = {}^{V}R_{Uij}^{-1}.{}^{V}v_{uij} \tag{2.12}$$

Here, l_{sij} is the instantaneous length of the suspension spring, and can be calculated by

$$l_{sij} = z_{aij} - z_{uij} + l_{staticij} \tag{2.13}$$

with $l_{staticij}$ is the static spring length.

2.1.1 Vehicle Three Dimensional Dynamics

After deriving the kinematic relations of the multibody system, the dynamic equations of motion can be established from the direct application of the conservation of linear and angular momentums in the vector formulation. The corresponding translational equations are introduced as

$$
\begin{aligned}
&({}^{V}\dot{v}_V + {}^{I}\omega_V \times {}^{V}v_V) \\
&\qquad = \sum_{i,j=1}^{2} \left\{ {}^{V}F_{sij} + {}^{V}F_{dij} + {}^{V}F_{arbij} + {}^{V}F_{tij} \right\} \\
&\qquad - m\,{}^{V}R_I \begin{bmatrix} 0 \\ 0 \\ 1 \end{bmatrix} g + {}^{V}F_{aero} + {}^{V}F_{inc}
\end{aligned}
\tag{2.14}
$$

The term in the brackets on the left-hand side of the equation represents the acceleration vector of the body center of mass and is given in the kinematics section. The right-hand side expresses the global external forces applied to the vehicle body. Analogously, the body rotational equations of motion are introduced in the following explicit form

$$
\begin{aligned}
&\begin{bmatrix} I_x & 0 & 0 \\ 0 & I_y & 0 \\ 0 & 0 & I_z \end{bmatrix} . {}^{I}\dot{\omega}_V + {}^{I}\omega_V \times \left(\begin{bmatrix} I_x & 0 & 0 \\ 0 & I_y & 0 \\ 0 & 0 & I_z \end{bmatrix} . {}^{I}\omega_V \right) \\
&\qquad = \sum_{i,j=1}^{2} \left\{ {}^{V}r_{aij} \times \left({}^{V}F_{sij} + {}^{V}F_{dij} + {}^{V}F_{arbij} + {}^{V}F_{tij} \right) \right\} \\
&\qquad + M_{aero}
\end{aligned}
\tag{2.15}
$$

The left-hand side of equation 2.15 is the rate of change of angular momentum of the vehicle body with respect to its center of mass while the right-hand side is global external moments about the same point. The offsets from the center of mass to the pitch and roll centers are disregarded. In the above governing equations, F_{aero} and M_{aero} are the external aerodynamic force and moment, $F_{inc}$is the road resistive load from the inclination and bank angles. ${}^{V}F_{sij}$, ${}^{V}F_{dij}$, ${}^{V}F_{arbij}$ and ${}^{V}F_{tij}$ are the forces resulting from the suspension spring, damper, anti-roll bar, and tire-ground contact, respectively.

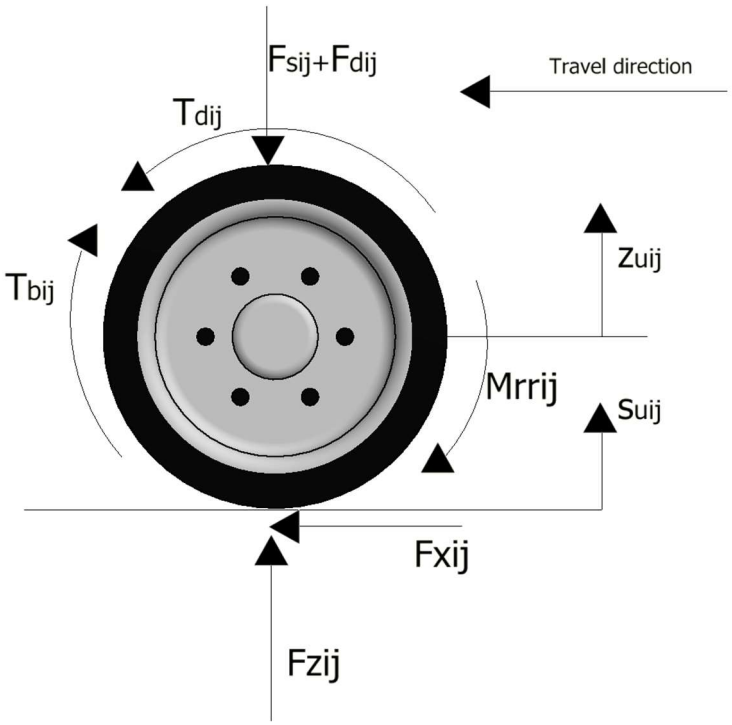

Figure 2.2. Wheel Free Body Diagram

The wheel motion can be excited either by the external forces and moments or by the road bumps as demonstrated in Figure 2.2. The application of the linear momentum in the vertical direction of the unsprung mass results in the following set of equations in a vector form

$$m_{uij}\ddot{z}_{uij} = F_{zij} - F_{sij} - F_{dij} - F_{arbij} - m_{uij}g + k_{tij}s_{uij} + C_{tij}\dot{s}_{uij} \tag{2.16}$$

Where m_u is the unsprung mass of each corner, k_t and C_t are the vertical stiffness and damping of the tire, respectively. The wheels can also be excited by the road bumps and irregularities s_u.

Finally, the rotational dynamics of the wheel can be described by the direct application of the conservation of angular momentum in the wheel body-fixed frame of reference.

$$J_{uyij}\dot{\omega}_{yij} = T_{dij} - T_{bij} - r_{ij}F_{txij} - M_{rrij} \tag{2.17}$$

J_{uy} is the mass moment of inertial of the wheel and $\dot{\omega}_y$ is its rotational acceleration. The external torques acting on a wheel are the driving torque T_d, the braking torque T_b , the rolling resistance torque M_{rr}, and the torque resulting from longitudinal force F_{txij} of the tire.

The driving resistance forces consist of the climbing, aerodynamic, and rolling resistance forces. The climbing resistance force is given by

$$F_{cl} = -mgsin\theta_g {}^{V}R_I \begin{bmatrix} 0 \\ 0 \\ 1 \end{bmatrix} \tag{2.18}$$

θ_g is the road slope angle. Accounting only for the longitudinal drag force and the pitching moment, the aerodynamic force and moment are represented as

$${}^{V}F_{aero} = \frac{1}{2}\rho_a C_D A_s \sqrt{v_w^2 + {}^{I}v_{Vx}^2} \begin{bmatrix} 1 \\ 0 \\ 0 \end{bmatrix} \tag{2.19}$$

$${}^{V}M_{aero} = \frac{1}{2}\rho_a C_D A_s d_{aero} \sqrt{v_w^2 + {}^{I}v_{Vx}^2} \begin{bmatrix} 0 \\ 1 \\ 0 \end{bmatrix} \tag{2.20}$$

ρ_a is the density of air, C_D is the dimensionless drag coefficient often determined experimentally, A_s is the projected surface area, $d_{aero}$is the offset from the resultant aerodynamic force application point to the center of mass of the vehicle, and v_w is the airstream velocity positive opposite to the driving direction.

Assuming linear behavior for the spring and the damper, the suspension stiffness and damping forces resulting from massless springs and dampers can be calculated as

$$^{V}F_{sij} = -^{V}R_I k_{sij}\left[\left(z_{aij} - z_{uij}\right) + \left(l_{statij} - l_{0ij}\right)\right]\begin{bmatrix}0\\0\\1\end{bmatrix} \tag{2.21}$$

$$^{V}F_{dij} = -^{V}R_I c_{sij}\left(\dot{z}_{aij} - \dot{z}_{uij}\right)\begin{bmatrix}0\\0\\1\end{bmatrix} \tag{2.22}$$

These forces are assumed to act orthogonal to the road plane. The moment generating from the antiroll bars and acting about the longitudinal axis of the vehicle is given by [11]

$$^{V}M_{arbf} = k_{arbf}\left[\left(z_{afl} - z_{ufl}\right) - \left(z_{afr} - z_{ufr}\right)\right]\begin{bmatrix}1\\0\\0\end{bmatrix} \tag{2.23}$$

$$^{V}M_{arbr} = k_{arbr}\left[\left(z_{arl} - z_{url}\right) - \left(z_{arr} - z_{urr}\right)\right]\begin{bmatrix}1\\0\\0\end{bmatrix} \tag{2.24}$$

Where k_{arbf} and k_{arbr} are the torsional stiffnesses of the front and rear antiroll bars, respectively.

To calculate the forces generating from the tire-road interaction, the longitudinal slip defined by [84]

$$\sigma_{ij} = \frac{^{U}v_{uxij} - r_{ij}\dot{\omega}_{yij}}{max\left(\left|^{U}v_{uxij}\right|, \left|r_{ij}\dot{\omega}_{yij}\right|\right)} \tag{2.25}$$

is required with $^{U}v_{uxij}$ is the *x* component of the wheel absolute velocity expressed in the wheel body-fixed frame. Moreover, the slip angle is given by

$$\alpha_{ij} = \delta - tan^{-1}\frac{{}^{U}v_{uyij}}{max\left(\left|{}^{U}v_{uyij}\right|, \left|r_{ij}\dot{\omega}_{yij}\right|\right)} \tag{2.26}$$

provided ${}^{U}v_{uyij}$ is the y component of the wheel absolute velocity expressed in the wheel body-fixed frame.

Having the slip quantities, the tire forces can be introduced. The longitudinal and lateral tire forces are derived using the tire model while the vertical component is formulated using the tire elasticity as

$${}^{U}F_{zij} = \begin{cases} k_{tij}\left(z_{uij} - s_{uij}\right) + c_{tij}\left(\dot{z}_{uij} - \dot{s}_{uij}\right) & \text{Normal motion} \\ 0 & \text{Wheel lift} - \text{off} \end{cases} \tag{2.27}$$

There is a broad spectrum of tire models available in the literature with varying accuracy and complexity. The well-grounded magic formula [100] and Dugoff tire models are used in this research. The magic formula tire model is used for validating the vehicle model while the Dugoff model is used in the context of vehicle response to a tire blowout. The governing equations, as well as the numerical data for the magic formula used in this research, can be found in appendix A. Dugoff's tire model can act as a precise portrayal for the tire forces generation mechanism in a steady-state regime and is capable to capture the combined longitudinal and lateral slips. Neglecting the relaxation lengths, the following equations are used to calculate the tire forces [3]

$${}^{U}F_{xij} = \frac{C_{aij}\sigma_{ij}}{\left(1 - \sigma_{ij}\right)} f\left(\lambda_{ij}\right) \tag{2.28}$$

$${}^{U}F_{yij} = \frac{C_{bij}tan\alpha_{ij}}{\left(1 - \sigma_{ij}\right)} f\left(\lambda_{ij}\right) \tag{2.29}$$

C_{aij} and C_{bij} represent the longitudinal and cornering stiffnesses determined by

$$C_{aij} = \left.\frac{\partial F_{xij}}{\partial \sigma_{ij}}\right|_{\sigma_{ij}=0} \tag{2.30}$$

$$C_{bij} = \left.\frac{\partial F_{yij}}{\partial \alpha_{ij}}\right|_{\alpha_{ij}=0} \tag{2.31}$$

calculated at the nominal wheel load. $f(\lambda_{ij})$ is given by

$$f(\lambda_{ij}) = \begin{cases} (2-\lambda_{ij})\lambda_{ij} & if\ \lambda_{ij} < 1 \\ 1 & if\ \lambda_{ij} \geq 1 \end{cases} \tag{2.32}$$

where

$$\lambda_{ij} = \frac{\mu F_{zij}(1-\sigma_{ij})}{2\left\{(C_{aij}\sigma_{ij})^2 + (C_{bij}tan\alpha_{ij})^2\right\}^{\frac{1}{2}}} \tag{2.33}$$

is a dummy variable. The rolling resistance torque is assumed to be expressed as

$$M_{rrij} = R_w C_{rij} F_{zij} \tag{2.34}$$

C_{rij} is the coefficient of rolling resistance. Finally, the tire forces are transformed to the vehicle body-fixed frame through the transformation

$$\begin{aligned} {}^{V}\begin{bmatrix} F_{xij} \\ F_{yij} \\ F_{zij} \end{bmatrix} &= {}^{V}R_{U_{ij}}\ {}^{U}\begin{bmatrix} F_{xij} \\ F_{yij} \\ F_{zij} \end{bmatrix} \\ &= \begin{bmatrix} c\theta c\delta & -s\delta c\theta & -s\theta \\ c\delta s\theta s\phi - s\delta c\phi & c\phi c\delta - s\phi s\theta s\delta & c\theta s\phi \\ -s\delta s\phi + c\delta s\theta c\phi & -s\delta s\theta c\phi - c\delta s\phi & c\theta c\phi \end{bmatrix} {}^{U}\begin{bmatrix} F_{xij} \\ F_{yij} \\ F_{zij} \end{bmatrix} \end{aligned} \tag{2.35}$$

The front steering angle δ is assumed to be related to the wheel steering angle δ_W through the steering ratio *SR* as

$$SR = \frac{\delta_W}{\delta} \tag{2.36}$$

The resulting equations are highly coupled, nonlinear, and capable to carry out simultaneous handling and ride analysis. The aforementioned equations are written in a vectorial compact form that does not highlight the inherent complexity of the vehicle system. To illuminate the whole picture, the expanded version of the body governing equations motion in y-direction for instance are

$$m\big[(c\psi s\theta s\phi - s\psi c\phi)\ddot{x} + \big(-s\psi s\theta s\phi\dot{\psi} + c\psi c\theta s\phi\dot{\theta} + c\psi s\theta c\phi\dot{\phi} - c\psi c\phi\dot{\psi} + s\psi s\phi\dot{\phi}\big)\dot{x} + (c\psi c\phi + s\psi s\theta s\phi)\ddot{y} + \big(-s\psi c\phi\dot{\psi} - c\psi s\phi\dot{\phi} + c\psi s\theta s\phi\dot{\psi} + s\psi c\theta s\phi\dot{\theta} + s\psi s\theta c\phi\dot{\phi}\big)\dot{y} + (c\theta s\phi)\ddot{z} + \big(-s\theta s\phi\dot{\theta} + c\theta c\phi\dot{\phi}\big)\dot{z} + \big\{-\dot{\theta}s\phi + \dot{\psi}c\theta c\phi\big\}\{(c\theta c\psi)\dot{x} + (s\psi c\theta)\dot{y} + (-s\theta)\dot{z}\} - \big\{\dot{\phi} - \dot{\psi}s\theta\big\}\{(s\psi s\phi + c\psi s\theta c\phi)\dot{x} + (s\psi s\theta c\phi - c\psi s\phi)\dot{y} + (c\theta c\phi)\dot{z}\}\big] =$$

$$-k_{sfl}c\theta s\phi\big[\big(z_{afl} - z_{ufl}\big) + \big(l_{statfl} - l_{0fl}\big)\big] - k_{sfr}c\theta s\phi\big[\big(z_{afr} - z_{ufr}\big) + \big(l_{statfr} - l_{0fr}\big)\big] - k_{srl}c\theta s\phi[(z_{arl} - z_{url}) + (l_{statrl} - l_{0rl})] - k_{srr}c\theta s\phi[(z_{arr} - z_{urr}) + (l_{statrr} - l_{0rr})] - c_{sfl}c\theta s\phi\big(\dot{z}_{afl} - \dot{z}_{ufl}\big) - c_{sfr}c\theta s\phi\big(\dot{z}_{afr} - \dot{z}_{ufr}\big) - c_{srl}c\theta s\phi(\dot{z}_{arl} - \dot{z}_{url}) - c_{srr}c\theta s\phi(\dot{z}_{arr} - \dot{z}_{urr}) + (c\delta s\theta s\phi - s\delta c\phi)\frac{C_{afl}\sigma_{fl}}{(1-\sigma_{fl})}f\big(\lambda_{fl}\big) + (c\phi c\delta - s\phi s\theta s\delta)\frac{C_{bfl}tan\alpha_{fl}}{(1-\sigma_{fl})}f\big(\lambda_{fl}\big) + k_{tfl}c\theta s\phi\big(z_{ufl} - s_{ufl}\big) + c_{tfl}c\theta s\phi\big(\dot{z}_{ufl} - \dot{s}_{ufl}\big) + (c\delta s\theta s\phi - s\delta c\phi)\frac{C_{afr}\sigma_{fr}}{(1-\sigma_{fr})}f\big(\lambda_{fr}\big) + (c\phi c\delta - s\phi s\theta s\delta)\frac{C_{bfr}tan\alpha_{fr}}{(1-\sigma_{fr})}f\big(\lambda_{fr}\big) + k_{tfr}c\theta s\phi\big(z_{ufr} - s_{ufr}\big) + c_{tfl}c\theta s\phi\big(\dot{z}_{ufr} - \dot{s}_{ufr}\big) + s\theta s\phi\frac{C_{arl}\sigma_{rl}}{(1-\sigma_{rl})}f(\lambda_{rl}) + c\phi\frac{C_{brl}tan\alpha_{rl}}{(1-\sigma_{rl})}f(\lambda_{rl}) + k_{trl}c\theta s\phi(z_{url} - s_{url}) + c_{trl}c\theta s\phi(\dot{z}_{url} - \dot{s}_{url}) + mgc\theta s\phi - mg\sin\big(\theta_g\big)c\theta s\phi$$

$$\left(\ddot{\theta}c\phi - \dot{\theta}\dot{\phi}s\phi + \ddot{\psi}c\theta s\phi - \dot{\psi}\dot{\theta}s\theta s\phi + \dot{\psi}\dot{\phi}c\theta c\phi\right)I_y + \left(-\dot{\theta}s\phi + \dot{\psi}c\theta c\phi\right)\left(\dot{\phi} - \dot{\psi}s\theta\right)I_x -$$

$$\left(\dot{\phi} - \dot{\psi}s\theta\right)\left(-\dot{\theta}s\phi + \dot{\psi}c\theta c\phi\right)I_z = -l_z\left\{k_{sfl}s\theta\left[\left(z_{afl} - z_{ufl}\right) + \left(l_{statfl} - l_{0fl}\right)\right] +\right.$$

$$c_{sfl}s\theta\left(\dot{z}_{afl} - \dot{z}_{ufl}\right) + c\theta c\delta\frac{C_{afl}\sigma_{fl}}{(1-\sigma_{fl})}f\left(\lambda_{fl}\right) - s\delta c\theta\frac{C_{bfl}tan\alpha_{fl}}{(1-\sigma_{fl})}f\left(\lambda_{fl}\right) - k_{tfl}s\theta\left(z_{ufl} -\right.$$

$$\left.s_{ufl}\right) - c_{tfl}s\theta\left(\dot{z}_{ufl} - \dot{s}_{ufl}\right)\Big\} - l_f\left\{-k_{sfl}c\theta c\phi\left[\left(z_{afl} - z_{ufl}\right) + \left(l_{statfl} - l_{0fl}\right)\right] -\right.$$

$$c_{sfl}c\theta c\phi\left(\dot{z}_{afl} - \dot{z}_{ufl}\right) + \left(-s\delta s\phi + c\delta s\theta c\phi\right)\frac{C_{afl}\sigma_{fl}}{(1-\sigma_{fl})}f\left(\lambda_{fl}\right) + \left(-s\delta s\theta c\phi -\right.$$

$$c\delta s\phi\left)\frac{C_{bfl}tan\alpha_{fl}}{(1-\sigma_{fl})}f\left(\lambda_{fl}\right) + k_{tfl}c\theta c\phi\left(z_{ufl} - s_{ufl}\right) + c_{tfl}c\theta c\phi\left(\dot{z}_{ufl} -\right.\right.$$

$$\left.\dot{s}_{ufl}\right)\Big\} - l_z\left\{k_{sfr}s\theta\left[\left(z_{afr} - z_{ufr}\right) + \left(l_{statfr} - l_{0fr}\right)\right] + c_{sfr}s\theta\left(\dot{z}_{afr} - \dot{z}_{ufr}\right) +\right.$$

$$c\theta c\delta\frac{C_{afr}\sigma_{fr}}{(1-\sigma_{fr})}f\left(\lambda_{fr}\right) - s\delta c\theta\frac{C_{bfr}tan\alpha_{fr}}{(1-\sigma_{fr})}f\left(\lambda_{fr}\right) - k_{tfr}s\theta\left(z_{ufr} - s_{ufr}\right) - c_{tfr}s\theta\left(\dot{z}_{ufr} -\right.$$

$$\left.\dot{s}_{ufr}\right)\Big\} - l_f\left\{-k_{sfr}c\theta c\phi\left[\left(z_{afr} - z_{ufr}\right) + \left(l_{statfr} - l_{0fr}\right)\right] - c_{sfr}c\theta c\phi\left(\dot{z}_{afr} - \dot{z}_{ufr}\right) +\right.$$

$$\left(-s\delta s\phi + c\delta s\theta c\phi\right)\frac{C_{afr}\sigma_{fr}}{(1-\sigma_{fr})}f\left(\lambda_{fr}\right) + \left(-s\delta s\theta c\phi - c\delta s\phi\right)\frac{C_{bfr}tan\alpha_{fr}}{(1-\sigma_{fr})}f\left(\lambda_{fr}\right) +$$

$$k_{tfr}c\theta c\phi\left(z_{ufr} - s_{ufr}\right) + c_{tfr}c\theta c\phi\left(\dot{z}_{ufr} - \dot{s}_{ufr}\right)\Big\} - l_z\left\{k_{sfl}s\theta\left[\left(z_{arl} - z_{url}\right) +\right.\right.$$

$$\left.\left(l_{statrl} - l_{0rl}\right)\right] + c_{srl}s\theta\left(\dot{z}_{arl} - \dot{z}_{url}\right) + c\theta\frac{C_{arl}\sigma_{rl}}{(1-\sigma_{rl})}f\left(\lambda_{rl}\right) - c_{trl}s\theta\left(\dot{z}_{url} - \dot{s}_{url}\right)\Big\} +$$

$$l_r\left\{-k_{srl}c\theta c\phi\left[\left(z_{arl} - z_{url}\right) + \left(l_{statrl} - l_{0rl}\right)\right] - c_{srl}c\theta c\phi\left(\dot{z}_{arl} - \dot{z}_{url}\right) +\right.$$

$$s\theta c\phi\frac{C_{arl}\sigma_{rl}}{(1-\sigma_{rl})}f\left(\lambda_{rl}\right) - s\phi\frac{C_{brl}tan\alpha_{rl}}{(1-\sigma_{rl})}f\left(\lambda_{rl}\right) + k_{trl}c\theta c\phi\left(z_{url} - s_{url}\right) + c_{trl}c\theta c\phi\left(\dot{z}_{url} -\right.$$

$$\left.\dot{s}_{url}\right)\Big\} - l_z\left\{k_{srr}s\theta\left[\left(z_{arr} - z_{urr}\right) + \left(l_{statrr} - l_{0rr}\right)\right] + c_{srr}s\theta\left(\dot{z}_{arr} - \dot{z}_{urr}\right) +\right.$$

$$c\theta\frac{C_{arl}\sigma_{rl}}{(1-\sigma_{rl})}f\left(\lambda_{rl}\right) - c_{trl}s\theta\left(\dot{z}_{url} - \dot{s}_{url}\right)\Big\} + l_r\left\{-k_{srr}c\theta c\phi\left[\left(z_{arr} - z_{urr}\right) +\right.\right.$$

$$\left.\left(l_{statrr} - l_{0rr}\right)\right] - c_{srr}c\theta c\phi\left(\dot{z}_{arr} - \dot{z}_{urr}\right) + s\theta c\phi\frac{C_{arr}\sigma_{rr}}{(1-\sigma_{rr})}f\left(\lambda_{rr}\right) -$$

$$s\phi\frac{C_{brr}tan\alpha_{rr}}{(1-\sigma_{rr})}f\left(\lambda_{rr}\right) + k_{trr}c\theta c\phi\left(z_{urr} - s_{urr}\right) + c_{trr}c\theta c\phi\left(\dot{z}_{urr} - \dot{s}_{urr}\right)\Big\} +$$

$$\frac{1}{2}\rho_a C_D A_s d_{aero}\sqrt{v_w^2 + {}^I v_{Vx}^2}$$

2.2 Model Validation

In order to evaluate the validity of the proposed nonlinear fourteen degrees of freedom vehicle model, the response of the developed vehicle model is compared with the results from the high-fidelity multibody dynamic package MSC Adams.

According to the study conducted by Kutluay [89], the double lane change, sine-sweep, and step steering maneuvers as defined according to ISO-3888/1 and ISO 7401:2003 [90, 91] cover a broad range of working conditions and they are suitable to assess the behavior of the vehicle. The double lane change test is a closed-loop scenario in which a driver interferes with the dynamics of the vehicle by means of a driver model (a PID controller in MSC Adams model). To compensate for the disturbances from the driver, the fourteen degrees of freedom model is excited by the same inputs (steering and traction/braking torques) as MSC Adams model. The simulations are carried out using identical vehicle and tire parameters. Vehicle geometric parameters are obtained directly from the vehicle model template while the tire parameters are measured with the assistance of the tire virtual testing in MSC Adams. The numerical values used in the magic formula model are taken from MSC Adams tire library and the tire properties file can be found in appendix A. Additionally, kinematic and compliance analyses are executed to quantify the suspensions and steering characteristics. The numerical values of the critical parameters utilized in the simulations are presented in Table 2.1.

Figures 2.3-2.5 show the steering input used to excite both models together with the comparison between their responses (yaw rate, roll rate, and lateral acceleration). It is apparent that the proposed fourteen degrees of freedom vehicle model shows sufficient agreement with the MBD model and therefore this platform can adequately replicate the dynamic behavior of the vehicle.

Table 2.1. Vehicle and Tire Parameters Used in the Simulation for Validation

Vehicle sprung mass	995 kg
Front left unsprung mass	54.5 kg
Front right unsprung mass	54.5 kg
Rear left unsprung mass	61.5 kg
Rear right unsprung mass	61.5 kg
Vehicle mass moment of inertia about its roll axis	200 $kg.m^2$
Vehicle mass moment of inertia about its pitch axis	500 $kg.m^2$
Vehicle mass moment of inertia about its yaw axis	600 $kg.m^2$
Wheel mass moment of inertia about its spin axis	1 $kg.m^2$
The distance between vehicle c.g. and front axle	1.233 m
The distance between vehicle c.g. and rear axle	1.327 m
Front track width	1.57 m
Rear track width	1.57 m
Unsprung mass c.g. height	0.401 m

Wheel radius	0.326 *m*
Front left suspension stiffness	36500 *N/m*
Front right suspension stiffness	36500 *N/m*
Rear left suspension stiffness	36500 *N/m*
Rear right suspension stiffness	36500 *N/m*
Front left suspension damping	3493 *N.s/m*
Front right suspension damping	3493 *N.s/m*
Rear left suspension damping	3493 *N.s/m*
Rear right suspension damping	3493 *N.s/m*
Friction coefficient	0.9
Tire longitudinal stiffness	70000 *N*
Tire cornering stiffness	95000 *N/rad*
Rolling resistance coefficient	0.02
Tire vertical stiffness	310000 *N/m*
Tire vertical damping	3100 *N.s/m*

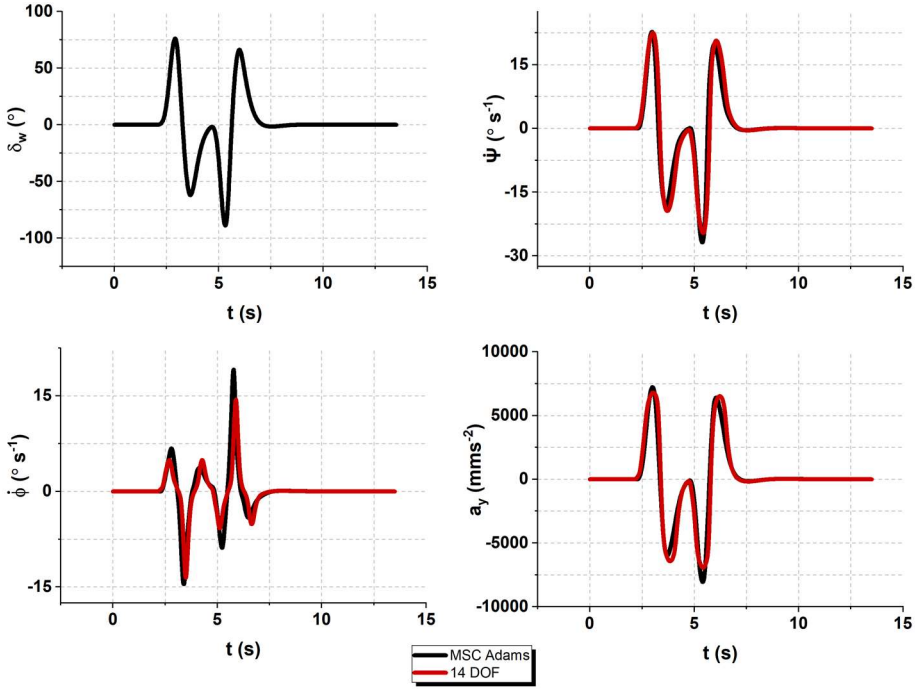

Figure 2.3. Double Lane Change Scenario Response

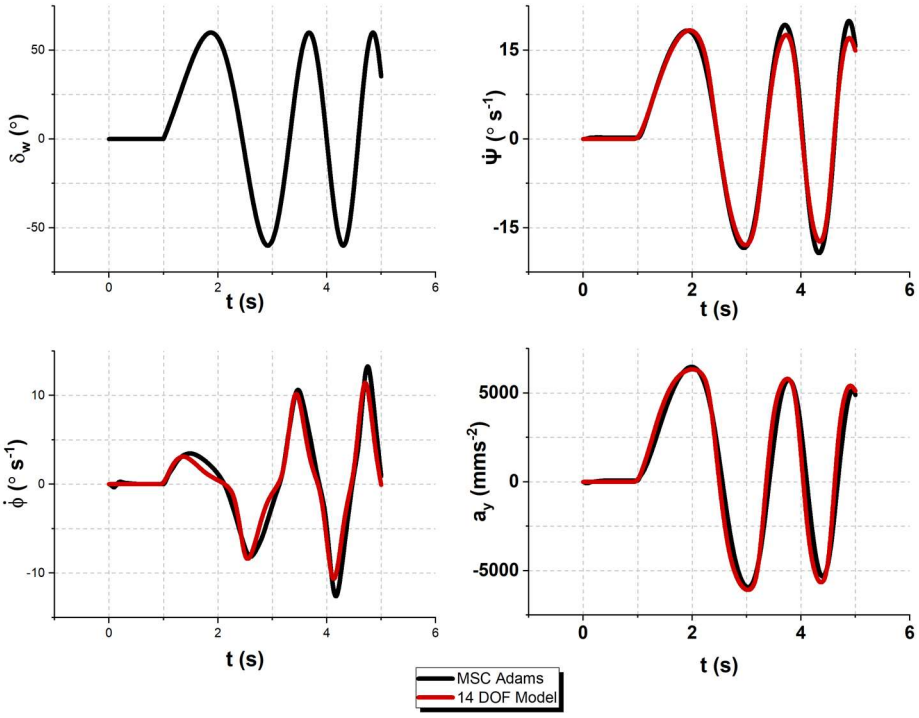

Figure 2.4. Swept-Sine Steering Scenario Response

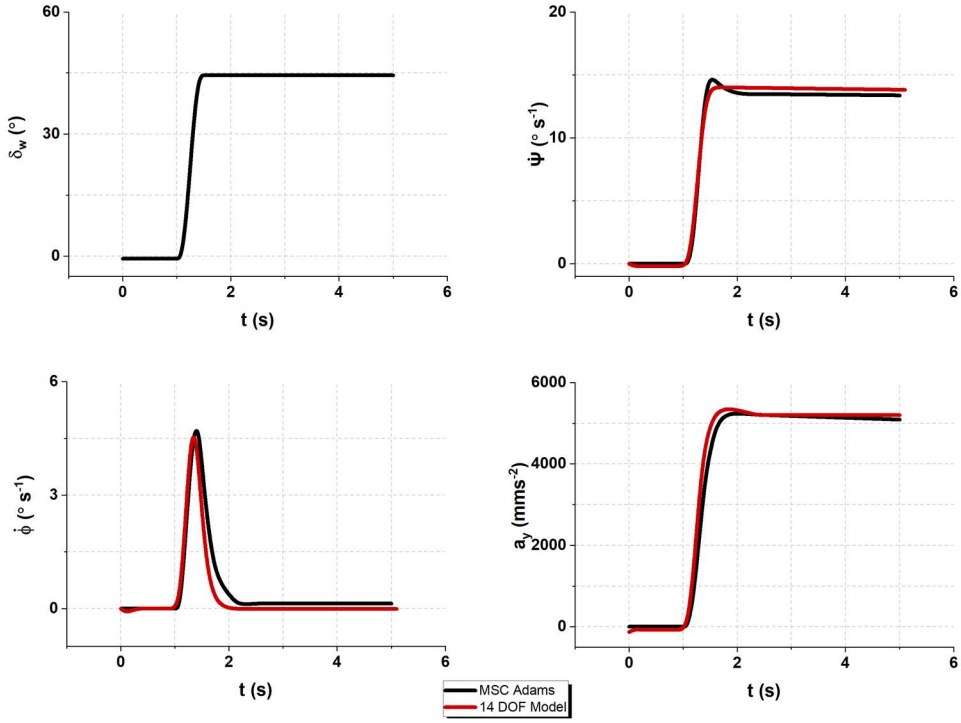

Figure 2.5. Step Steering Scenario Response

2.3 Tire Blowout Analysis

Modeling the tire forces in the normal operation of the vehicle is an intriguing and challenging topic of research. Analyzing this highly nonlinear vehicle component in a failure/post-failure environment is a very challenging part. A preliminary attempt to investigate the tire forces redistribution throughout the blowout was conducted by Blythe [37]. In his study, four well-instrumented maneuvers were carried out involving rear tire blowout in a steady-state regime. It was concluded that there are specific tire parameters that will change as a result of this rapid loss in inflation pressure. Moreover, finite element models with detailed tire components and material properties have been presented to improve the tire model accuracy for this complicated scenario [45, 54, 58, 59]. However,

these high-fidelity models have neither been combined with vehicle dynamic models nor been used to build a safety control system, because they lack the computational efficiency required in the context of multibody dynamics algorithms. Therefore, this study relies on the simplified tire forces reconstruction along with the well-grounded and Dugoff's tire models for the analysis and control of the inevitable consequences of the tire blowout phenomenon.

Assuming linear variation throughout the deflation time, calibrated multipliers for the tire stiffness and rolling resistance are used to model the blown tire as indicated in Figure 2.6 [37, 44]. The blowout out is initiated at T_{start} where the inflation pressure is at the nominal operating point, and it takes $\Delta T_{duration}$ seconds for the tire to be fully deflated. The rolling resistance coefficient is assumed to increase to 30 times its nominal value while the stiffnesses are assumed to reduce to 10 percent of their nominal values through linear interpolations.

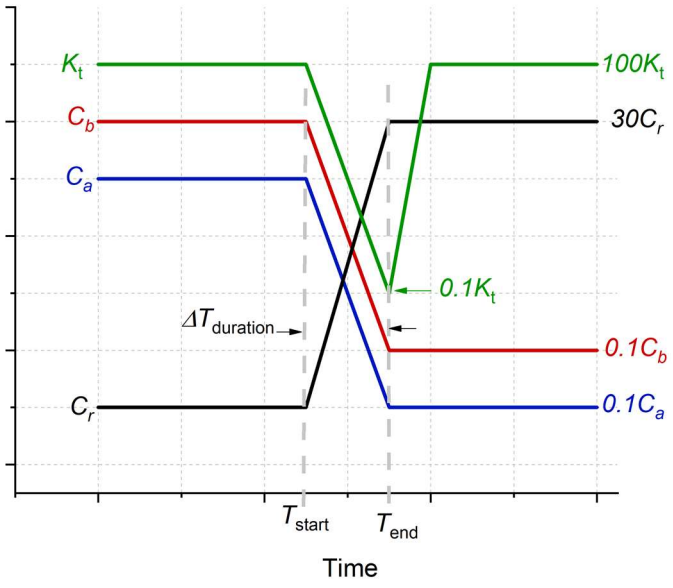

Figure 2.6. Tire Parameters Changes During Air Loss [37, 44]

To examine the effect of the tire blowout on the dynamic behavior of the vehicle, a series of tests incorporating tire blowout is conducted in both rectilinear and curvilinear maneuvers with different tire burst locations. Table 2.2 introduces the parameter chosen for the blowout simulations.

Table 2.2. Parameters Used in Tire Blowout Simulations

T_{start}	5^{th} second
$\Delta T_{duration}$	0.1 seconds
Simulation total time	10 seconds
Longitudinal stiffness multiplier*	0.1
Cornering stiffness multiplier*	0.1
Vertical stiffness multiplier	0.1
Rolling resistance multiplier*	30

** Tire blowout parameters multipliers are taken from the work done in [37]*

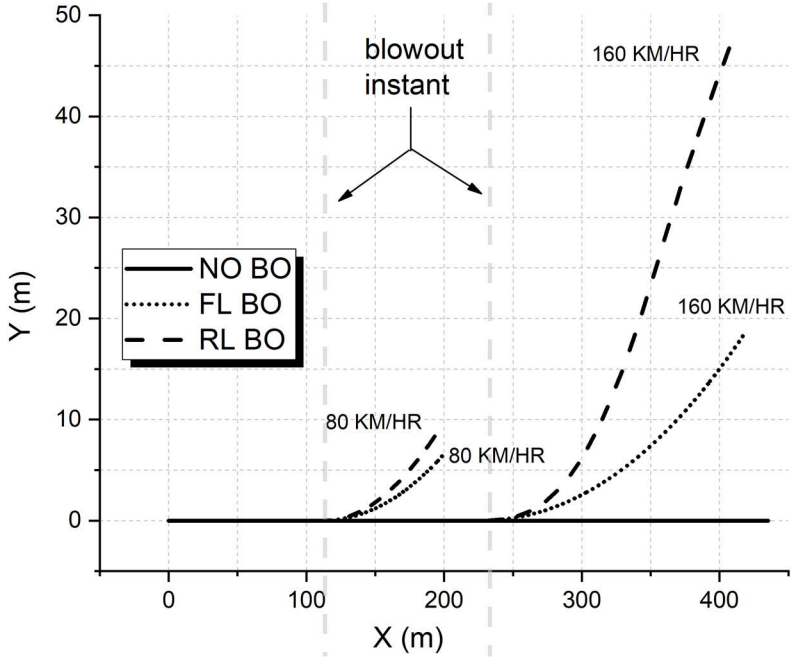

Figure 2.7. Vehicle Trajectory in Straight BO Scenario

2.3.1 Rectilinear Motion

The vehicle is moving at 80 km/hr speed, the blowout occurs at the fifth second and lasts for 0.1 seconds. The steering angle is kept at zero and the driver does not intervene with vehicle motion. The time history for the trajectories, translational and angular velocities of the body mass center, and tire forces are recorded and plotted in Figures 2.7 to 2.11.

The reduction of the longitudinal stiffness combined with the increase in the rolling resistance force reduces the total longitudinal force in the side of the blown tire, which in turn induces a yaw moment that pushes the vehicle towards the blown tire direction. This can be depicted in Figure 2.7 where it can also be noticed that the lateral deviation increases as the traveling speed increases. Therefore, tire blowout accident is more hazardous in highways where this deviation may lead to colliding other vehicles or the guardrail.

Figure 2.8-a highlights the translational speed of the vehicle body in longitudinal, lateral, and vertical directions. The increase in the rolling resistance magnifies the total vehicle motion damping and the vehicle traveling speed reduces as a result. Concurrently, the reorientation of the vehicle posture with respect to the road indicates that the motion of the vehicle is dominated by the yaw disturbance. Hence, it can be deduced that not only the vehicle deviates from its trajectory, but also it starts spinning as revealed in Figure 2.8-b. Insignificant motions are excited in the lateral, vertical, roll, and pitch directions right after tire blowouts. Afterward, these excitations gradually vanish while the time progresses after reaching their peaks. In fact, these out-of-plane excitations would

presumably increase in the presence of ground inputs. On the other hand, Figure 2.9 illustrates that the vertical motion experiences spikes because of the tire blowout before returning to their steady motion. Moreover, the spinning speed of the wheels is reduced because of the enlarged contact area between the tire and the road as well as the increased rolling resistance force.

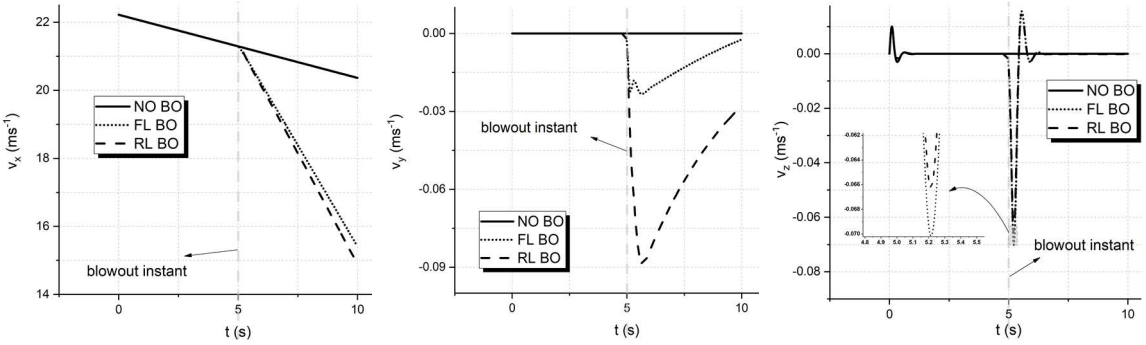

a- Translational velocities

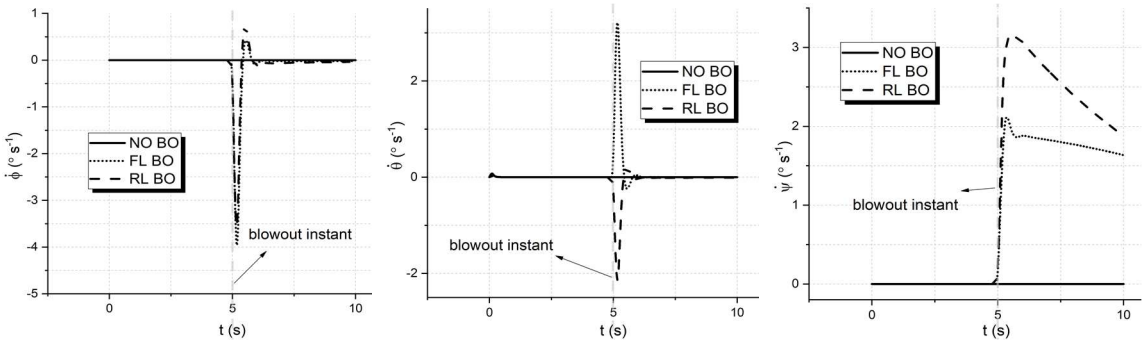

b- Rotational velocity

Figure 2.8. Vehicle Translational and Rotational Velocities in Straight Line BO

A)Translational B) Rotational

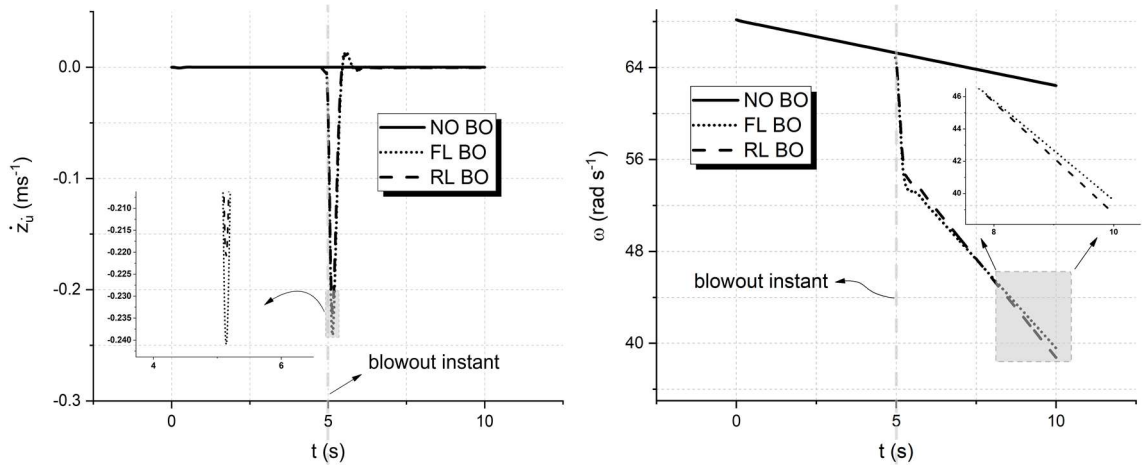

Figure 2.9. Wheel Vertical and Rotational Speeds in Straight Line BO

In addition, the change in tire mechanical properties resulting from blowout triggers the transfer and redistribution of tire forces. The nonuniformity of the rotational speed among the wheels following a tire blowout longitudinal and lateral tire forces stemmed from the generation of the longitudinal slips and slip angles, respectively. This is clear in Figure 2.10 where it can also be observed that the rolling resistance of the blown tire is dramatically changed and the vertical tire force is redistributed. The vertical forces reduce sharply for the blown tire and its diagonal opposite tire while increase for the other two tires following the blowout. The change in the total longitudinal force of the burst tire with respect to the other tires commences the yawing moment that leads to the distinctive vehicle blowout behavior of departing the lane.

Finally, to examine the effect of the blowout duration – the time it takes for the tire inflation pressure to reduce from its nominal operating point to zero-, the maximum

lateral offset is plotted against blowout duration in Figure 2.11. Obviously, the more gradual the inflation pressure reduction is the less the amount of vehicle lateral deviation.

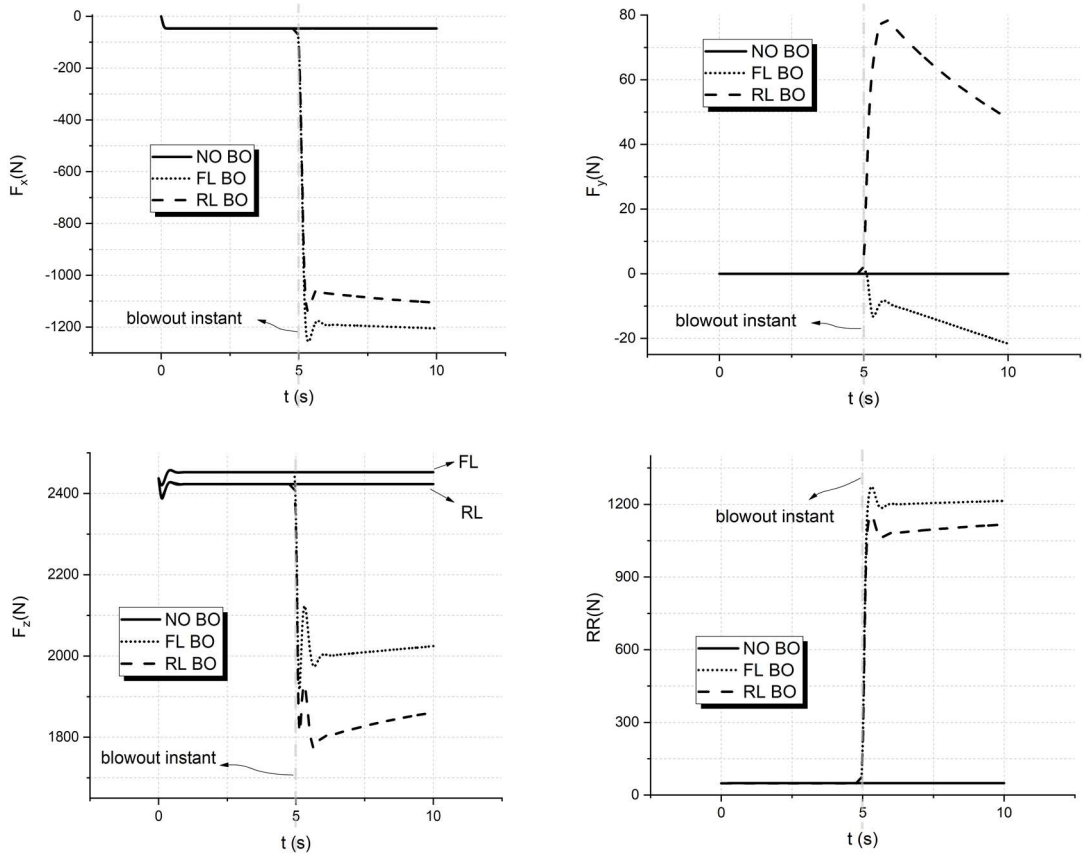

Figure 2.10. Tire Forces Redistribution in Straight Line BO

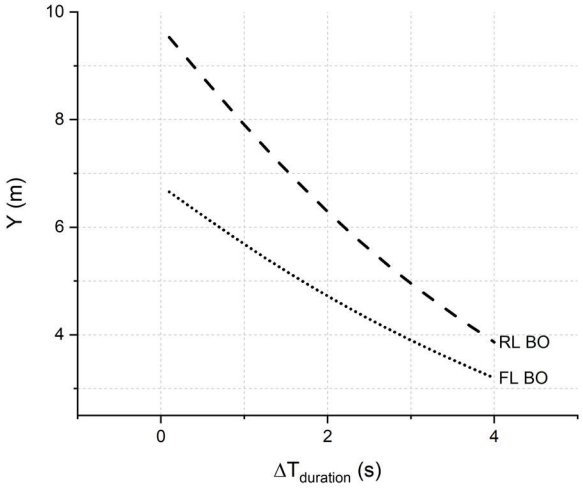

Figure 2.11. Effect of Blowout Duration on Vehicle Lateral Displacement

2.3.2 Curvilinear Motion

In this section, the vehicle is subjected to a tire blowout while turning left. Four driving maneuvers are performed for each individual tire blowout case. Firstly, the vehicle is accelerated to a speed of 80 km/hr and starts turning at the fourth second while cruising. Then, the blowout is triggered at the fifth second and lasts for 0.1 seconds. Due to the symmetry of the selected vehicle, the right turn results are simply the mirror of the left turn. As can be shown in Figure 2.12, excessive understeer and oversteer occur in a cornering maneuver for front and rear tire blowouts, respectively. This results from the rolling resistance-induced yaw moment as well as the reduction in cornering stiffness. Similar to the straight-line motion, this deviation becomes more severe as the speed increases. Larger deviations can be noticed in the case of front-outer and rear-inner tire blowout. When a rear tire is deflated, its cornering stiffness and thus its lateral tire force decreases. This reduction reduces the grip and allows the centrifugal forces to push the rear tire outwards and subsequently, the posture of the vehicle tends inwards of the curved trajectory.

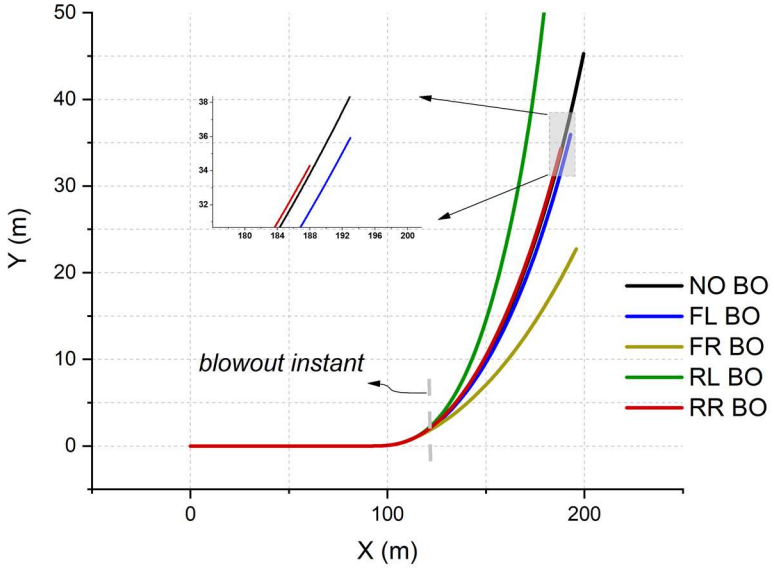

Figure 2.12. Vehicle Trajectory in a Cornering BO Scenario

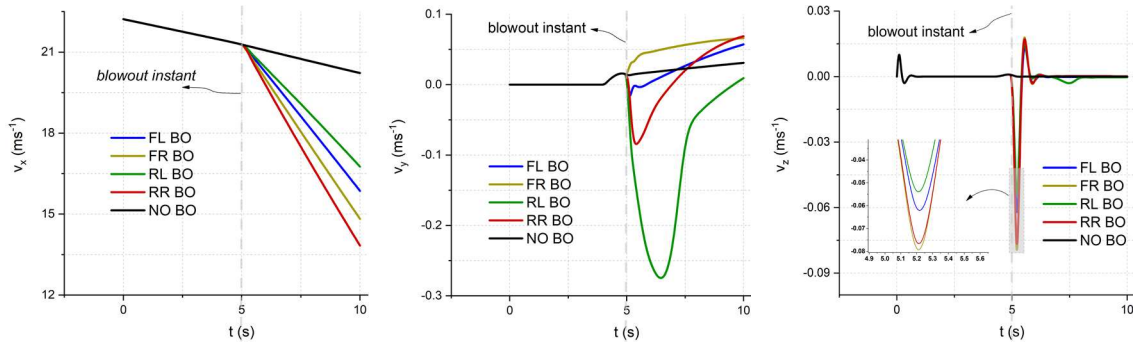

(a) Translational velocity

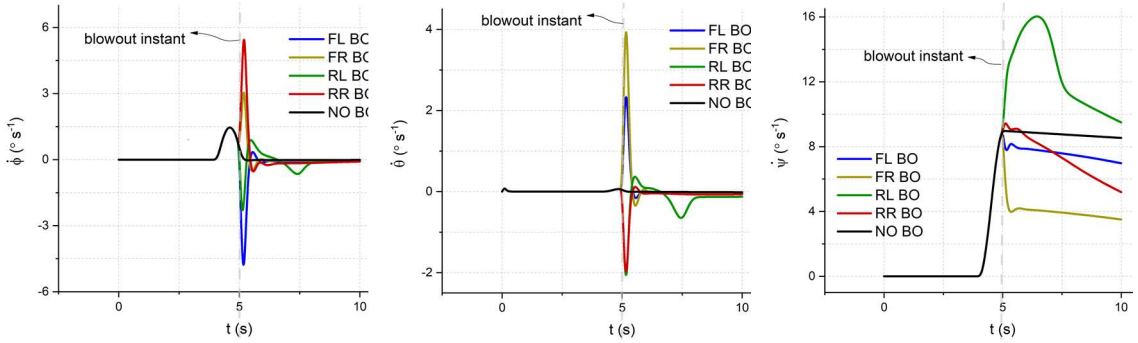

(b) Rotational velocity

Figure 2.13. Vehicle Translational and Rotational Velocities in Cornering BO

A)Translational B) Rotational

Figure 2.13-a shows the translational speed of the vehicle body in longitudinal, lateral, and vertical directions. The rapid increase in the rolling resistance force acts as a braking torque that decreases the longitudinal speed of the vehicle. The vehicle lateral velocity is also disturbed by the blowout in a more significant manner compared with the straight-line motion, especially for the rear-inner tire blowout case. Similarly, with reference to the straight-line tire blowout case, the vehicle shows more noticeable excitations in the roll, pitch, and bounce motions. Simultaneously, a remarkable change in the vehicle yaw rate is observed in Figure 2.13-b. This abrupt nonuniform yawing motion combined with

the lateral deviations make stabilizing the vehicle quite challenging for the driver. Similar to the straight line case, Figure 2.14 demonstrates how the wheel's vertical motion shows some excitations stemmed by the tire blowout before returning to their steady motion as well as how the spinning speed of the wheels reduces.

Furthermore, the tire forces undergo dramatic redistribution right after tire burst as shown in Figure 2.15. These substantial changes in the tire loads are expected to inspire severe damage to the tire structure, and this justifies why the dynamic behavior of the vehicle is tremendously affected in the curvilinear motion scenario.

The modeling setup used in this research bears a close qualitative resemblance to the experiments conducted in [37, 44, 48].

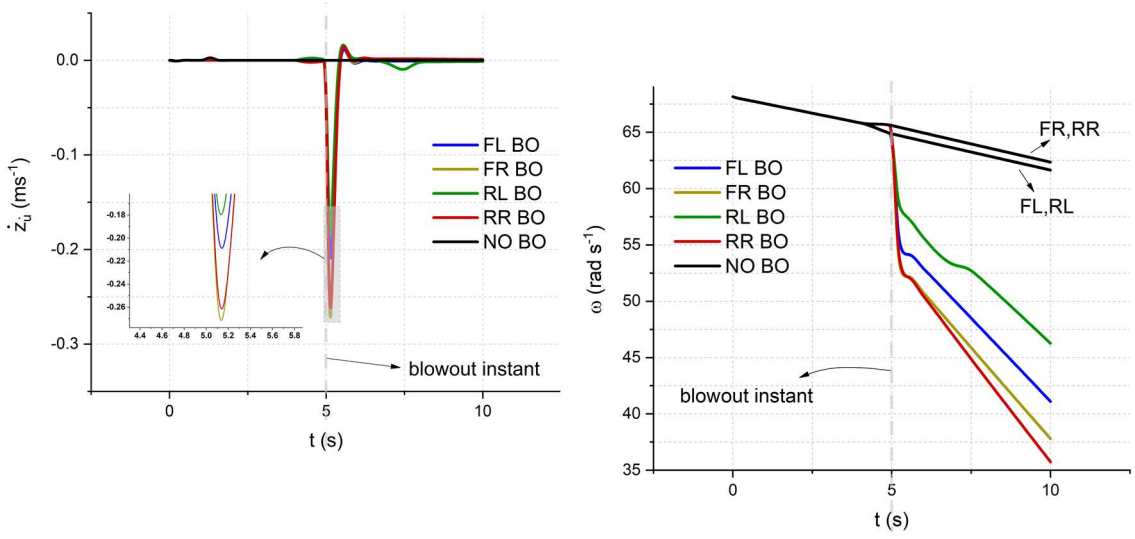

Figure 2.14. Wheel Vertical and Rotational Speeds in Cornering BO

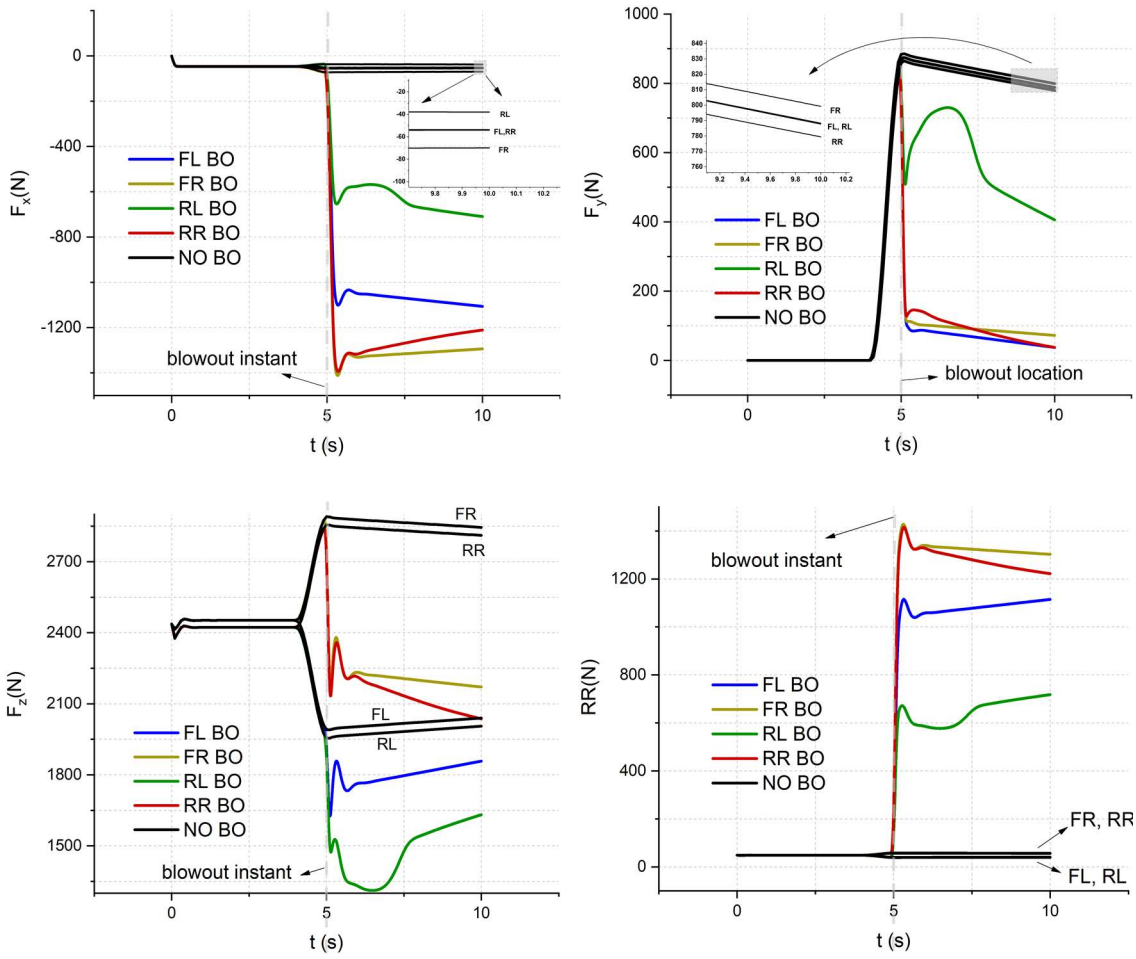

Figure 2.15. Tire Forces Redistribution in Cornering BO

The analysis carried out in this study so far implies that the handling dynamics of the vehicle subjected to a tire blowout are tremendously affected. The results are only valid in the absence of any interventions from the driver. It can be clearly revealed that the motion of the vehicle is significantly dominated by the yaw disturbance. The vehicle with such severe transients cannot be easily stabilized by the driver following a tire blowout. Consequently, designing an automatic control system against this safety threat is essential.

Although the vehicle may experience a rollover caused by the tire blowout as reported in [49, 74], the vast majority of the studies in the literature have only focused on the effect of the tire blowout on the handling dynamics of the vehicle. Even in [37], the pivotal study that the other authors have relied on to replicate the effect of the tire blowout, the test vehicle was fitted with outriggers to prevent the rollover accident during the experiment. Therefore, the remaining work sheds new light on the roll dynamics of the vehicle exposed to a tire blowout.

The vehicle numerical data introduced in Table 2.1 represent a sedan vehicle. The dynamical analysis conducted for this vehicle did not detect any rollover as a result of a tire blowout. On the other hand, sport utility vehicles (SUVs) are known to have more tendency to rollover accidents compared with sedans due to their higher center of gravity [110]. Therefore, to investigate the effect of the blowout on the roll dynamics of SUVs, the height of the vehicle was increased to 65 cm – a typical SUV c.g. height-. The analyses were repeated for the new vehicle. The study is limited to the region where the vehicle is inherently stable in the roll direction. Specifically, the study is limited to the rollover driven by the blowout. Although being very conservative, the simplified rollover threshold is utilized to detect the rollover. As reported in [110], the SUVs will rollover if the lateral acceleration exceeds around 0.75g.

During the straight-line motion of the vehicle, no rollover was detected as a result of the tire blowout because the lateral accelerations induced by the tire blowout are insufficient to trigger a vehicle rollover. On the other hand, as the lateral acceleration builds-up during

a left turn, the roll dynamic behavior of the vehicle is enormously affected by the tire blowout. It is well-known that the higher the total lateral tire forces the more susceptible the vehicle to rollover, while the higher the difference between the outer and inner vertical tire forces the more stable the vehicle in the roll direction. Figure 2.16 shows the lateral tire forces for different tire blowout events compared with the no blowout case. Clearly, the lateral tire forces increase dramatically in the case of a rear right tire blowout. Furthermore, in the case of a rear outer tire blowout, the lateral and vertical tire forces of the front left as well as rear left approaches zero at around the sixth seconds. Having zero tire forces in the inner tires during cornering implies that these tires leave the ground and the vehicle tipped up on two wheels. Subsequently, the vehicle experiences an outward rollover. These results are consistent with the results of the lateral acceleration shown in Figure 2.17 where the rear right tire blowout generates the highest lateral acceleration. This increase in the total lateral tire forces increases the lateral acceleration until the rollover threshold is exceeded. On the other hand, Figure 2.18 illustrates the time history for the vertical tire forces with and without tire blowout for different tire blowout scenarios. In all cases except the front right tire blowout, following the tire blowout instant, the outer vertical tire forces increase while the forces in the inner wheels decrease. This vertical force redistribution has a roll stabilizing effect. Conversely, the decrease in the difference between the outer and the inner vertical forces in the case of front right tire blowout has a roll destabilizing effect. However, when combined with the reduction in the lateral force, the vehicle does not experience rollover in the front right tire blowout case. This can be also found in Figure 2.17 where the lateral acceleration in the front right tire blowout case decreases. Figure 2.19 demonstrates the roll angle response of the vehicle to different tire

blowout events. Again, it can be observed that the case of rear right tire blowout produces high roll angles. To sum up, the vehicle may suffer from rollover only in the case of a rear outer tire blowout.

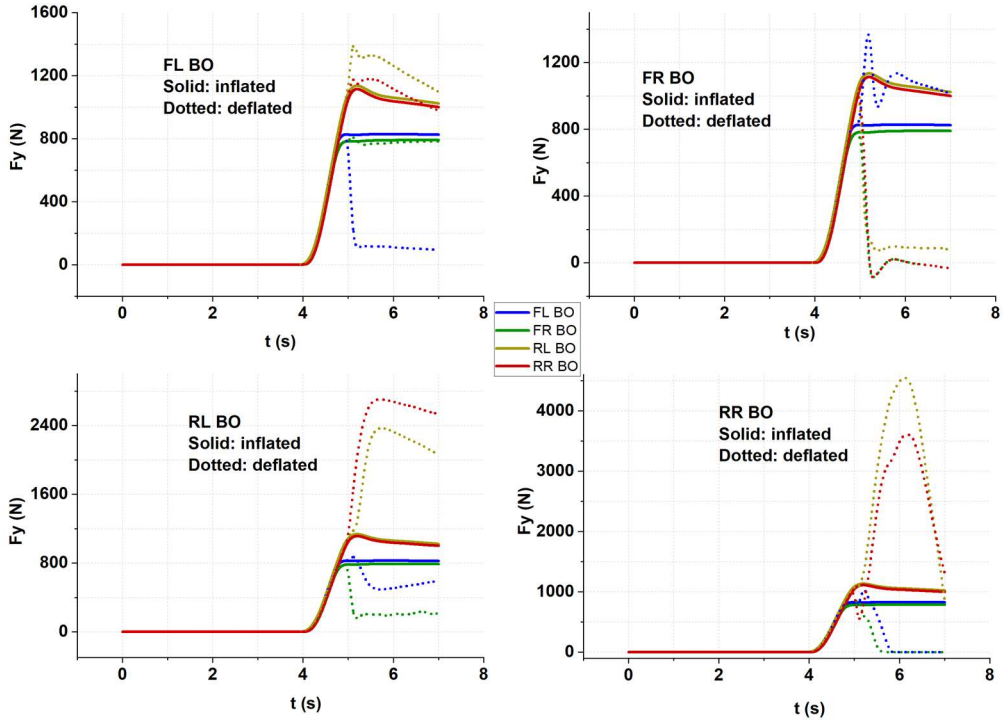

Figure 2.16. Tire Lateral Forces for Different Tire Blowout Scenarios

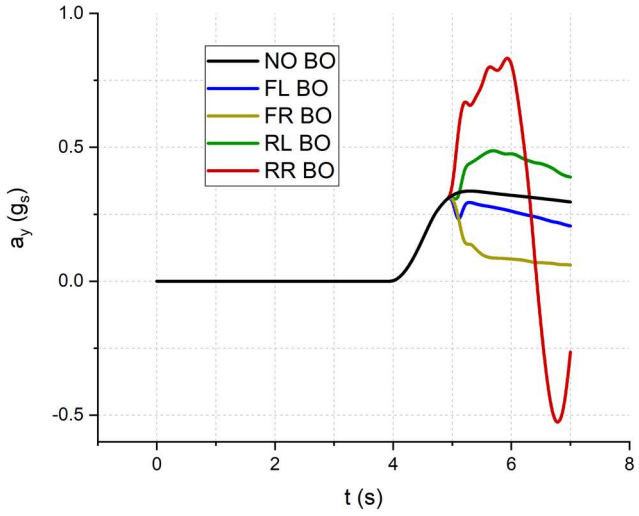

Figure 2.17. Lateral Acceleration With/Without a Blowout

The results that have been introduced so far are for a vehicle without an anti-roll bar. To examine the effect of the antiroll bar in the roll dynamics of the vehicle subjected to a tire blowout, the simulation studies were repeated considering a vehicle with an antiroll bar of a stiffness of 2500 N/m. Moreover, another factor that mitigates the vehicle's tendency to rollover is the road cross-slope angle. The simulation was also repeated for a 10% banked road for the vehicle suffering from a rear right tire blowout. Figures 2.20 and 2.21 illustrate the effect of the antiroll bar as well as the transverse slope angle on the vehicle lateral acceleration and roll angle, respectively. It can be concluded that for a passive system subjected to a rear outer tire blowout, the existence of an antiroll bar or a cross-slope angle moderates the lateral acceleration and makes the vehicle less vulnerable to rollover following a tire blowout.

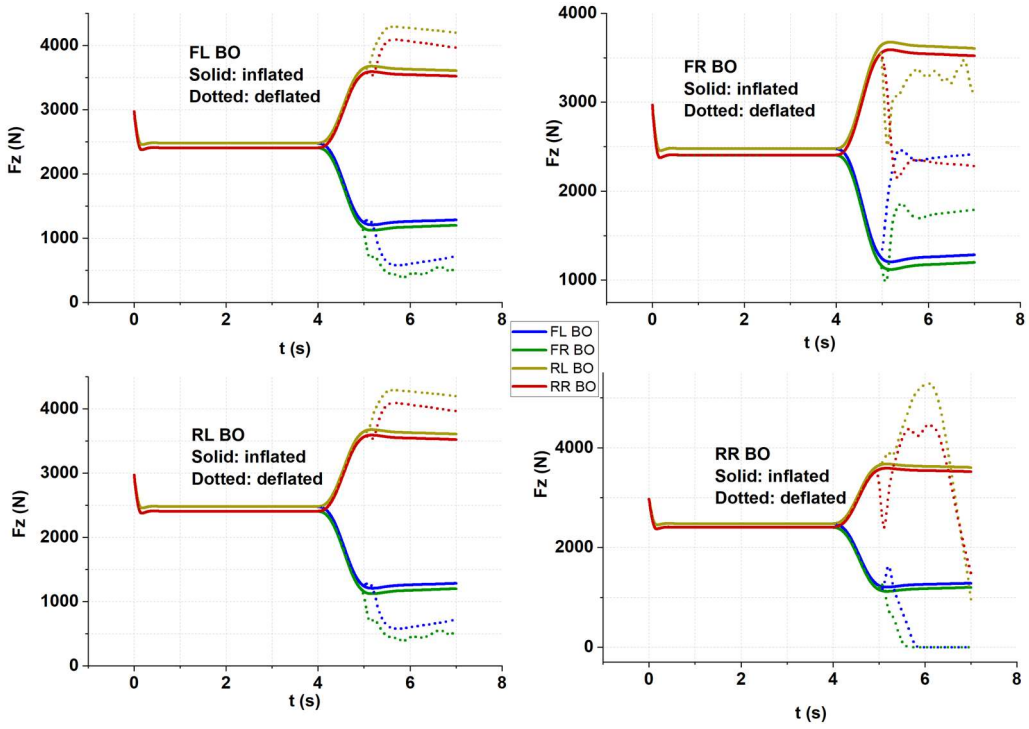

Figure 2.18. Tire Vertical Forces for Different Tire Blowout Scenarios

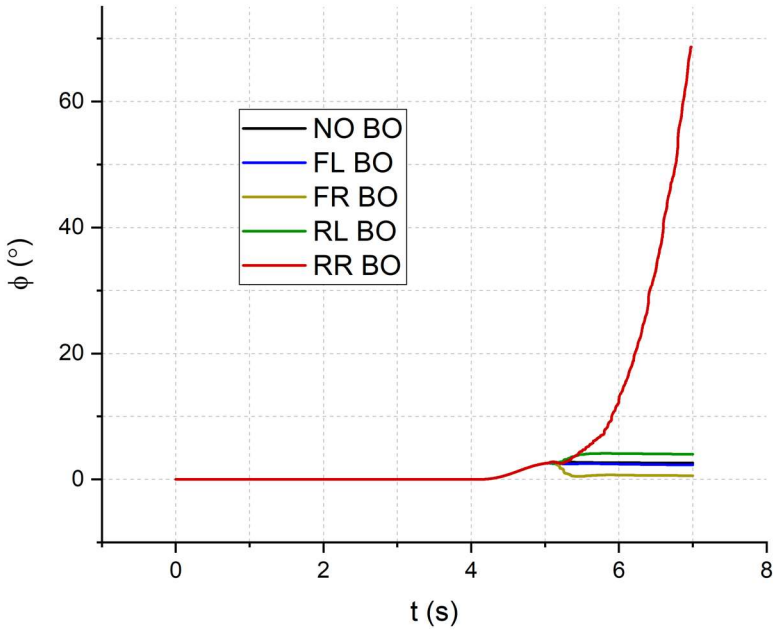

Figure 2.19. Roll Angle for Different Tire Blowout Cases

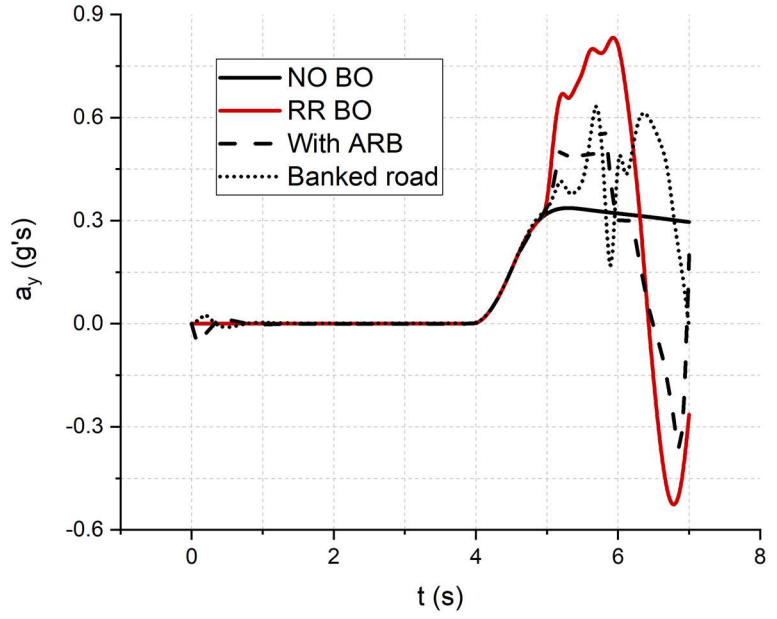

Figure 2.20. Effect of the ARB and the Transverse Slope

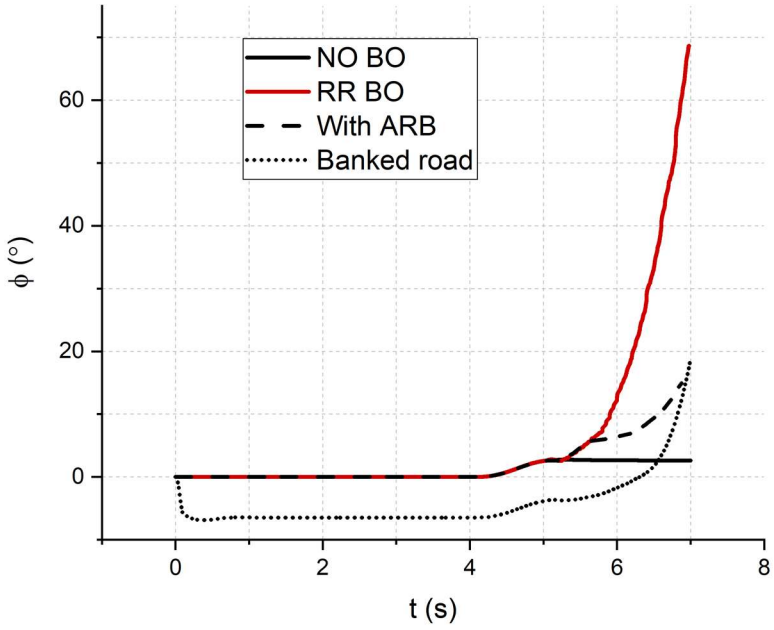

Figure 2.21. Roll Angle Response With the ARB Installed

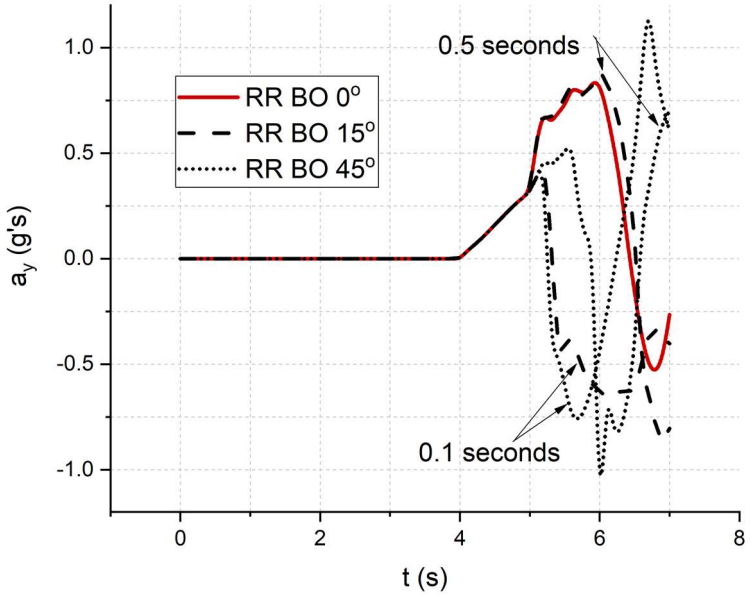

Figure 2.22. Lateral Acceleration Response for Different Steering Reactions

Another rudimentary factor that can contribute to the vehicle's propensity to rollover is the driver's reaction to the tire blowout. The driver will typically react to the tire blowout by either steering, braking, or a combination of both. To examine the effect of possible

driver reactions from the driver on the roll attitude of the vehicle, the simulations were repeated with the driver in the loop.

Firstly, steering-only driver inputs are considered. The steering reaction input has a magnitude and a reaction delay time. As demonstrated in Figures 2.22 and 2.23 where 0.1 and 0.5 seconds reaction times, as well as 15° and 45° steering inputs are considered, small steering angles in the opposite direction with short delay time can resist the rollover. On the other hand, if large steering angles are commanded to the vehicle, the potential to the rollover inward of the curve is increased. Moreover, even for small steering angles, if the delay time is relatively large (in the simulation, the maximum reaction time below which the vehicle can be stabilized for the small steering angle is 0.4 seconds after the blowout instant), the vehicle will rollover outward. The steering in the opposite direction was chosen because the driver will likely do that to avoid spinning out from the curve.

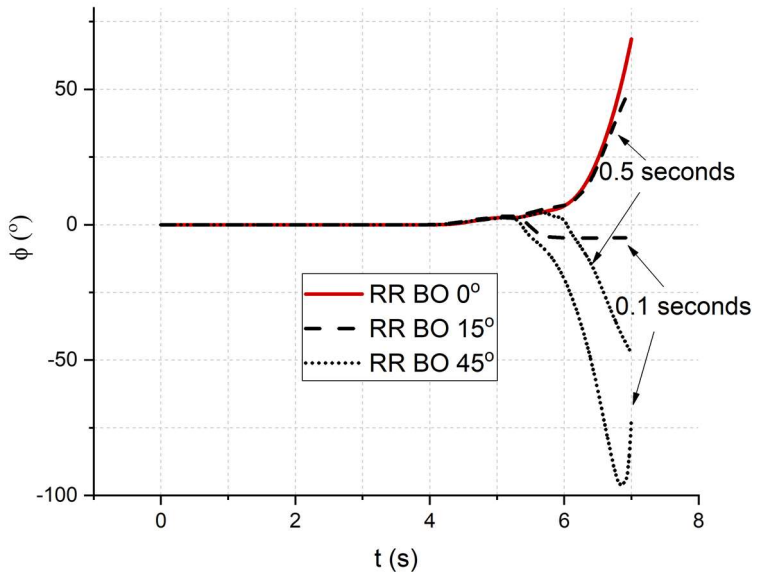

Figure 2.23. Roll Angle Response for Different Steering Reactions

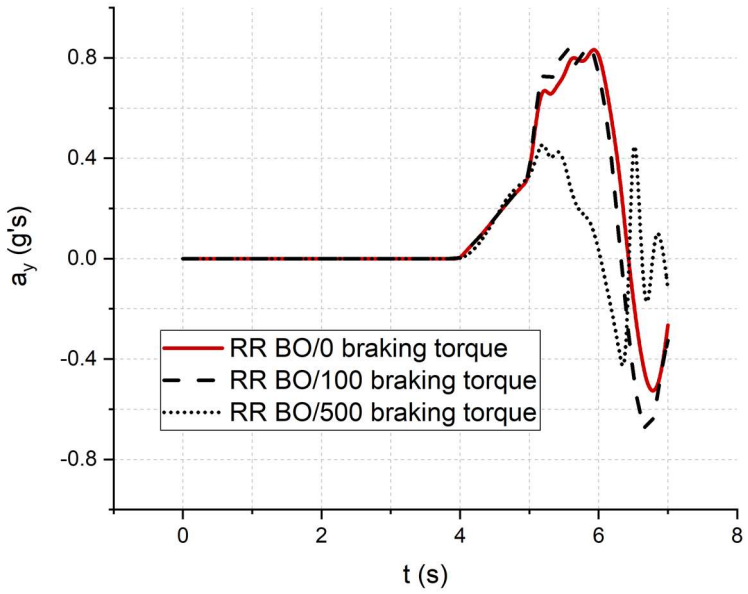

Figure 2.24. Lateral Acceleration Response for Different Braking Reactions

Then, the braking effect was studied. Again, the braking input has a magnitude and a reaction time. The system was tested for braking only inputs from the driver following the blowout. In the absence of any steering inputs from the driver, the braking diminishes the vehicle's tendency to rollover if the response time was relatively short and the amount of braking is large. Otherwise, the vehicle will rollover outward. In the simulation, the critical reaction time after which the vehicle cannot be stabilized by braking-only is 1.1 seconds after the blowout instant. Figures 2.24 and 25 show the lateral acceleration and the roll angle response for 0.1 seconds delay time. It can be observed that the application of a 100 N.m braking torque is not sufficient to stabilize the vehicle while 500 N.m torque is adequate. Then the braking input was combined with the steering input. It was found that the application of the braking besides the steering improves the roll stability of the vehicle compared with the steering-alone reaction by increasing the span of the possible reaction time of the steering. For instance, applying 500 N.m with delays of 0.1

or 0.5 combined with any combination of a steering reaction of 15° and 45° delayed by 0.1 and 0.5 seconds is appropriate to guarantee roll stability. On the other hand, the 100 N.m is insufficient to avoid the rollover unless small steering input is applied quickly. Table 2.3 summarizes the results of the simulation for all the possible combinations. Because of the broad disparity in driver possible reactions, this judicious interplay between the braking and steering following a tire blowout cannot be easily accomplished by an average driver. Finally, not surprisingly, the application of either a tractive torque or a steering angle in the direction of the blown tire can precipitate the rollover of the vehicle.

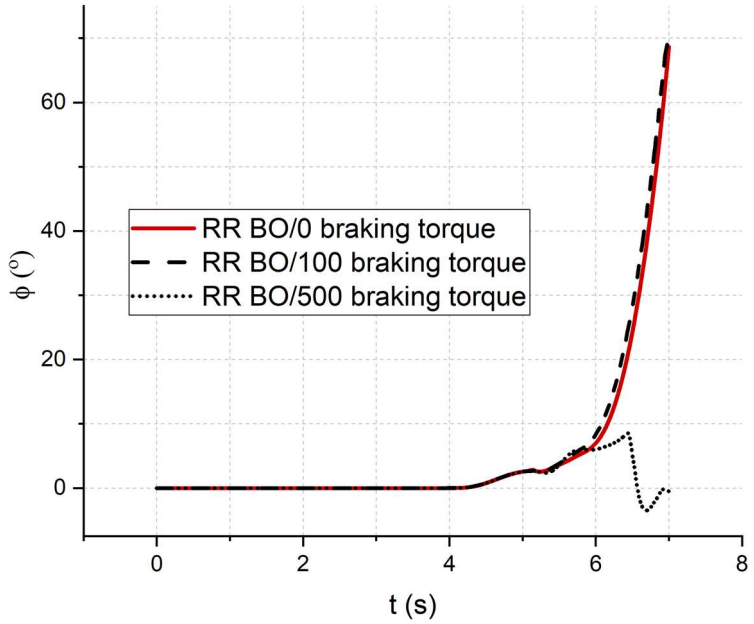

Figure 2.25. Roll Angle Response for Different Braking Reactions

The analysis carried out in this chapter implies that the dynamics of the vehicle subjected to a tire blowout are tremendously affected. It can be clearly revealed that the motion of the vehicle is significantly dominated by the yaw disturbance. The vehicle with such severe

transients cannot be easily stabilized by the driver following a tire blowout. Consequently, designing an automatic control system against this safety threat is essential.

Table 2.3. Rollover Test For Different Combinations of Reaction Times and Magnitudes of Steering and Braking

Steering angle magnitude (deg)	Steering input delay (s)	Braking torque magnitude (N.m)	Braking torque delay (s)	Rollover?
45	0.1	500	0.1	No
45	0.5	500	0.1	No
15	0.1	500	0.1	No
15	0.5	500	0.1	No
45	0.1	100	0.1	Yes
45	0.5	100	0.1	Yes
15	0.1	100	0.1	No
15	0.5	100	0.1	Yes
45	0.1	500	0.5	No
45	0.5	500	0.5	No
15	0.1	500	0.5	No
15	0.5	500	0.5	No
45	0.1	100	0.5	Yes
45	0.5	100	0.5	Yes
15	0.1	100	0.5	No
15	0.5	100	0.5	Yes

CHAPTER 3

TIRE BLOWOUT SAFETY CONTROL SYSTEM DESIGN

It has been unambiguously shown that the directional stability of the vehicle experiencing a tire blowout is tremendously affected and cannot be easily controlled by the average driver. Furthermore, improper driver steering or braking/accelerating reactions are even more threatening. In this section, an active automatic safety control system is designed and evaluated. The objective of the proposed control system is to maintain the vehicle's desired steady-state trajectory in the presence of disturbances from the tire blowout. Given the vehicle speed and the steering wheel input from the driver, the controller calculates the desired yaw rate and sideslip angle.

The first step of designing the controller is to build a control-oriented model accurate enough to reflect major system dynamic characteristics. Since the most dominant intrinsic instability occurs in the yaw motion, a seven degrees of freedom handling control-oriented model is considered in this study to design the controller and evaluate the closed-loop system. Before diving into the detailed control design derivation, the sliding model nonlinear control design technique is introduced.

3.1 Sliding Mode Control

Sliding model control is a well-known nonlinear variable structure robust control design tool. Designing a control system in the presence of uncertainties is a very important problem in the practical controller design. These uncertainties are the mismatches

between the actual physical system and its mathematical representation arise from external disturbances and approximated model dynamics. Besides its robustness, SMC has the advantages of its finite-time convergence, ability to tackle linear and nonlinear systems, and its reduced order custom compensated dynamics.

In Figure 3.1, the sliding manifold is defined by $s(t)=0$. Following the finite time taken for the system to reach the sliding phase, the system commences sliding along the defined sliding manifold and stays on it thereafter towards the origin [92, 93].

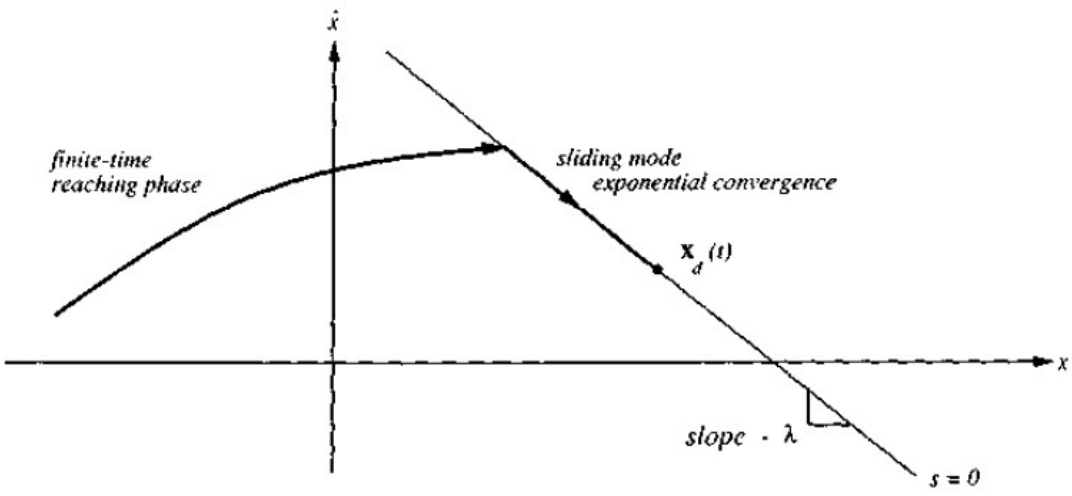

Figure 3.1. A Typical Phase Portrait Plot Under SMC [93]

The main pitfall of the SMC is the phenomenon known as chattering. In the vicinity of the sliding surface, the feedback control produces high (but finite) amplitude and frequency switching behavior as indicated in Figure 3.2. This behavior is problematic in

many practical control systems and many techniques have been developed to attenuate this drawback.

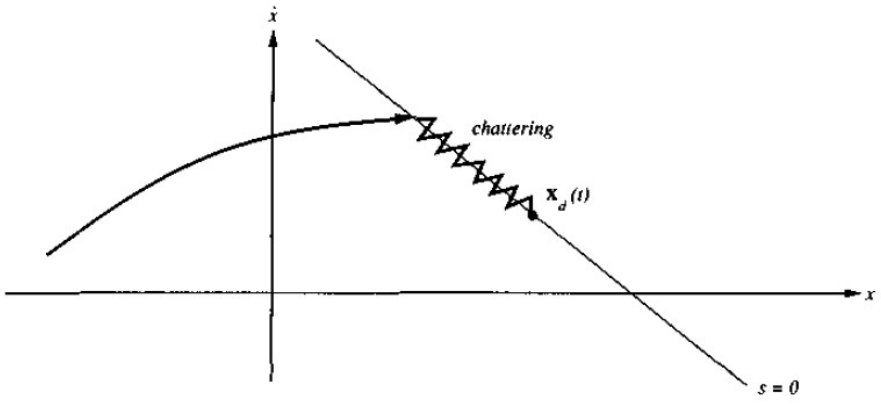

Figure 3.2. Chattering Problem [93]

3.2 Vehicle Nonlinear Control Design

In this section, a moving vehicle subjected to a tire blowout is considered (Figure 3.3). The vehicle dynamic model has seven degrees of freedom: the position of the center of gravity in the longitudinal (x) and lateral directions (y), the yaw rotation, and the rotational degree of freedom corresponding to each of the four wheels about their spin axis. Dugoff's tire model is used to express the tire forces resulting from the interaction between the tire and the road. The governing equations of motion are derived according to the following assumptions: 1) the aerodynamic forces are ignored, 2) the vertical, roll, and pitch motions are neglected, and 3) the bank and inclination angles, as well as the suspension kinematics, are not considered.

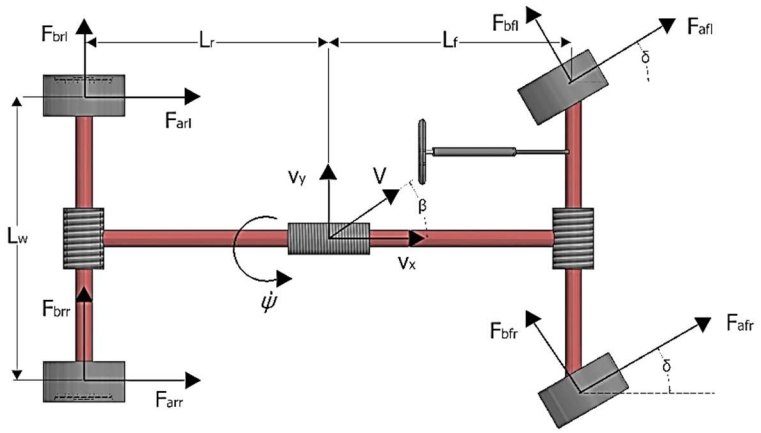

Figure 3.3. Seven DOF Handling Model

Applying the conservation of linear and angular momentums gives the following equations of motion for the vehicle

$$m\dot{v}_x = mv_y\dot{\psi} + F_{xfl} + F_{xfr} + F_{xrl} + F_{xrr} \tag{3.1}$$

$$m\dot{v}_y = -mv_x\dot{\psi} + F_{yfl} + F_{yfr} + F_{yrl} + F_{yrr} \tag{3.2}$$

$$I_z\ddot{\psi} = \frac{L_w}{2}\left(F_{xfr} - F_{xfl}\right) + \frac{L_w}{2}\left(F_{xrr} - F_{xrl}\right) + L_f\left(F_{yfl} + F_{yfr}\right) - L_r\left(F_{yrl} + F_{yrr}\right) \tag{3.3}$$

$$J_w\dot{\omega}_{ij} = T_{dij} - T_{bij} - F_{aij}R_w - F_{rij}R_w \tag{3.4}$$

Here: m is the vehicle mass, I_z is the vehicle mass moment of inertial about the z-axis, J_w is the wheel mass moment of inertia about the spinning axis, R is the wheel radius, F_{xij} and F_{yij} are the tire forces observed from the vehicle body-fixed frame, T_{dij} and T_{bij} correspond to the applied driving and braking torques, respectively. $v_{x,}v_y$, and $\dot{\psi}$ are the longitudinal, lateral, and rotational speeds of the vehicle center of mass respectively. i refers to front or rear, and j refers to left or right. Vehicle sideslip angle β is defined as the angle between the vehicle velocity vector and its longitudinal axis and it equals

$tan^{-1}(v_y/v_x)$. The following transformation can be performed between the wheel frame to the vehicle body-fixed frame

$$F_{xij} = F_{Aij}cos\delta - F_{Bij}sin\delta \tag{3.5}$$

$$F_{yij} = F_{Aij}sin\delta + F_{Bij}cos\delta \tag{3.6}$$

F_{rij} is the tire rolling resistance force. Assuming C_{rij} is the coefficient of rolling resistance, they can be calculated as

$$F_{rij} = C_{rij}F_{zij} \tag{3.7}$$

Equations (2.28) and (2.29) were used to determine the tire forces as in the previous chapter and repeated here for convenience:

$$F_{Aij} = \frac{C_a\sigma_{ij}}{(1-\sigma_{ij})}f(\lambda_{ij}) \tag{3.8}$$

$$F_{Bij} = \frac{C_b tan\alpha_{ij}}{(1-\sigma_{ij})}f(\lambda_{ij}) \tag{3.9}$$

Where C_a and C_b represent the longitudinal and cornering stiffnesses and $f(\lambda_{ij})$ is given by

$$f(\lambda_{ij}) = \begin{cases} (2-\lambda_{ij})\lambda_{ij} & if\ \lambda_{ij} < 1 \\ 1 & if\ \lambda_{ij} \geq 1 \end{cases} \tag{3.10}$$

provided the dummy variable λ_{ij} is determined by the following relation

$$\lambda_{ij} = \frac{\mu F_{zij}(1-\sigma_{ij})}{2\left\{(C_a\sigma_{ij})^2 + (C_b tan\alpha_{ij})^2\right\}^{\frac{1}{2}}} \tag{3.11}$$

Given ω_{ij} is the wheel rotational speed, the longitudinal slip takes the form

$$\sigma_{ij} = \begin{cases} \dfrac{R\omega_{ij} - v_{aij}}{v_{aij}} & during\ braking \\ \dfrac{R\omega_{ij} - v_{aij}}{R\omega_{ij}} & during\ acceleration \end{cases} \tag{3.12}$$

The longitudinal and lateral velocities at the center of the contact patch of each tire are related to the velocities of the vehicle center of mass as

$$v_{afl} = \left(v_x - \frac{\dot{\psi}L_w}{2}\right)cos\delta + \left(v_y + \dot{\psi}L_f\right)sin\delta \tag{3.13}$$

$$v_{afr} = \left(v_x + \frac{\dot{\psi}L_w}{2}\right)cos\delta + \left(v_y + \dot{\psi}L_f\right)sin\delta \tag{3.14}$$

$$v_{arl} = v_x - \frac{\dot{\psi}L_w}{2} \tag{3.15}$$

$$v_{arr} = v_x + \frac{\dot{\psi}L_w}{2} \tag{3.16}$$

$$v_{bfl} = -\left(v_x - \frac{\dot{\psi}L_w}{2}\right)sin\delta + \left(v_y + \dot{\psi}L_f\right)cos\delta \tag{3.17}$$

$$v_{bfr} = -\left(v_x + \frac{\dot{\psi}L_w}{2}\right)sin\delta + \left(v_y + \dot{\psi}L_f\right)cos\delta \tag{3.18}$$

$$v_{brl} = v_y - \dot{\psi}L_r \tag{3.19}$$

$$v_{brr} = v_y - \dot{\psi}L_r \tag{3.20}$$

The slip angles for a front-wheel driving vehicle are expressed by

$$\alpha_{fl} = \delta_{ij} - tan^{-1}\left\{\frac{v_y + \dot{\psi}L_f}{v_x - \dot{\psi}\left(\frac{L_w}{2}\right)}\right\} \tag{3.21}$$

$$\alpha_{fr} = \delta_{ij} - tan^{-1}\left\{\frac{v_y + \dot{\psi}L_f}{v_x + \dot{\psi}\left(\frac{L_w}{2}\right)}\right\} \tag{3.22}$$

$$\alpha_{rl} = -tan^{-1}\left\{\frac{v_y - \dot{\psi}L_r}{v_x - \dot{\psi}\left(\frac{L_w}{2}\right)}\right\} \tag{3.23}$$

$$\alpha_{rr} = -tan^{-1}\left\{\frac{v_y - \dot{\psi}L_r}{v_x + \dot{\psi}\left(\frac{L_w}{2}\right)}\right\} \tag{3.24}$$

To account for the longitudinal and lateral load transfer, the following equations are used:

$$F_{zfl} = \frac{mgL_r}{2(L_f + L_r)} - \frac{m(\dot{v}_x - v_y\dot{\psi})h}{2(L_f + L_r)} - \frac{m(\dot{v}_y + v_x\dot{\psi})h}{2L_w} \tag{3.25}$$

$$F_{zfr} = \frac{mgL_r}{2(L_f + L_r)} - \frac{m(\dot{v}_x - v_y\dot{\psi})h}{2(L_f + L_r)} + \frac{m(\dot{v}_y + v_x\dot{\psi})h}{2L_w} \tag{3.26}$$

$$F_{zrl} = \frac{mgL_f}{2(L_f + L_r)} + \frac{m(\dot{v}_x - v_y\dot{\psi})h}{2(L_f + L_r)} - \frac{m(\dot{v}_y + v_x\dot{\psi})h}{2L_w} \tag{3.27}$$

$$F_{zrl} = \frac{mgL_f}{2(L_f + L_r)} + \frac{m(\dot{v}_x - v_y\dot{\psi})h}{2(L_f + L_r)} + \frac{m(\dot{v}_y + v_x\dot{\psi})h}{2L_w} \tag{3.28}$$

In order to verify the validity of the proposed nonlinear seven degrees of freedom handling model, the derivations are compared with the publications studying the handling motion of the vehicle, like in [3, 112]. Next, the response of the vehicle is compared with the results from the high-fidelity multibody dynamic package MSC Adams. According to

the study conducted by [95], the double lane change maneuver as defined according to ISO-3888/1 is suitable to assess the handling behavior of the vehicle.
Figure 3.4 shows the steering input used to excite both models together with the comparison between their responses. It is apparent that the proposed control-oriented vehicle model can adequately replicate the handling dynamic behavior of the vehicle.

The desired states represent the steady-state vehicle cornering motion. During a steady-state motion, the vehicle has zero angular acceleration and sideslip angle rate. The expressions for the desired yaw rate and sideslip angle are derived from the bicycle model dynamics by setting the angular acceleration and the sideslip angle rate to zero (see [3], [98], and [112], for example). These desired states expressions are widely used in the development of the general vehicle handling control systems design to stabilize the vehicle against understeering and oversteering, which are also induced by the tire blowout during vehicle cornering.

The calculations of the target bounded yaw rate and slip angle are according to the steady-state curvilinear motion of the single-track model presented in [3]. However, in this study the equations are modified to account for different tire blowout locations as

$$\dot{\psi}_{target} = \begin{cases} \dot{\psi}_{des} & if\ |\dot{\psi}_{des}| \leq \dot{\psi}_{upper_{bound}} \\ \dot{\psi}_{upper_{bound}} & if\ |\dot{\psi}_{des}| > \dot{\psi}_{upper_{bound}} \end{cases} \tag{3.29}$$

where

$$\dot{\psi}_{upper_{bound}} = 0.85\frac{\mu g}{v_x}$$

$$\dot{\psi}_{des} =$$

$$\frac{(C_{bfl}+C_{bfr})(C_{brl}+C_{brr})(L_f+L_r)}{(C_{bfl}C_{brl}+C_{bfr}C_{brl}+C_{bfl}C_{brr}+C_{bfr}C_{brr})(L_f+L_r)^2+mV^2\{L_r(C_{brr}+C_{brl})-L_f(C_{bfl}+C_{bfr})\}}V\delta$$

and

$$\beta_{target} = \begin{cases} \beta_{des} & if\ |\beta_{des}| \le \beta_{upper_{bound}} \\ \beta_{upper_{bound}} sgn(\beta_{des}) & if\ |\beta_{des}| > \beta_{upper_{bound}} \end{cases} \quad (3.30)$$

$$\beta_{upper_{bound}} = tan^{-1}(0.02\mu g)$$

$$\beta_{des} = \frac{(C_{bfl}+C_{bfr})\delta - \{mV^2 + L_f(C_{bfl}+C_{bfr}) - L_r(C_{brr}+C_{brl})\}}{(C_{bfl}+C_{bfr}+C_{brl}+C_{brr})}\dot{\psi}_{des}$$

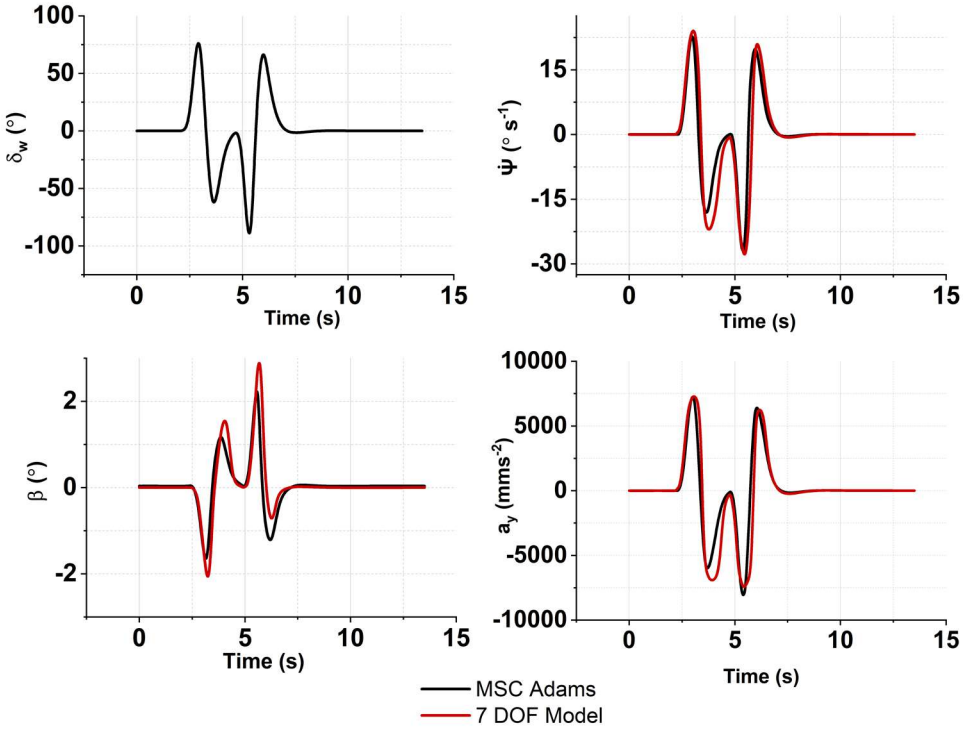

Figure 3.4. Comparison Between the Proposed Model and MSC Adams for DLC Maneuver

To achieve these desired states, an independent distributive braking torque with pre-assumed proportions for the normal three tires was proposed by Zhang et al. [94]. However, their approach is not well-suited to deal with different vehicle maneuvers and is only limited to straight-line motion. Therefore, a novel control strategy that handles different vehicle motion scenarios using a single front wheel actuator has been proposed. Furthermore, this scheme minimizes the computational effort required for the optimization algorithms in the distributive control counterpart. This is important because the available effective control time is just a few seconds in such instances. The basic idea is to produce a regulated amount of braking/driving torque on one of the front wheels apart from the blown tire. Specifically, a yawing moment is induced that counteracts and balances out the disturbance experienced by the vehicle. Such an apparatus does not need any extra actuators because the independent braking/driving torque distribution is already implemented in the ESC system which by itself (hardware & software algorithm) is incapable of stabilizing the vehicle under such a severe transient [25]. The controller is selectively activated by the front left (to handle FR and RR blowouts) and the front right (to handle FL and RL blowouts) input torques to handle each tire blowout case during both straight line and cornering motion. The flat tire side is excluded from the application of controlled input torques to prevent the movement between the hub and the tire not to mention wheel locking. A schematic diagram for the proposed nonlinear controller is shown in Figure 3.5.

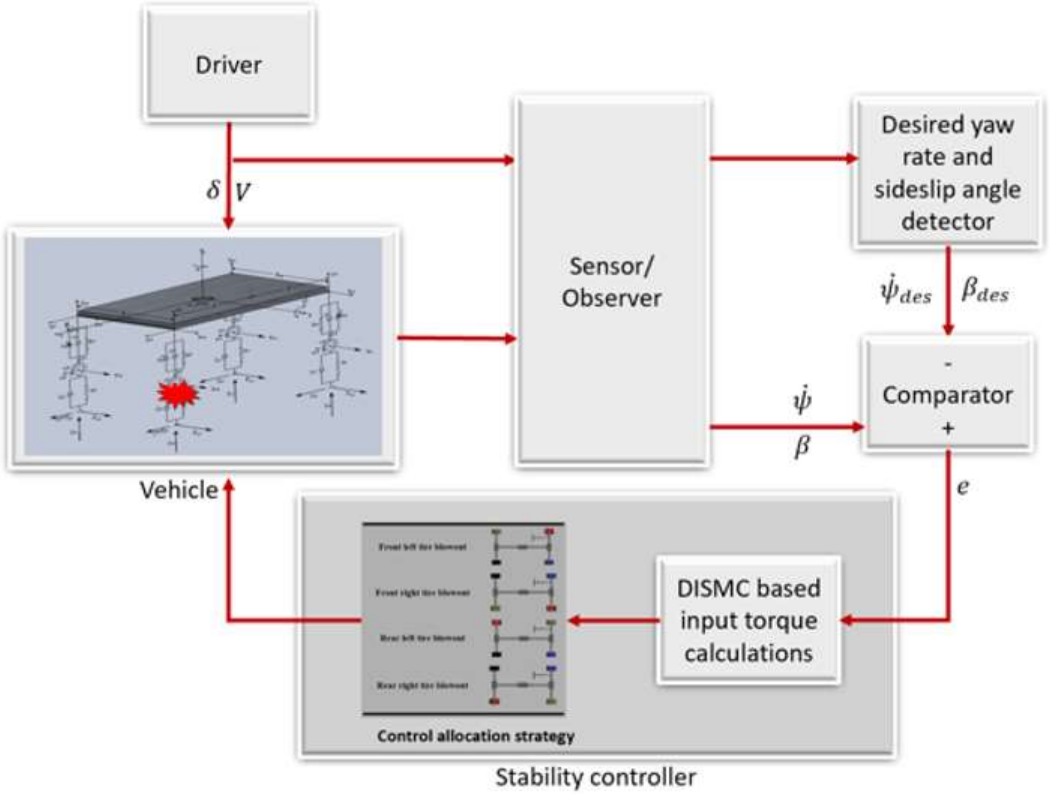

Figure 3.5. Block Diagram for the Proposed Controller

The conventional sliding mode controller is widely used because of its finite-time convergence as well as its invariance property against external disturbances and model uncertainties when the system approaches the sliding surface. In addition, this nonlinear controller encompasses large operating points of the system, unlike linearization-based controllers. Nevertheless, systems controlled by such variable structure controllers suffer from the relative complexity of the controller practical implementation, aside from the chattering phenomenon driven by the high frequency switching action of the controller which might be problematic to some dynamical systems. To remove the steady-state errors, a nonlinear Double Integral Sliding Mode Controller (DISMC) technique has been proposed. The reader can refer to the studies [111, 114] to practice the procedure of the

DISMC although it was applied to different systems. A strong reachability condition has been used to design the controller which decreases the chattering phenomena by reducing the slope of saturation function (instead of the discontinuous sign function). Designing of the switching surface is generally taken as a linear combination of the state tracking error dynamics and its derivative, given in [96] as

$$s = \left[\frac{d}{dt} + \xi\right]^{n-1} e(x) \tag{3.31}$$

In the above equation, ξ is a positive constant and *n* represents the order of the sliding surface. If one assumes *n=1*, the sliding manifold can be represented as the error dynamics which is defined as the difference between the target value and the actual dynamical value of the system expressed as $s = e(x)$. In the control synthesis of DISCM, the sliding manifold is considered as the sum of error and its integral terms and can be represented as

$$s = a_1 e_1 + a_2 e_2 + a_3 e_3 + a_4 e_4 \tag{3.32}$$

where

$$e_1 = \dot{\psi} - \dot{\psi}_{ref}$$

$$e_2 = \int (\dot{\psi} - \dot{\psi}_{ref})\, dt$$

$$e_3 = \int \left\{ \int (\dot{\psi} - \dot{\psi}_{ref}))\, dt \right\} dt$$

$$e_4 = (\beta - \beta_{ref})$$

a_1, a_2, a_3, and a_4 are constants used as the gains for the error quantities. Their optimal values are determined through improved methods based on Hurwitz Stability Theorem. Nonetheless, in this study, these parameters have been tuned manually to reduce the

computational burden of the controller. The integral terms of the error dynamics are employed to minimize the steady-state deviations in the system dynamics from their corresponding desired reference values. For the convergence of system dynamics to the reference value, the time derivative of the sliding surface should approach zero. In other words

$$\dot{s} = a_1\dot{e}_1 + a_2\dot{e}_2 + a_3\dot{e}_3 + a_4\dot{e}_4 \tag{3.33}$$

Substituting the values of derivatives of the error dynamics and considering $\dot{s} = -K|s|^{\alpha} sat\left(\frac{s}{\eta}\right)$, where η is the width of the boundary layer and $sat\left(\frac{s}{\eta}\right)$ is defined as

$$sat\left(\frac{s}{\eta}\right) = \begin{cases} 1 & \left|\left(\frac{s}{\eta}\right)\right| \leq 1 \\ sgn\left(\frac{s}{\eta}\right) & \left|\left(\frac{s}{\eta}\right)\right| > 1 \end{cases} \tag{3.34}$$

Equation 3.33 can be rewritten as:

$$\begin{aligned} a_1(\ddot{\psi} - \ddot{\psi}_{ref}) + a_2(\dot{\psi} - \dot{\psi}_{ref}) \\ + a_3\left(\int(\dot{\psi} - \dot{\psi}_{ref})\, dt\right) \\ + a_4(\dot{\beta} - \dot{\beta}_{ref}) + K|s|^{\alpha} sat\left(\frac{s}{\eta}\right) = 0 \end{aligned} \tag{3.35}$$

By substituting the value of $\ddot{\psi}$ in the above equation, one can calculate the nonlinear control value for the driving torque by separating T_{dfj} in one side of the equation, where j represents left and right side actuators. Including the absolute value of sliding surface in the $\dot{s}$ equation empowers the controller to increase the speed of convergence as the

distance of the system variable from the sliding manifold increases. The chattering problem is reduced by tuning the slope of the saturation function (section 3.2 and appendix A). The parameter η is imposed in the saturation function term to adjust its slope. Appendix A highlights how the chattering problem is attenuated, where three values for η are simulated: 0.5 (which is the one chosen for the simulations in chapter 3), 1, and 1.5. The responses of the sideslip angle, yaw rate, lateral acceleration, and the input torque are shown, and the effect of η is demonstrated (see appendix A). Using equation 3.35 and considering front left driving torque as the system actuator while taking the rest of braking and driving torques equal to zero, the control equation can be obtained as

$$T_{dfl} = \left\{\frac{L_f sin\delta}{R_w I_z} - \frac{L_w cos\delta}{2R_w I_z}\right\}^{-1} \left\{-\frac{K}{a_1}|s|^{\alpha} sat\left(\frac{s}{\eta}\right) - \right\} \frac{a_2}{a_1}\left[\left(\dot{\psi} - \dot{\psi}_{ref}\right)\right] - \frac{a_3}{a_1}\left(\int\left[\left(\dot{\psi} - \dot{\psi}_{ref}\right)\right] dt\right) + \ddot{\psi}_{ref} + \frac{a_4}{a_1}\left(\dot{\beta}_{ref} - \frac{v_x\dot{v}_y - v_y\dot{v}_x}{v_x^2 + v_y^2}\right) - \frac{L_f}{I_z}\left(F_{Bfl} + F_{Bfr}\right)cos\delta + \frac{L_r}{I_z}\left(F_{Brl} + F_{Brr}\right) - \frac{L_w}{2I_z}\left(F_{Bfl} - F_{Bfr}\right)sin\delta - \frac{L_w}{2I_z}\left(\frac{-J_w\dot{\omega}_{rr} - F_{rrr}R_w}{R_w} - \frac{-J_w\dot{\omega}_{rl} - F_{rrl}R_w}{R_w}\right) - \frac{L_f}{I_z}\left(\frac{-J_w\dot{\omega}_{fl} - F_{rfl}R_w}{R_w} + \frac{-J_w\dot{\omega}_{fr} - F_{rfr}R_w}{R_w}\right) sin\delta - \left\{\frac{L_w}{2I_z}\left(\frac{-J_w\dot{\omega}_{fr} - F_{rfr}R_w}{R_w} - \frac{-J_w\dot{\omega}_{fl} - F_{rfl}R_w}{R_w}\right) cos\delta \right\} \quad (3.36)$$

Similarly, using front right driving torque as the actuator and the remaining braking and driving torques equal to zero, the actuator driving signal is

$$T_{dfr} = \left\{\frac{L_f sin\delta}{R_w I_z} + \frac{L_w cos\delta}{2R_w I_z}\right\}^{-1} \left\{-\frac{K}{a_1}|s|^{\alpha} sat\left(\frac{s}{\eta}\right) - \right\} \frac{a_4}{a_1}\left(\dot{\beta}_{ref} - \frac{v_x\dot{v}_y - v_y\dot{v}_x}{v_x^2 + v_y^2}\right) - \frac{L_f}{I_z}\left(F_{Bfl} + F_{Bfr}\right)cos\delta + \frac{L_r}{I_z}\left(F_{Brl} + F_{Brr}\right) - \frac{L_w}{2I_z}\left(F_{Bfl} - F_{Bfr}\right)sin\delta - \frac{L_w}{2I_z}\left(\frac{-J_w\dot{\omega}_{rr} - F_{rrr}R_w}{R_w} - \frac{-J_w\dot{\omega}_{rl} - F_{rrl}R_w}{R_w}\right) - \frac{L_f}{I_z}\left(\frac{-J_w\dot{\omega}_{fl} - F_{rfl}R_w}{R_w} + \frac{-J_w\dot{\omega}_{fr} - F_{rfr}R_w}{R_w}\right) sin\delta - \left\{\frac{L_w}{2I_z}\left(\frac{-J_w\dot{\omega}_{fr} - F_{rfr}R_w}{R_w} - \frac{-J_w\dot{\omega}_{fl} - F_{rfl}R_w}{R_w}\right) cos\delta \right\} \quad (3.37)$$

Lemma 1: given the vehicle planar motion governed by equations 3.1-3.4, the control laws expressed in equations 37 and 38 guarantee asymptotic stability of the feedback closed-loop system if and only if the values of *K* are positive.

Proof: To demonstrate the stability of the proposed controller, a positive definite Lyapunov energy function candidate is taken as $V = \frac{1}{2} s^2$. To satisfy the stability condition of the Lyapunov criterion, it is required to have at least a negative semi-definite time derivative of the Lyapunov candidate function to ensure the existence of sliding mode in the neighborhood of the sliding surface. To prove the reachability condition, the derivative of the Lyapunov candidate function is $\dot{V} = s\dot{s}$.

By substituting the value of $\dot{s} = -K|s|^{\alpha} sat\left(\frac{s}{\eta}\right)$, the previous equation can be rewritten as

$$\dot{V} = s\left(-K|s|^{\alpha} sat\left(\frac{s}{\eta}\right)\right)$$

Hence,

$$\dot{V} \leq 0 \leftrightarrow \quad K > 0 \quad \blacksquare$$

From the aforementioned equation, it has been proved that using T_{dfl} and T_{dfr} calcul ated in equations 37 and 38 will guarantee the convergence of system states to the desired reference values in a finite time interval. The values of *K* should be positive to satisfy the Lyapunov theorem.

3.3 Closed-Loop System Simulation and Evaluation

MATLAB/Simulink environment has been utilized to evaluate the effectiveness of the proposed controller for different tire blowout scenarios in both straight and curved paths. The study considers a four-wheel independently actuated electric ground vehicle. Initially, the vehicle is accelerated to 80 km/hr and this speed is held constant thereafter. The braking and accelerating pedals are kept unpressed throughout the simulations, whereas the only inputs are exerted by the proposed controller and the pre-assumed steering input. This open-loop apparatus with a prespecified sequence of inputs might be considered theoretical in flavor. However, it is decently sufficient for the virtual prototyping phase of the project. Moreover, the inherent robustness of the sliding mode controller can be exploited to make the system invariant to the disturbances from the driver. In all tests, the blowout is initiated at the fifth second and lasts for 0.1 seconds. The front left input torque is applied when FR or RR blowout occurs while the front right input torque is applied for FL or RL blowouts. This is illustrated in Table 3.1 where the red tire refers to the flat tire while the blue one refers to the actuator side. The control parameters are tuned to fulfill the required tracking performance and they are fixed for all the tests and listed in Table 3.2.

Furthermore, it is assumed that all the required parameters can be fed back either directly through sensor measurements or using observers. In the following sections, eight blowout scenarios for the four tires are carried out during both straight and cornering motions on a straight, flat, dry road, and the performance of the controller is assessed.

Table 3.1. The Selective Control Strategy

Front left tire blowout	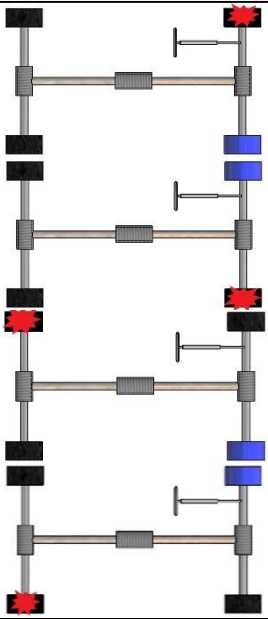
Front right tire blowout	
Rear left tire blowout	
Rear right tire blowout	

Table 3.2. Controller Parameters for the Individual Actuator Control

α	0.5
n	1
η	0.5
K	100
a_1	990000
a_2	5000000
a_3	30000000
a_4	1

3.3.1 Straight Line Motion

In this section, a straight-line trajectory is considered, in which neither lane departure nor vehicle spinning are allowed. The tire pressure monitoring system (TPMS) [102] detects the rapid loss in the inflation pressure and transmits a signal that triggers the controller

immediately. Four cases of tire blowouts events are conducted, and the closed-loop system response is simulated and evaluated. The control problem in the straight-line motion case is simply a regulation problem, in which the objective is to drive the states to zero.

When a front left tire blowout occurs, the controller applies an input torque in the opposite front side. Figure 3.6 illustrates the results for the trajectory, the sideslip angle, and the yaw rate with/without blowout as well as with/without control. In the absence of control, the vehicle dynamics abruptly change, and the vehicle departs its lane with the risk of colliding with other vehicles. Contrarily, it is obvious that the controller can efficiently stabilize the vehicle and drive the states to zero. In addition, as it can be seen in Figure 3.6, the controller does not only keep the vehicle lateral deviations within fractals of a meter, it also decelerates the vehicle until a complete stop. The sideslip angle and the yaw rate also return to their target trajectories.

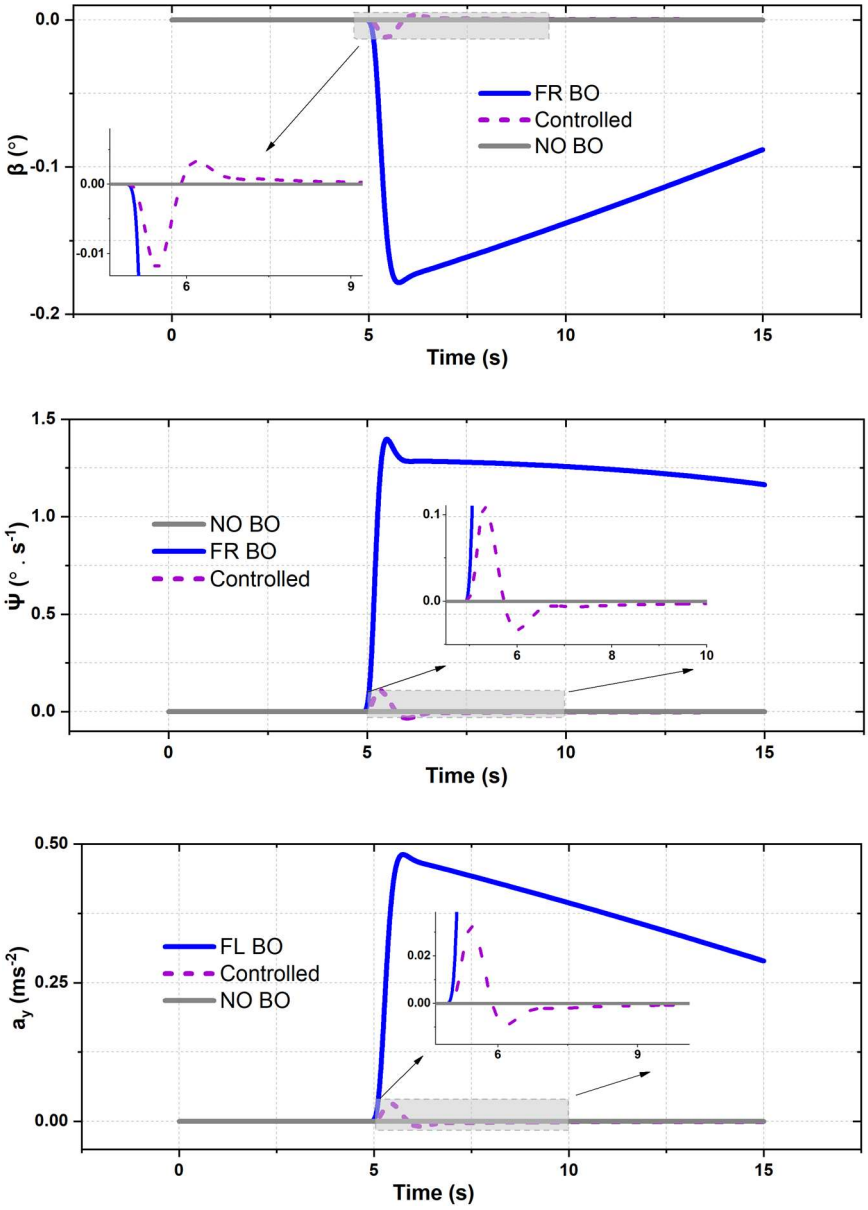

Figure 3.6. Vehicle Straight-Line Response to a Front Left Tire Blowout

When a front right tire blowout occurs, the front left wheel input torque is activated by the controller in order to control the vehicle dynamics and to follow the desired trajectory. The results regarding trajectory, side slip angle, and yaw rate for the front left tire are highlighted in Figure 3.7. It can be seen that the controller responds in the same

fashion as the front left tire blowout case, and the states, as well as the lateral deviation, are restricted within the respective desired values.

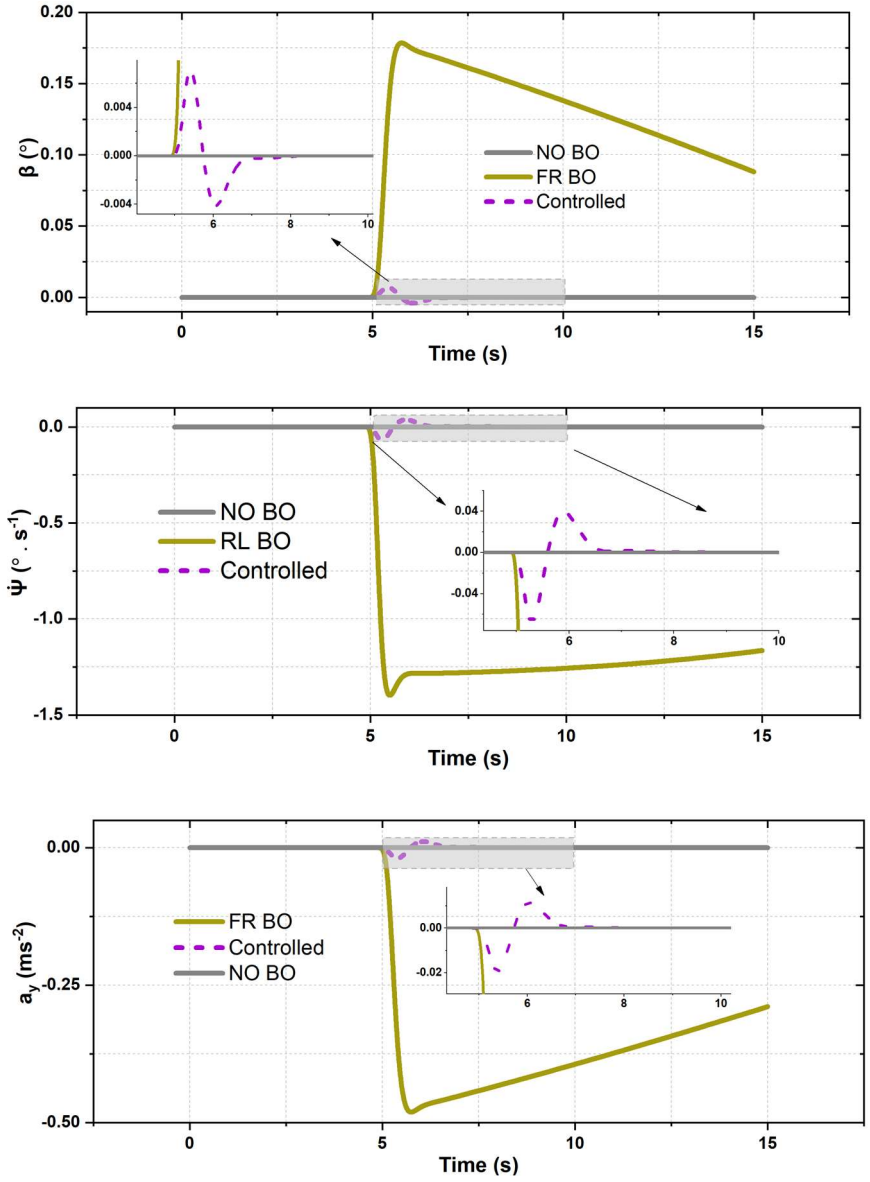

Figure 3.7. Vehicle Straight-Line Response to a Front Right Tire Blowout

For straight-line motion, from a quantitative measure of the lateral deviation perspective, the rear left tire blowout is more severe than the front left blowout. Following a rear left tire blowout, the front right input torque is activated, and the resulting effects are

recorded in Figure 3.7. A large lateral deviation from the straight-line path is highlighted in the Figure, while the dramatic changes in the sideslip angle and the yaw rate are shown in the second row of Figure 3.8.

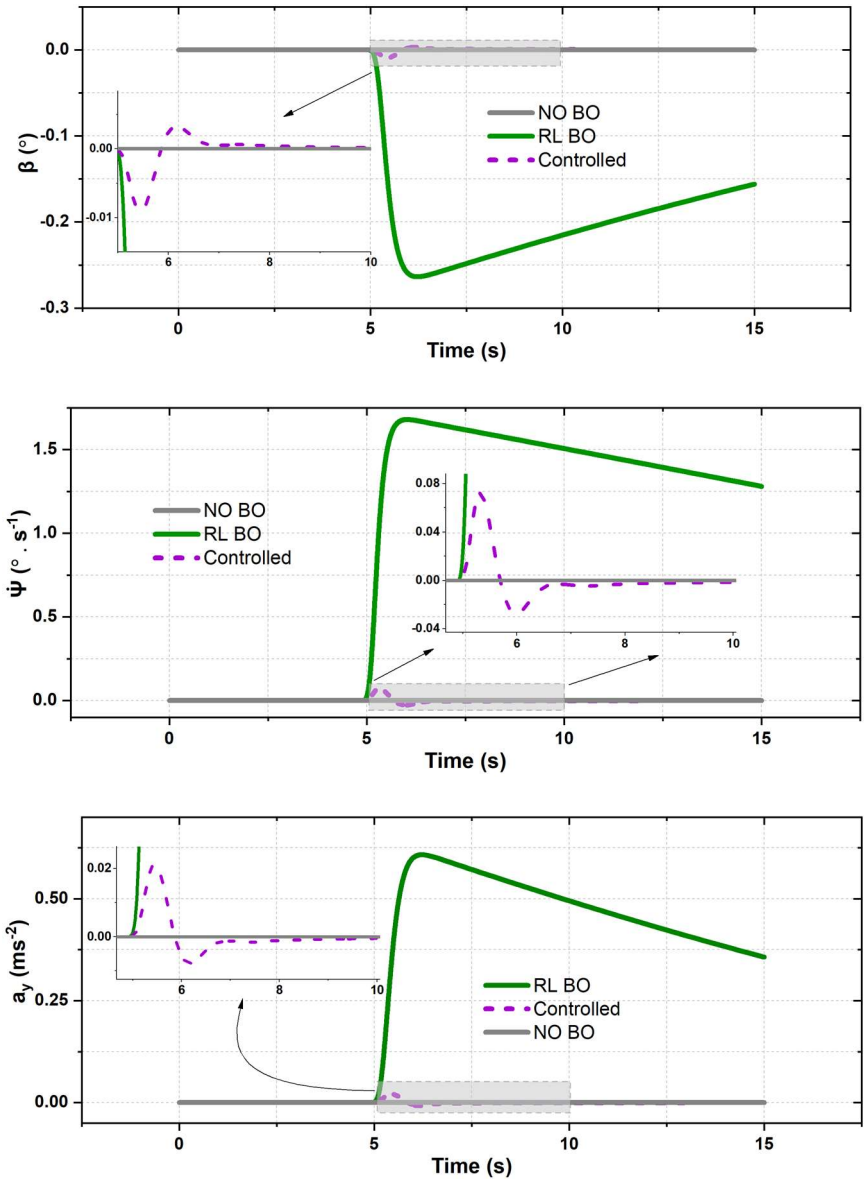

Figure 3.8. Vehicle Straight-Line Response to Rear Left Tire Blowout

In contrast, when the controlled driving torque is applied to the right front wheel, the dynamic responses ultimately converge to their target values, the vehicle again slows down, and the transverse deviations vanish.

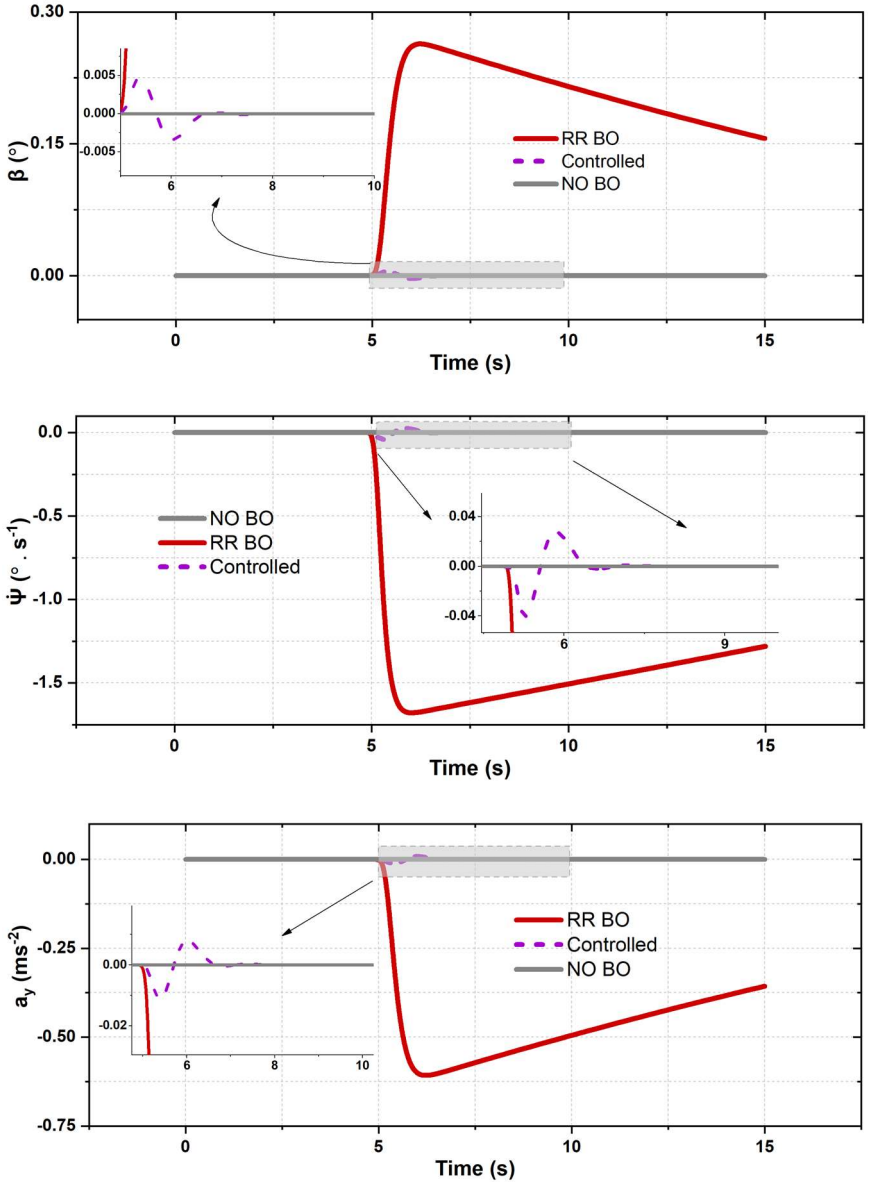

Figure 3.9. Vehicle Straight-Line Response to a Rear Right Tire Blowout

Similarly, for the rear right tire blowout, the controller activates the front left wheel input torque such that the vehicle follows the desired trajectory. Trajectory, side slip angle, and yaw rate results for the controlled and the uncontrolled cases are shown in Figure 3.9. With reference to the previous figures, due to symmetry, the vehicle exhibits the same open-loop and closed-loop results, and they are both included for completeness. The

proposed controller can drastically enhance the stability and the driving directionality performance using only a single actuator for straight-line motion. However, the actuation methodology consisting of either the in-wheel electric motor or hydraulic braking does not behave in such an ideal way; rather, the existence of delays and nonlinearities turns the system to be less perfect.

Input torques provided by the controller to stabilize the vehicle are illustrated in Figure 3.10. The symmetrical behavior is clearly demonstrated. It can also be observed that the front tire blowouts need more input torque to stabilize the vehicle than their rear counterparts. This is because the required moment needed to counteract the yawing blowout-induced moment a smaller arm in the case when a front tire blowout occurs. The time delay between sensing the blowout and generating the input torques as well as actuator dynamics are not incorporated in this research.

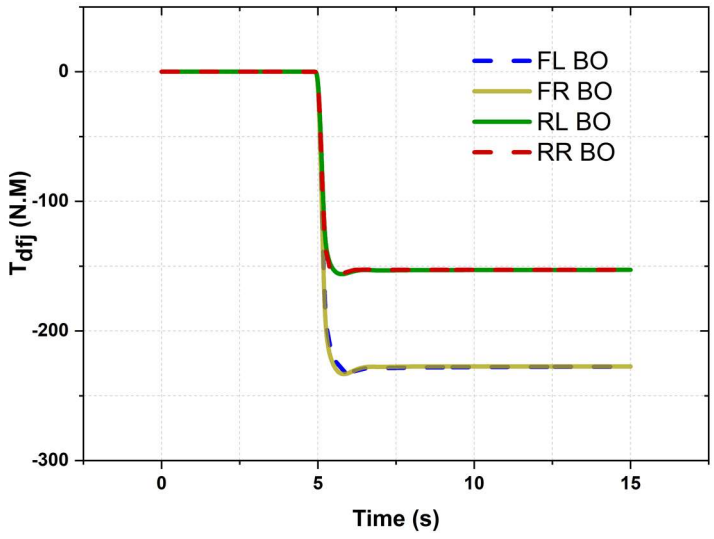

Figure 3.10. Input Control Torques in Straight Line Blowout-Single Actuator

3.3.2 Cornering Motion

In this section, the vehicle is subjected to a tire blowout while turning left. Four driving maneuvers are performed for each individual tire blowout case. Firstly, the vehicle is accelerated to a speed of 80 km/hr and starts turning at the fourth second while cruising. Then, the blowout is triggered at the fifth second and lasts for 0.1 seconds. Finally, the controller is activated right after the blowout. It is worth pointing out that in the state-of-the-art cornering tracking problem, the controller might be activated during the normal cornering prior to the blowout. This is because the vehicle will not necessarily follow desired steady-state motion derived from the linear single-track model. This is valid if the controller is activated as soon as any deviation from the steady-state behavior is detected. However, in the current study, the controller is triggered only by the Tire Pressure Monitoring System (TPMS) and stays deactivated in the absence of tire blowout. The lateral acceleration is spontaneously manipulated and its desired value is considered to be $v_x\dot{\psi}$ [3].

In response to a front left tire blowout, the controller produces front right wheel torque to stabilize the vehicle and follow the desired states. Sideslip angle, yaw rate, and lateral acceleration responses to the front left tire case are illustrated in Figure 3.11. It can be revealed from the figures that the controller can effectively drive the states to approach their target trajectories and hence reduce the understeer generated by the front left tire blowout. Since the intrinsic instability is dominated by the yaw rate, it has been given more weights in the sliding manifold equation compared with the sideslip angle. Therefore, its tracking performance is better than the one for the sideslip angle which in

turn does not exceed one degree in magnitude anyway. This trend is so common in underactuated systems.

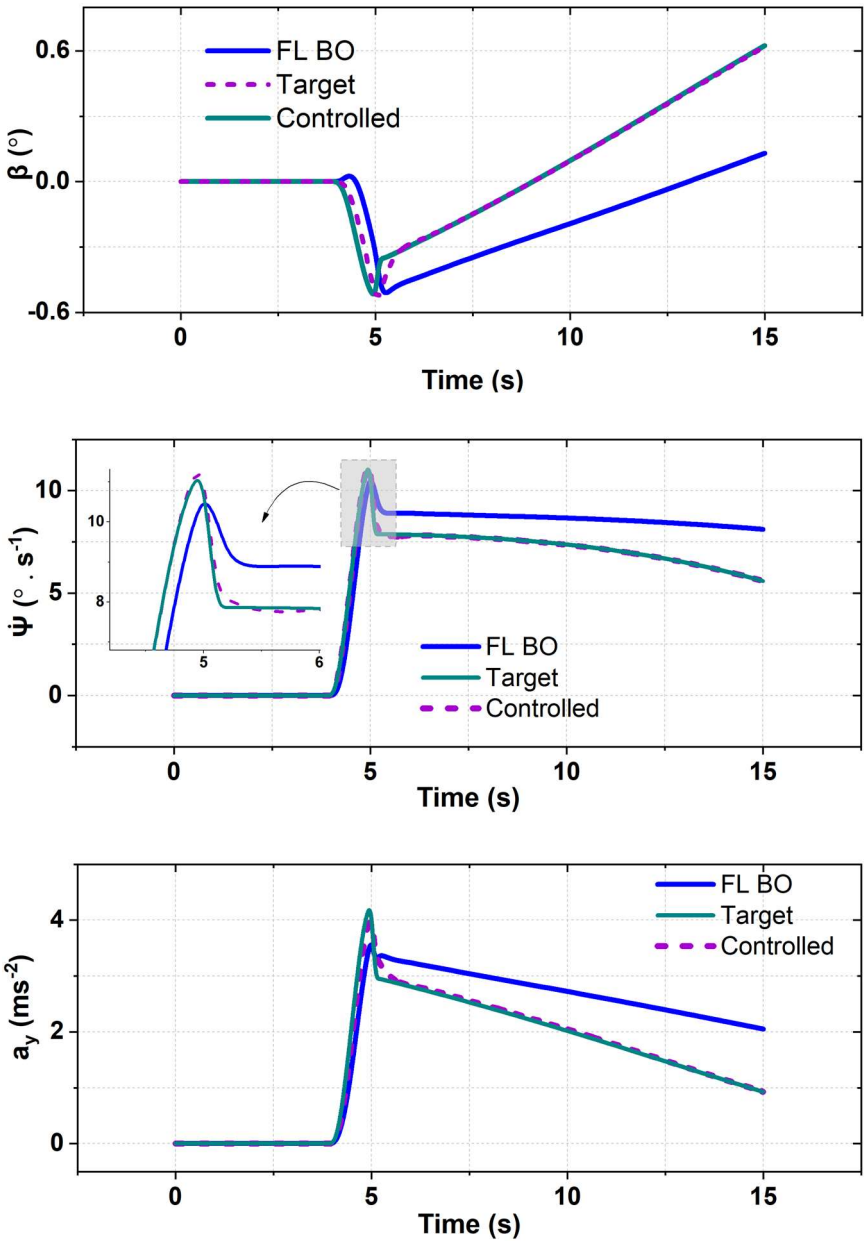

Figure 3.11. Vehicle Response To a Front Left Cornering Tire Blowout Scenario

Responding to the front right tire blowout, the front left wheel actuator is activated to control the vehicle dynamics and to follow the desired trajectory. Sideslip angle, yaw rate, and lateral acceleration results for the front left tire blowout with and without

control are presented in Figure 3.12. Following tiny oscillations, vehicle yaw rate and sideslip angle converge to their corresponding steady-state curves. Hence, the resulting excessive oversteering can successfully be minimized.

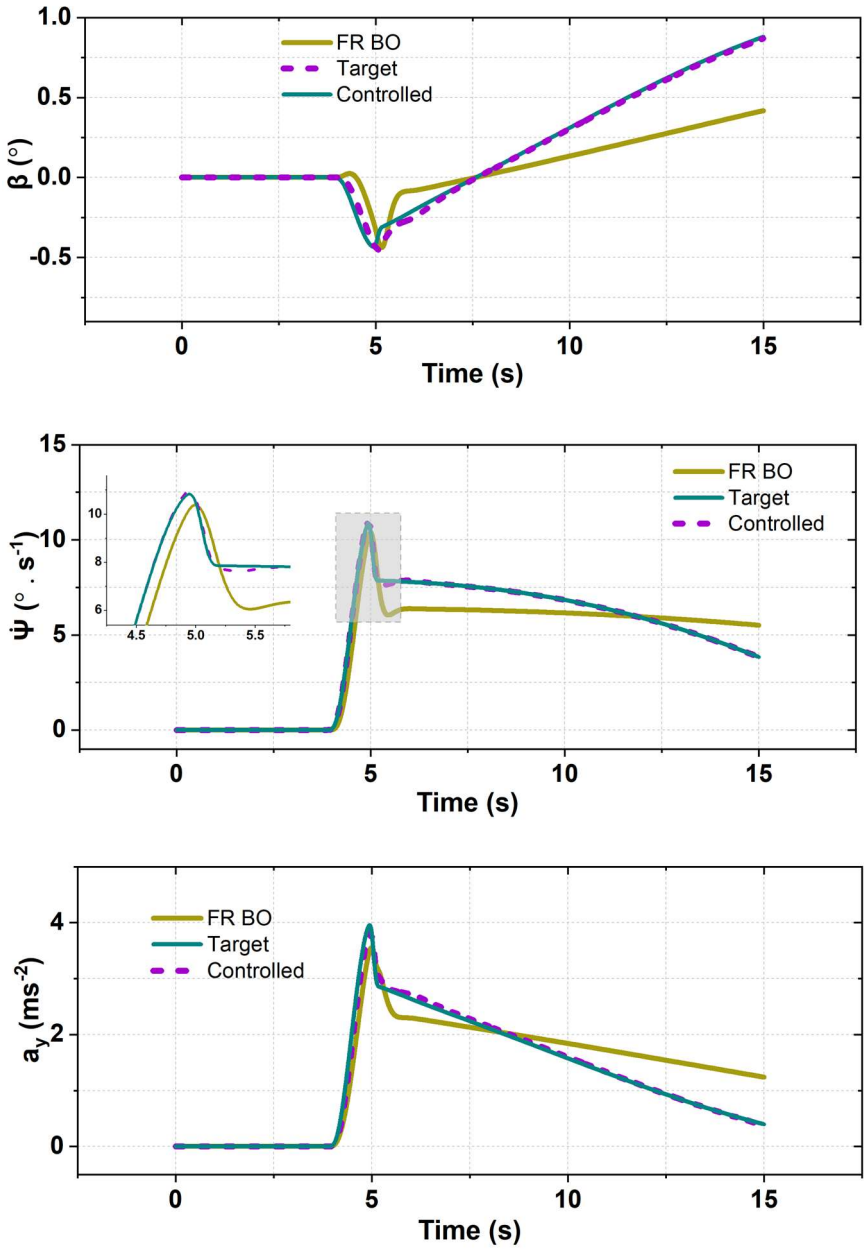

Figure 3.12. Vehicle Response to Front Right Cornering Tire Blowout Scenario

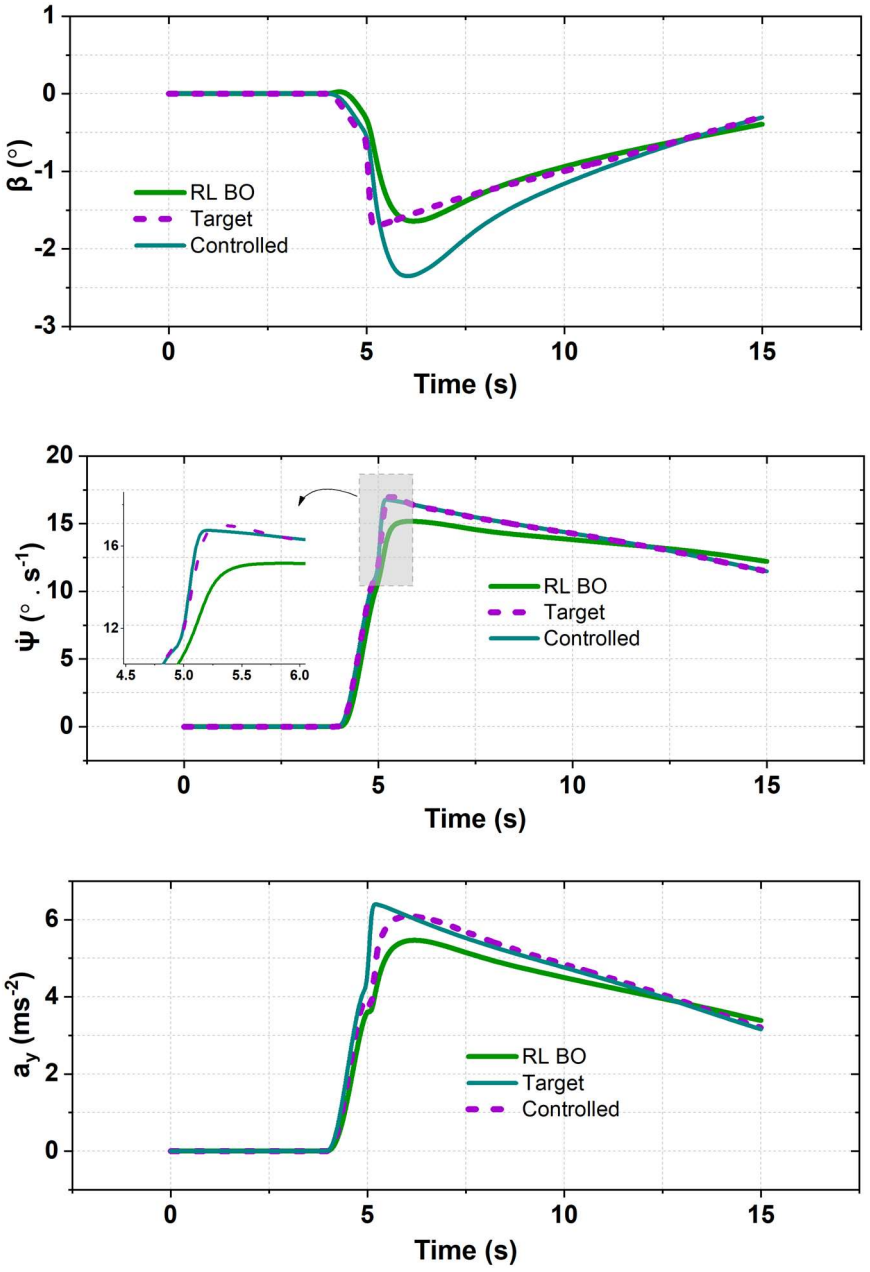

Figure 3.13. Vehicle Response to Rear Left Cornering Tire Blowout Scenario

In the same fashion, in the case of a rear left tire blowout, the controller activates the front right wheel actuator. Comparison of controlled and uncontrolled behavior of the vehicle following rear left tire blowout is highlighted in Figure 3.13.

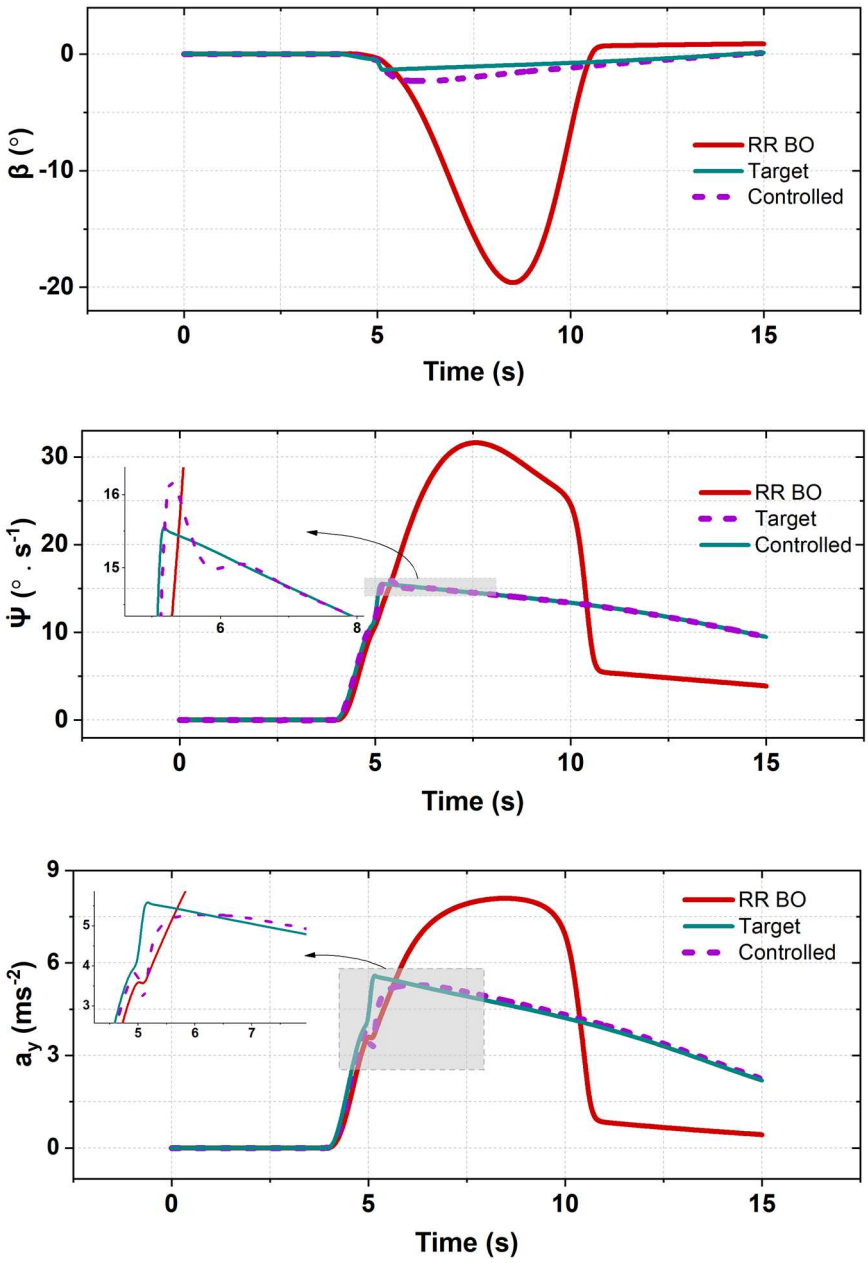

Figure 3.14. Vehicle Response to Rear Right Cornering Tire Blowout Scenario

When the inner rear tire blowout occurs, the vehicle starts spinning besides drifting from its original path. Stabilizing the vehicle by the driver in such circumstances is very challenging and almost impossible [37]. However, the controller can effectively minimize

the risk by applying an input torque in the front right wheel, resulting in the excellent directional stability characteristics revealed in Figure 3.14.

When rear right blowout occurs, the controller generates front left wheel torques to suppress the dramatic changes in the vehicle response to a tire blowout. Although its response is significantly different from those of other tires for the passive system, the controller effect on the vehicle subjected to rear right blowout concurs with the other cases. The vehicle exhibits tiny overshoot and oscillation following the blowout and perfectly tracks the desired states trajectories afterward. Due to the symmetry, identical results can be observed for clockwise cornering maneuver with different blowout scenarios.

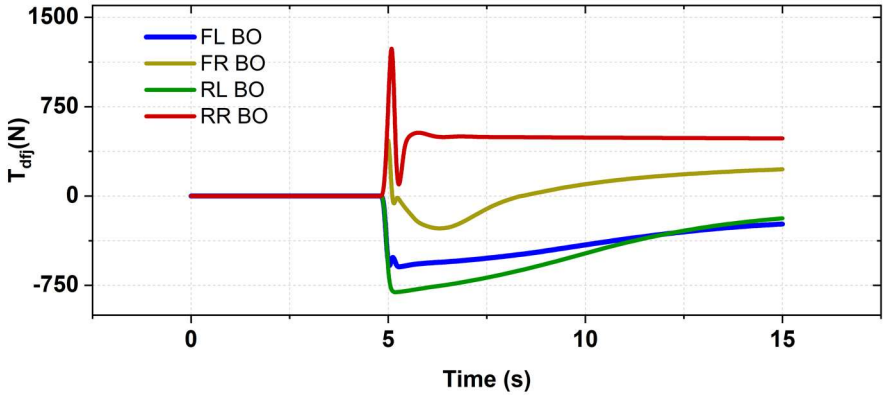

Figure 3.15. Input Control Torques in Cornering Blowout-Single Actuator

In the case of cornering, the input torque demand supplied by the controller to inhibit the tire blowout impact is presented in Figure 3.15. The control demand required from the actuator is high in the case of cornering. Quantitively, it is obvious that the case of rear tire blowout requires more torque to stabilize the vehicle compared with the front case. This is because the vehicle experiences more severe dynamics and excessive oversteering in rear

blowout cases. In all cases, the control demand reaches its peak as soon as the blowout signal is sparked and then starts decreasing steadily. The torque supplied to the front left wheel spikes at the moment of the blowout in the case of a rear right tire blowout in which the vehicle suffers a remarkable instability. Finally, by comparing Figures 3.10 and 3.15, it is apparent that the magnitude of the torque required in the cornering motion is greater in magnitude than in the case of its straight-line counterpart. Again, this is because, in cornering, the vehicle is subjected to severe under/over steering behaviors.

The transverse deviation of the vehicle path from its respective target trajectory measured from the lane center is demonstrated in Figure 3.16. The closed-loop system is tested for three vehicle speeds: 80 km/hr, 120 km/hr, and 160 km/hr during both straight-line and curvilinear maneuvers. Clearly, in comparison with the large lateral deviations for the passive system introduced in the previous chapter, when the controlled driving input torque is applied, the lateral deviations are vanished or are restricted within reasonable values.

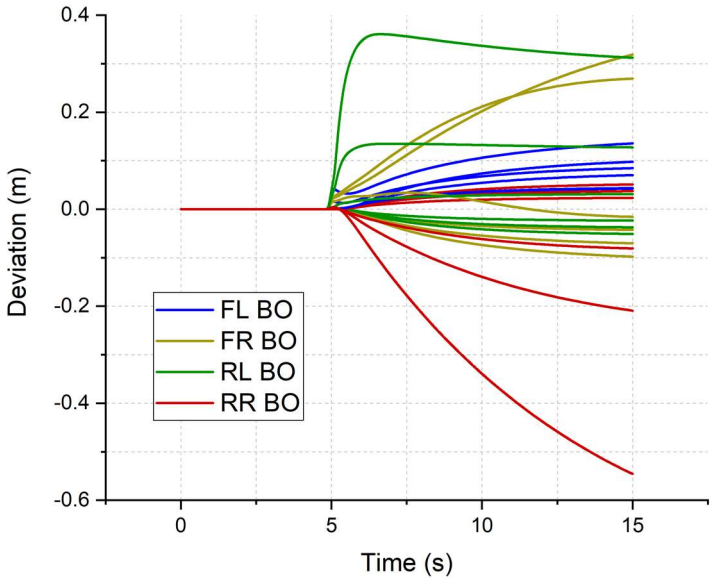

Figure 3.16. Lateral Deviations Of the Closed-Loop System for a Single Actuator

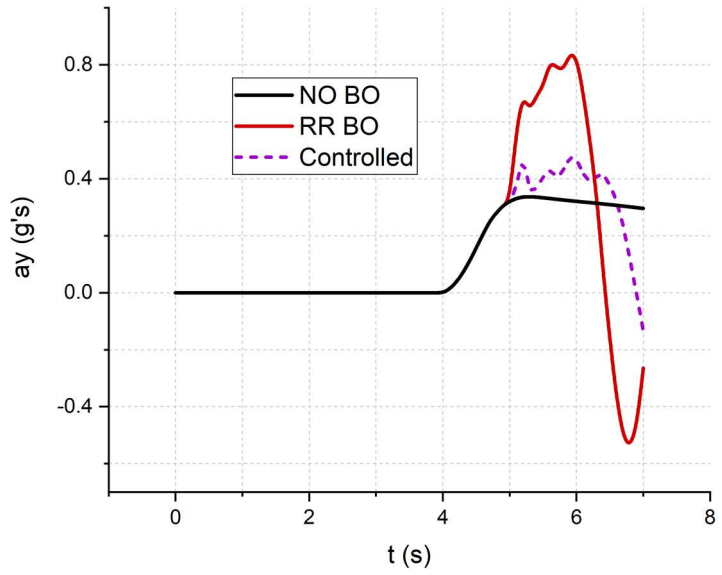

(a)

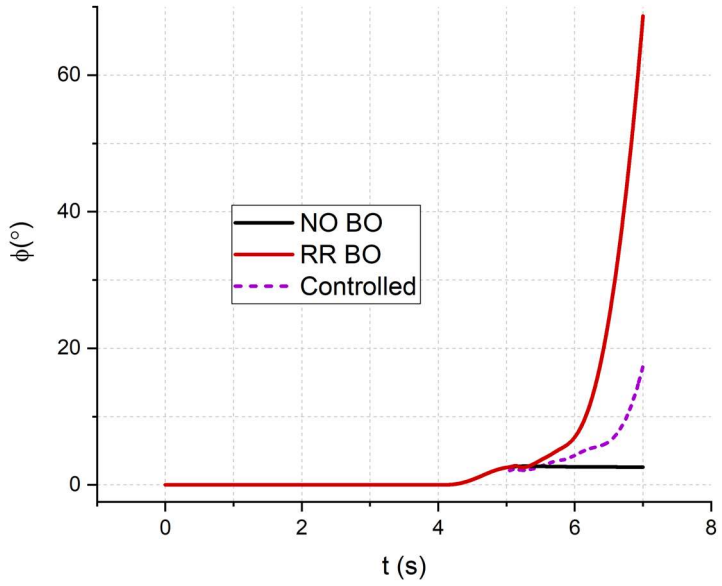

(b)

Figure 3.17. Fourteen DOF Closed-Loop Response (A) Lateral Acceleration (B) Roll Angle

Finally, the controller is connected to the fourteen degrees of freedom full vehicle model to examine the out-of-plane vehicle response. As expected, as the controller stabilizes the

vehicle handling motion, it reduces the lateral acceleration below. Thus, the vehicle will avoid the rollover accident because the lateral acceleration is below the rollover threshold and the roll angle is reduced significantly as illustrated in Figure 3.17.

3.3.3 Distributive Torque Control

One approach to reducing the torque requirements from a single actuator is to distribute the control demand among three motors. Due to the existence of the nonlinearities in the system, it is a very challenging task to come up with an optimum distribution strategy among the three tires. Instead, similar to the technique used in [94], a predetermined contribution of each of the three torque is implemented. The blown tire is not allowed to apply torques to prevent wheel locking. The wheels on the opposite side of the flat tire contribute by 50% and 60% while the wheel on the same side applies 10% in the reverse direction of the total torque. 50% of the total torque is taken by the wheel in the diagonal opposite to the flat tire. Table (3.3) summarizes this technique provided the red tire is the flat tire while the blue tires are the active ones.

For instance, if the front left tire blowout is considered, the total input torque can be expressed as

$$T_{tot} = \left\{\frac{0.6L_f sin\delta}{R_w I_z} + \frac{0.6L_w cos\delta}{2R_w I_z} + \frac{0.6L_w}{2I_z}\right\}^{-1} - \frac{K}{a_1}|s|^{\alpha} sat\left(\frac{s}{\eta}\right) - \frac{a_2}{a_1}\left(\dot{\psi} - \dot{\psi}_{ref}\right) - \frac{a_3}{a_1}\left(\int\left(\dot{\psi} - \dot{\psi}_{ref}\right)\, dt\right) + \ddot{\psi}_{ref} + \frac{a_4}{a_1}\left(\dot{\beta}_{ref} - \frac{v_x\dot{v}_y - v_y\dot{v}_x}{v_x^2+v_y^2}\right) - \frac{L_f}{I_z}\left(F_{bfl} + F_{bfr}\right)cos\delta + \frac{L_r}{I_z}\left(F_{brl} + F_{brr}\right) - \frac{L_w}{2I_z}\left(F_{bfl} - F_{bfr}\right)sin\delta - \frac{L_f}{I_z}\left(\frac{-J_w\dot{\omega}_{fl} - F_{rfl}R_w}{R_w} + \frac{-J_w\dot{\omega}_{fr} - F_{rfr}R_w}{R_w}\right)sin\delta - \frac{L_w}{2I_z}\left(\frac{-J_w\dot{\omega}_{fr} - F_{rfr}R_w}{R_w} - \frac{-J_w\dot{\omega}_{fl} - F_{rfl}R_w}{R_w}\right)cos\delta - \frac{L_w}{2I_z}\left(\frac{-J_w\dot{\omega}_{rr} - F_{rrr}R_w}{R_w} - \frac{-J_w\dot{\omega}_{rl} - F_{rrl}R_w}{R_w}\right) \quad (3.38)$$

Table 3.3. The Distributive Torque Control Strategy

Front left tire blowout	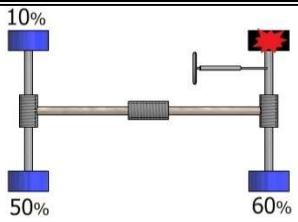
Front right tire blowout	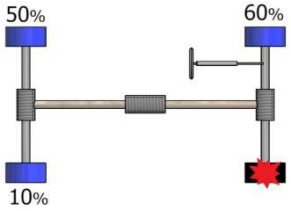
Rear left tire blowout	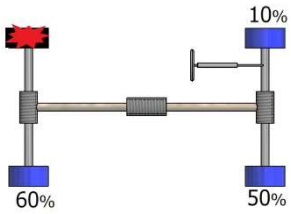
Rear right tire blowout	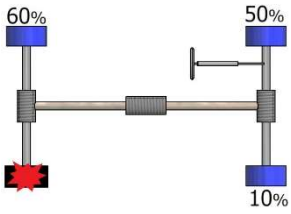

This torque is distributed among the front right, rear left, and rear right wheels according to the rule assigned in Table (3.3). It is worth pointing out that this proportional torque distribution law does not only reduce the effort required of the individual actuator but also improves the tracking performance of the closed-loop system by adding extra actuators.

Table 3.4. Controller Parameters for the Distributive Control

α	0.5
n	1
η	0.5
K	100
a_1	1000
a_2	500000000
a_3	300000000
a_4	1

The control parameters are tuned to achieve the required tracking performance while maintaining an acceptable amount of chattering. Their numerical values are fixed for all the tests and listed in Table 3.4.

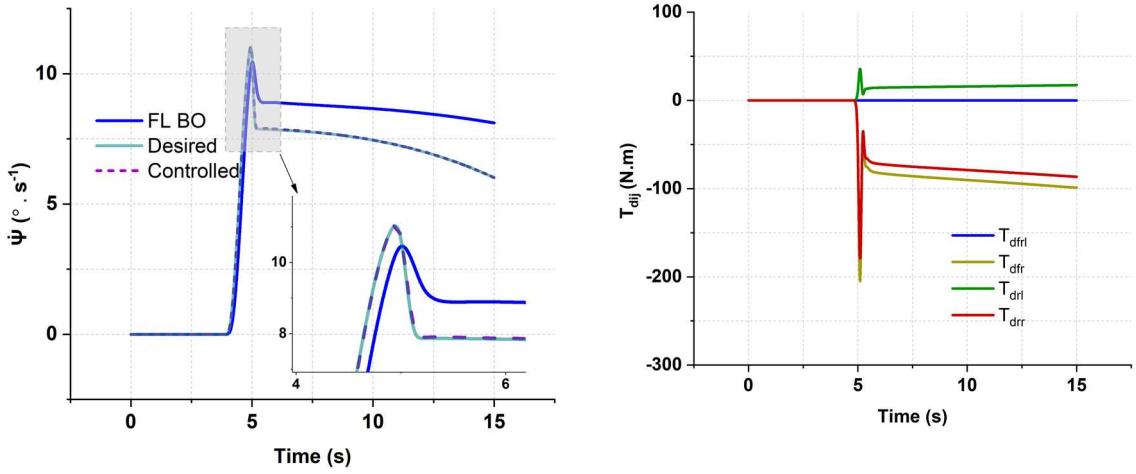

(a)

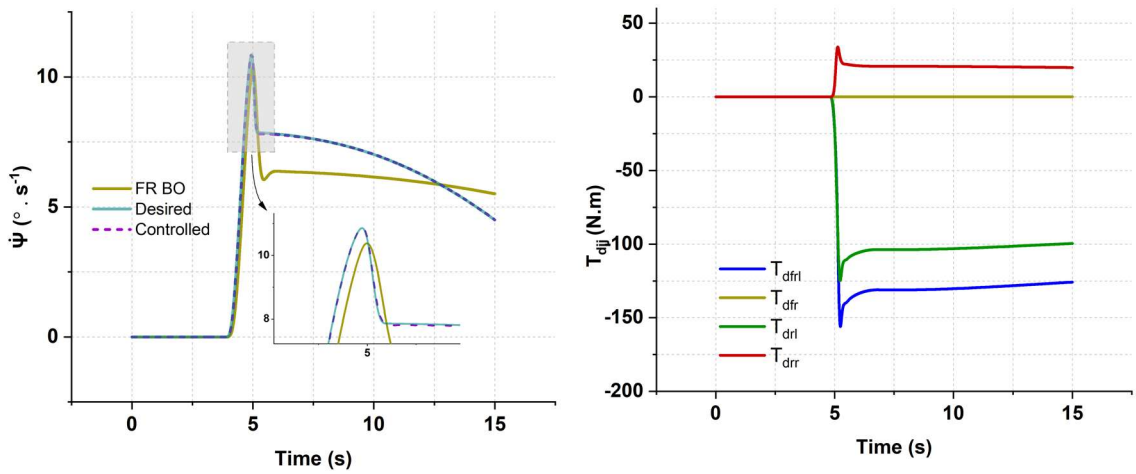

(b)

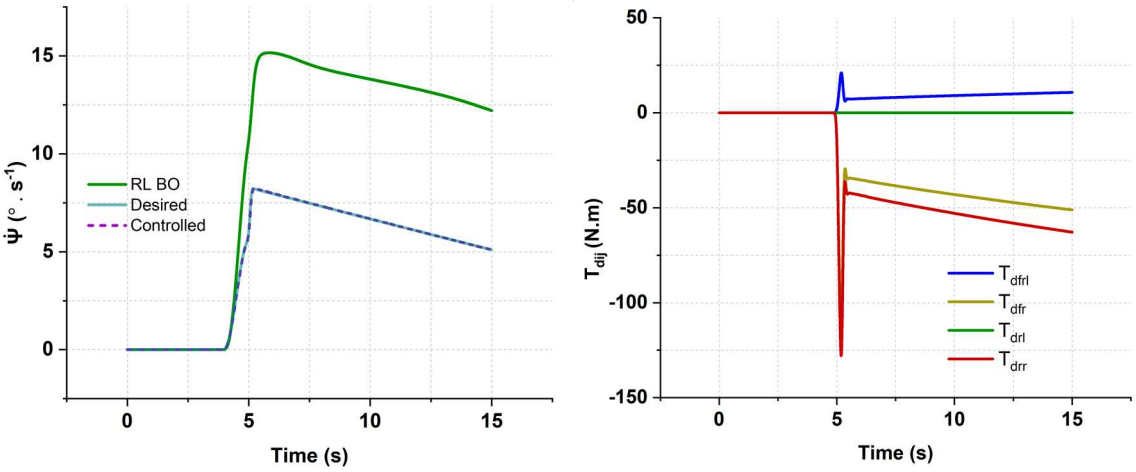

(c)

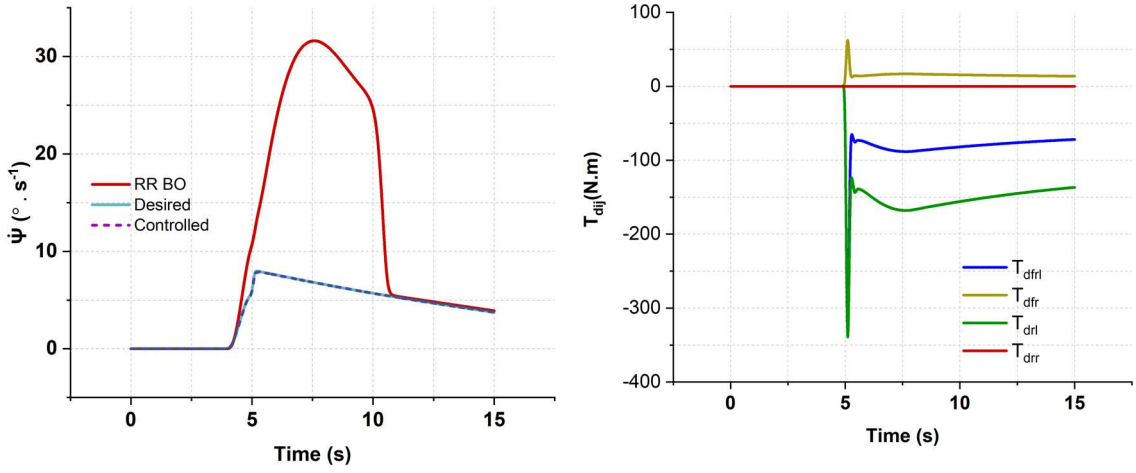

(d)

Figure 3.18. Distributive Torque Control Results (a) FL (b) FR (c) RL (d) RR

Figure 3.18 shows the results for the distributive torque controller. Clearly, the control effort does not exceed 500 N.m for any of the actuators in all possible situations. Moreover, the tracking performance of the distributive torque is advantageous over the individual actuator technique.

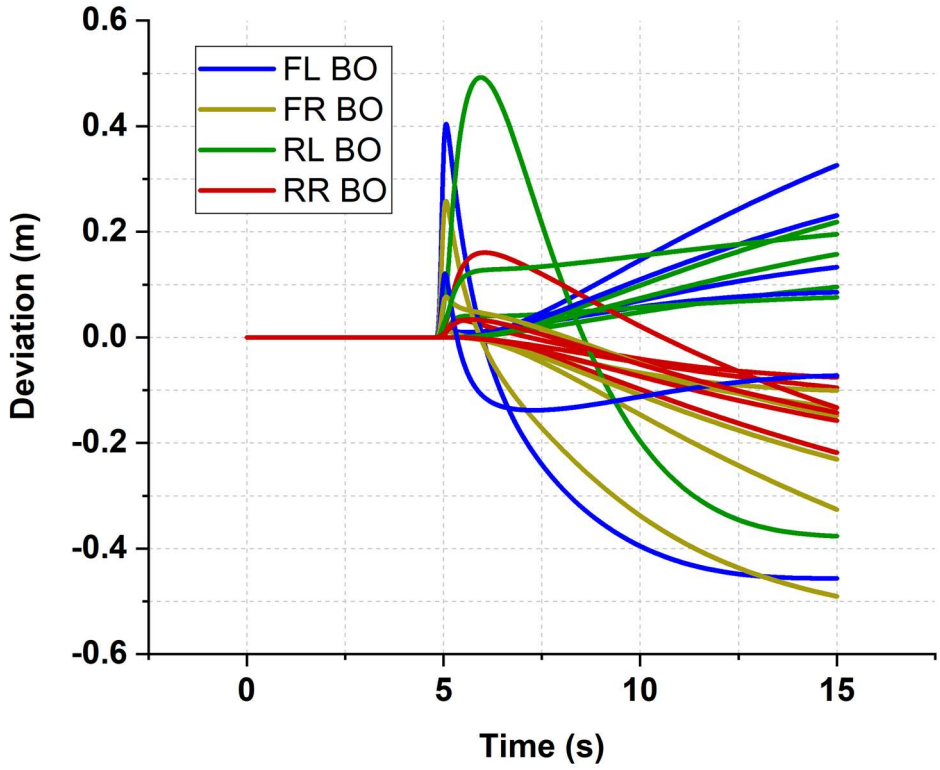

Figure 3.19. Lateral Deviations Of The Closed-Loop System for a Single Actuator

Again, the lateral deviation of the vehicle path from its respective desired trajectory measured from the lane center is demonstrated in Figure 3.19 for the multi-actuator controller. The closed-loop system is evaluated for three vehicle speeds: 80 km/hr, 120 km/hr, and 160 km/hr during both straight-line and curvilinear maneuvers. Obviously, the controller keeps the lateral deviations within reasonable values.

3.3.4 Single Actuator and Multi-actuator Comparison

There are several methodologies to induce a controlled stabilizing yaw moment by applying wheel torque either using an individual wheel torque or by multi-wheel torques. Superior tracking performance can be gained from the multi-wheel approach compared with single wheel torque [20]. In addition, using the multi-wheel torques approach, the control demand required from the actuator cannot be supplied by a single actuator in certain circumstances. On the other hand, the multi-wheel techniques technique suffers from some drawbacks, such as redundancy control and the computational burden associated with the optimization algorithms for the torque distribution among the wheels. Figure 3.20 shows the control demand needed in the cases of the single actuator and multi-actuator for the rear right tire blow scenario. Obviously, in the single actuator case, the input torque required from the actuator (front left wheel in this case) is higher than the individual control demand of each wheel. In fact, supplying the needed torque by the actuator is questionable (and unachievable in the case of an outer rear tire blowout) in the case of the single actuator control approach. However, in the multi-actuator approach, the control torque input required from the three wheels is moderate and is an onboard-achievable for passenger/commercial vehicle scale. Moreover, multi-actuator control achieves better tracking performance in comparison with the single actuator approach. This is clear in Figure 3.21 which illustrates the lateral deviations for the rear right tire blowout event with vehicle speeds of 80, 120, and 160 km/hr, where the lateral deviations for the multi-actuator control are smaller in magnitude compared with their single actuator counterparts.

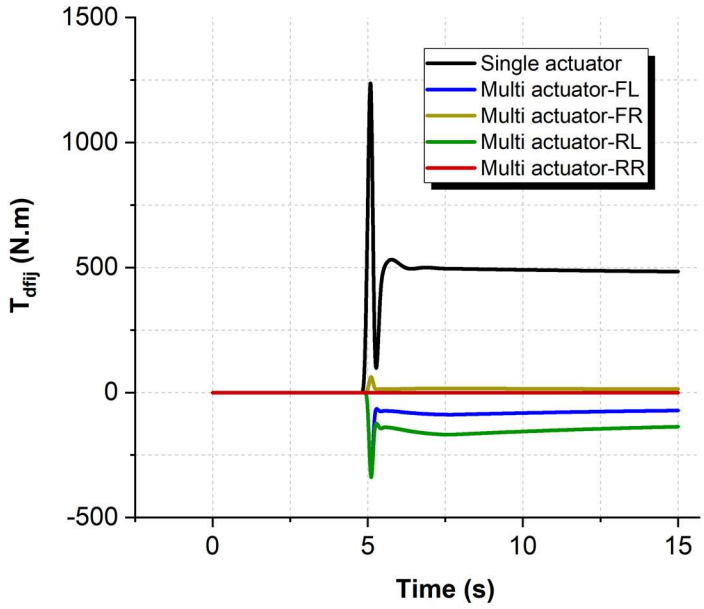

Figure 3.20. Input Torque Required From the Actuator for Single and Multi-Actuator Cases in A Rear Right Tire Blowout Event

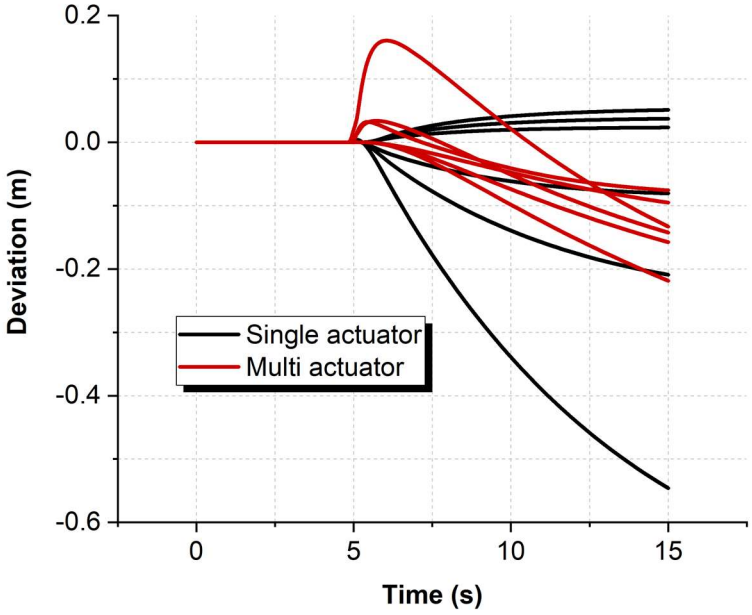

Figure 3.21. Deviations for Single and Multi-Actuator Controllers in a Rear Right Tire Blowout Event

3.3.5 Braking Torque Control

In the previous two sections, the system requires an actuator that is capable to supply positive and negative torques. In the differential braking systems, the stabilizing moment is induced using braking-only actuator. To apply the proposed controller in the context of differential braking, a new technique is introduced in this study to tackle this problem. The idea is to activate the front braking torque opposite to the flat tire. At any instance, if the system demands extra tractive torque, the controller activates a secondary braking torque input using one of the wheels opposite to the primary one excluding the flat tire. Table 3.5 presents this control strategy for all possible tire blowout cases. The blue tire indicates the primary actuator while the green tire refers to the secondary actuator.

Table 3.5. Control Strategy for the Braking Torque Controller

Front left tire blowout	
Front right tire blowout	
Rear left tire blowout	
Rear right tire blowout	

In all cases, the braking input control demand is governed by the general equation

$$\begin{aligned}
&\frac{L_f}{I_z}\left(\frac{-T_{bfl}-J_w\dot{\omega}_{fl}-F_{rfl}R_w}{R_w}+\frac{-T_{bfr}-J_w\dot{\omega}_{fr}-F_{rfr}R_w}{R_w}\right)sin\delta \\
&\quad+\frac{L_w}{2I_z}\left(\frac{-T_{bfr}-J_w\dot{\omega}_{fr}-F_{rfr}R_w}{R_w}-\frac{-T_{bfl}-J_w\dot{\omega}_{fl}-F_{rfl}R_w}{R_w}\right)cos\delta \\
&\quad+\frac{L_w}{2I_z}\left(\frac{-T_{brr}-J_w\dot{\omega}_{rr}-F_{rrr}R_w}{R_w}-\frac{-T_{brl}-J_w\dot{\omega}_{rl}-F_{rrl}R_w}{R_w}\right) \\
&\quad=-\frac{K}{a_1}|s|^{\alpha}sat\left(\frac{s}{\eta}\right)-\frac{a_2}{a_1}\left[\left(\dot{\psi}-\dot{\psi}_{ref}\right)+\left(\beta-\beta_{ref}\right)\right] \\
&\quad-\frac{a_3}{a_1}\left(\int\left[\left(\dot{\psi}-\dot{\psi}_{ref}\right)+\left(\beta-\beta_{ref}\right)\right]dt\right)+\ddot{\psi}_{ref}+\dot{\beta}_{ref}-\frac{v_x\dot{v}_y-v_y\dot{v}_x}{v_x^2+v_y^2} \\
&\quad-\frac{L_f}{I_z}\left(F_{bfl}+F_{bfr}\right)cos\delta+\frac{L_r}{I_z}\left(F_{brl}+F_{brr}\right)-\frac{L_w}{2I_z}\left(F_{bfl}-F_{bfr}\right)sin\delta
\end{aligned} \tag{3.39}$$

Control parameters used in the simulation are identical to the single-wheel tractive torque controller, and they are presented in Table 3.2. Figure 3.22 shows the closed-loop system response along with the control input demand for the braking torque controller. Obviously, the proposed braking controller significantly enhances the tracking performance of the system.

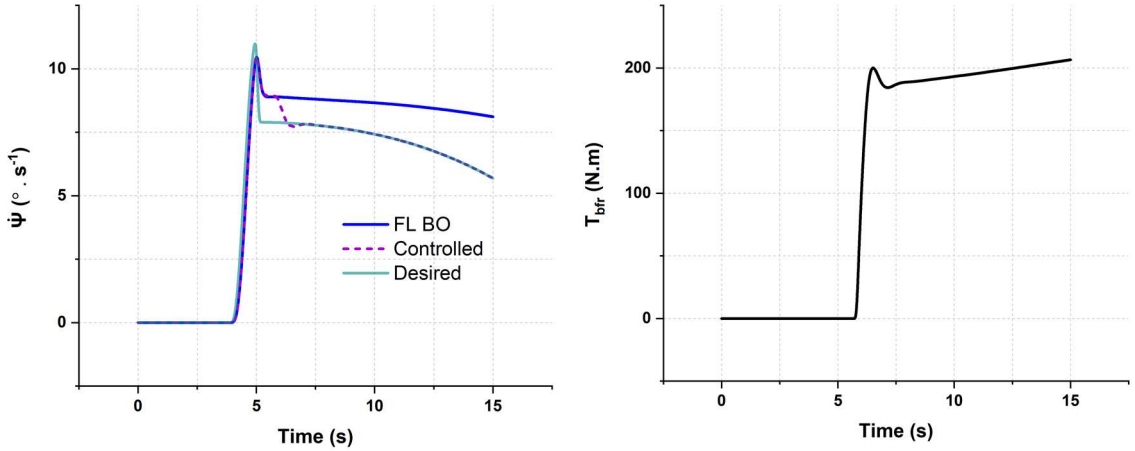

(a)

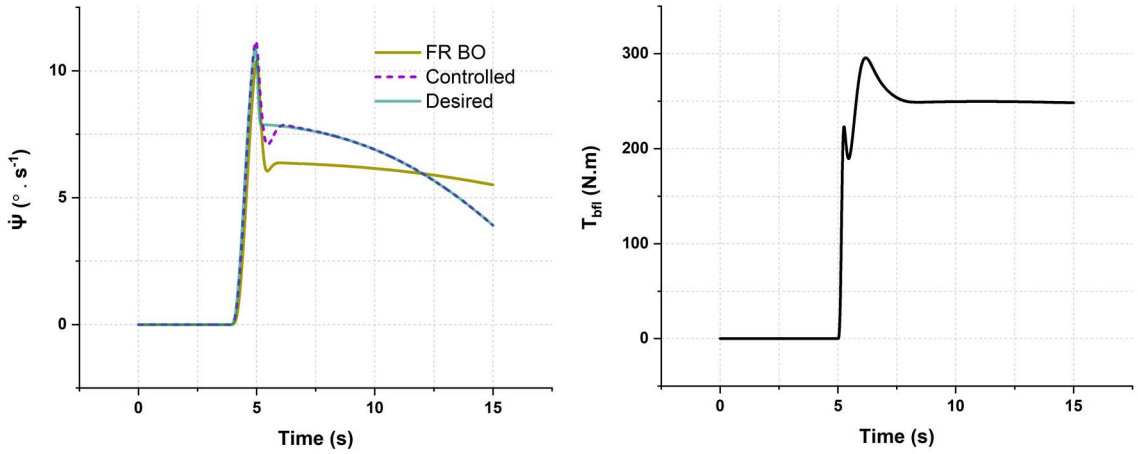

(b)

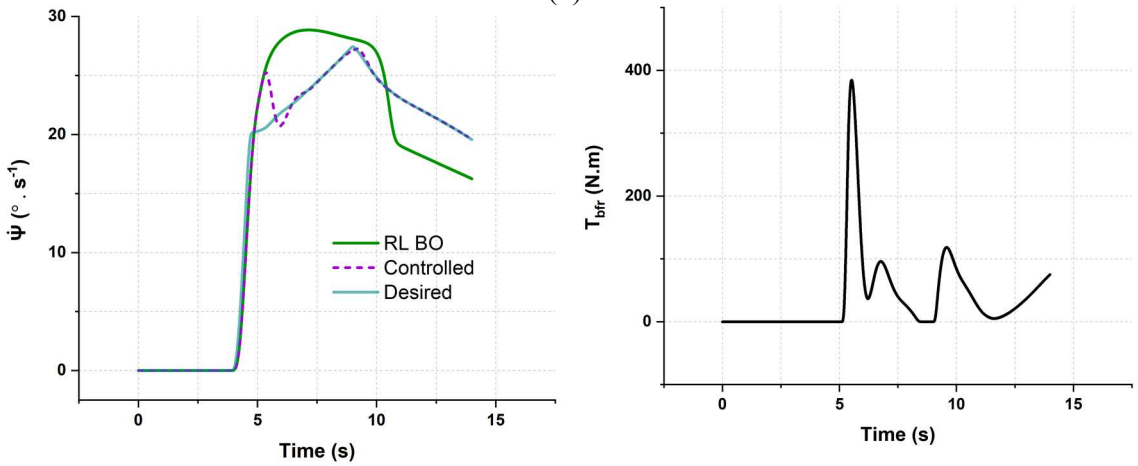

(c)

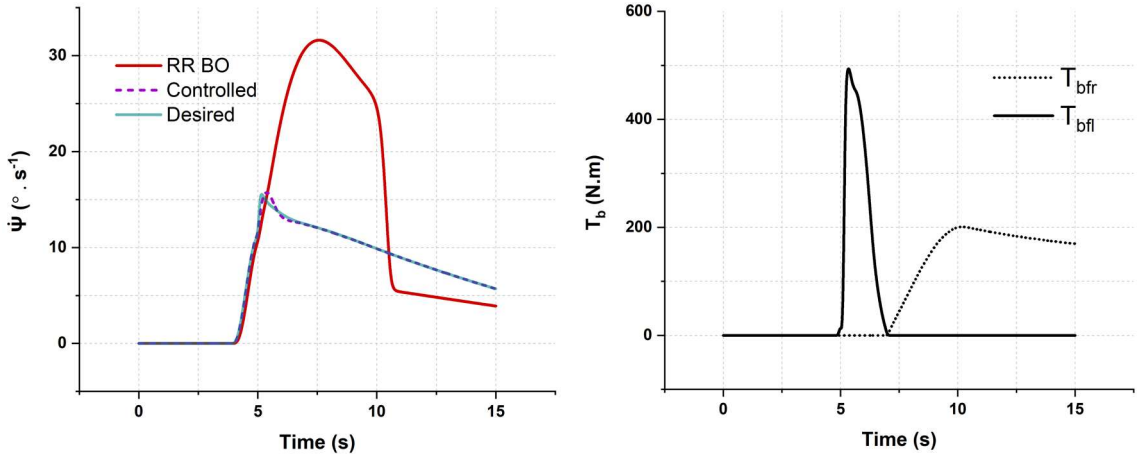

(d)

Figure 3.22. Distributive Braking Torque Control Results (A) FL (B) FR (C) RL (D) RR

3.4 Comparison with the PID Controller

To show the advantages of utilizing the nonlinear seven degrees of freedom model over the single-track model, using a ramp steering input, the handling diagrams for the single-track model, the seven degrees of freedom model, and MSC Adams model are plotted in Figure 3.23 For small accelerations, all three models exhibit quite similar behavior. Nevertheless, as the lateral acceleration increases, the bicycle model starts to deviate while the nonlinear model continues to have a trend analogous to the full vehicle model.

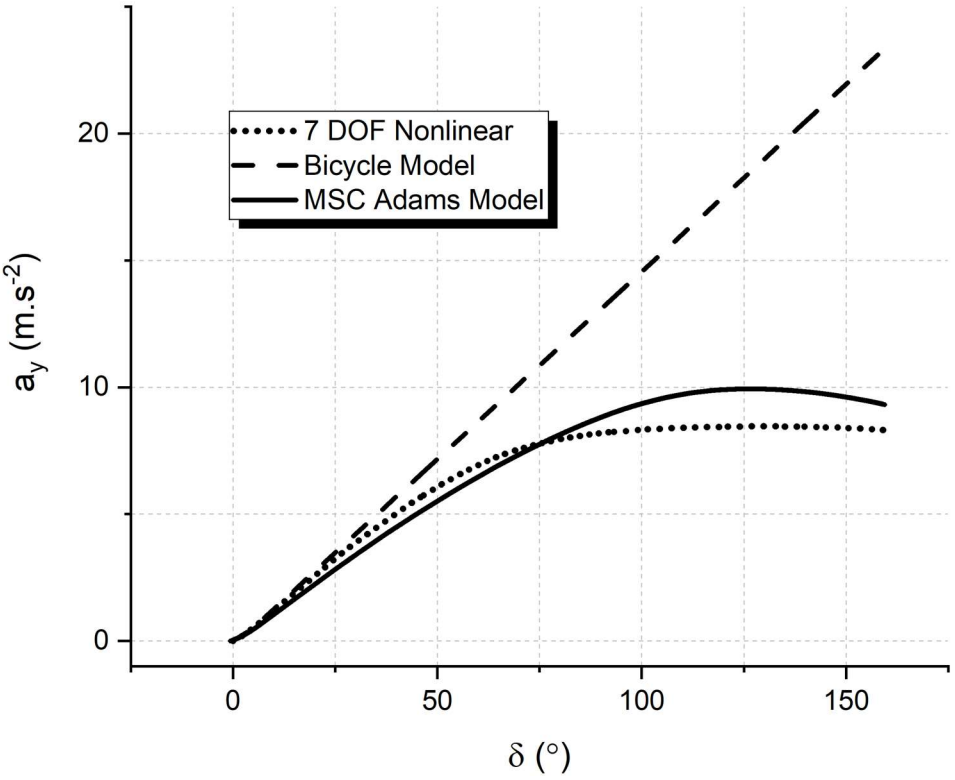

Figure 3.23. Handling Diagrams for Bicycle Model, 7 DOF Nonlinear Model, and MSC Adams Model

As previously stated, the presented mathematical model of the vehicle is a novel control-oriented model. No benchmark case was found in the literature for the purpose of performance comparison of the proposed safety controller. Therefore, a comparative analysis of proposed DISMC with conventional Proportional Integral Derivative (PID) has been conducted. PID controller has dominated the practical engineering systems for decades. It has a simple structure consisting of the linear combination of the error between the actual states and their corresponding desired states through proportional, integral, and derivative gains that can be conveniently tuned. Nevertheless, the conventional PID controller is a linear technique and it is predominantly valid near the equilibrium point the system is linearized around. In addition, unless self-learning strategies are used, the PID controller has difficulties in handling systems with varying parameters like the vehicle which can move with different velocities for instance. The Implemented PID controller is tuned using the trial and error method.

3.4.1 Straight-Line Motion

It has been observed during the straight-line motion that the PID tracks the desired reference. Figure 3.24 illustrates the sideslip angle and yaw rate responses of the vehicle for open-loop and closed-loop systems of the vehicle under the action of the PID controller in the case of the front left tire blowout. In comparison to the proposed DISMC, the PID controller depicts larger overshoots and a longer time to approach the target states. In fact, from a safety perspective, these overshoots cannot be ignored in a heavily congested road.

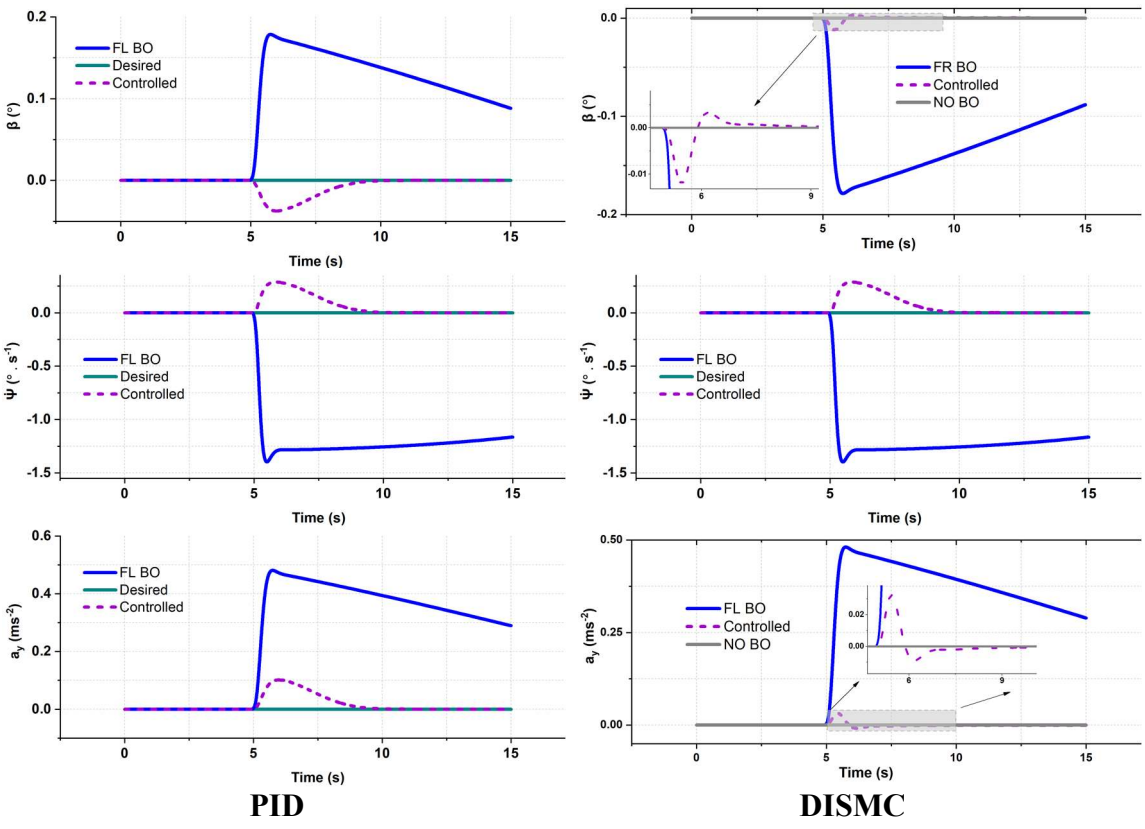

Figure 3.24. PID-DISMC Performance During Straight-Line Motion

3.4.2 Cornering Motion

Unsurprisingly, equilibrium points of the systems change during the curvilinear motion. Sideslip angle and yaw rate time evolution during a cornering maneuver with the front left tire blowout are presented in Figure 3.25. It is apparent that the PID controller fails to track the desired reference. The overshoots and recovery time are too large to be even considered.

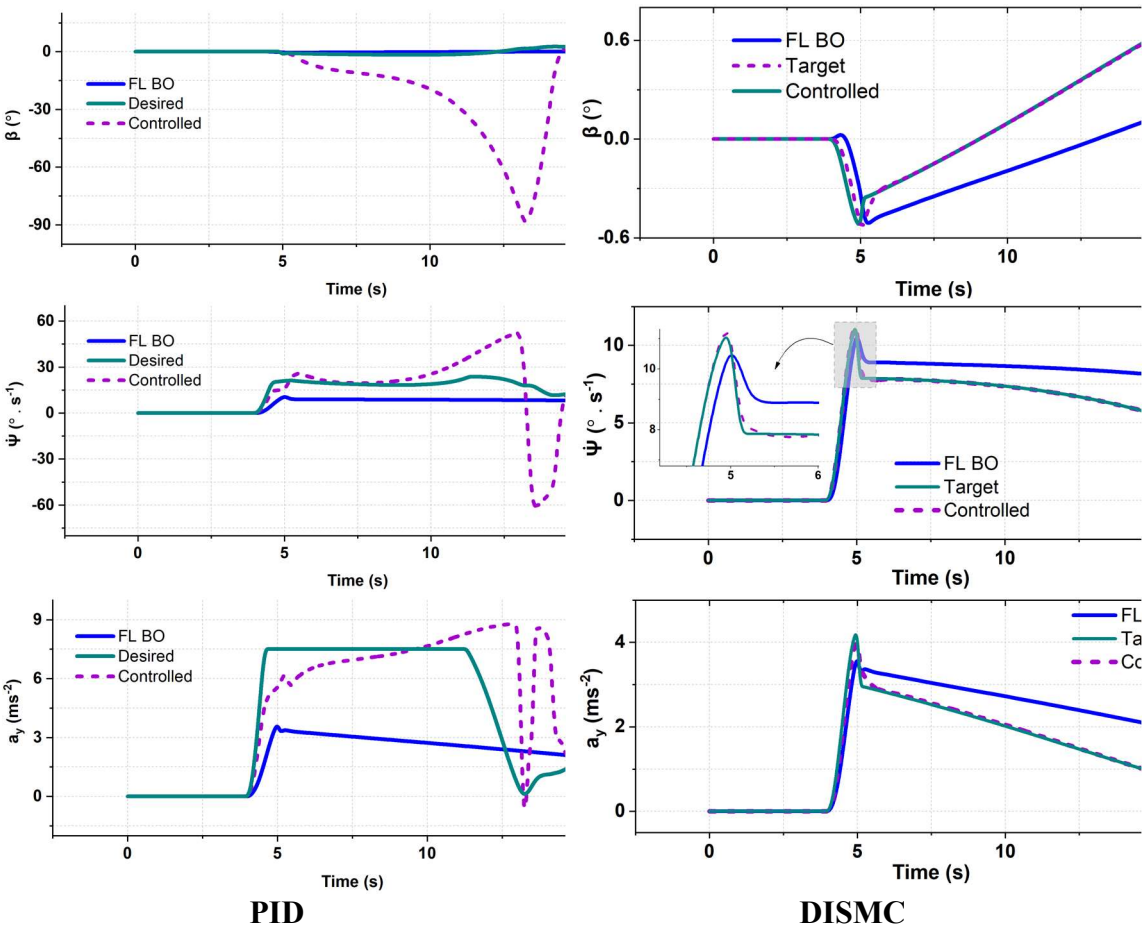

Figure 3.25. PID-DISMC Performance During Cornering Motion

Taken together, these results suggest that the DISMC outperforms the conventional PID controller. This emphasizes the need for such a nonlinear, fast, and robust controller due to its fast convergence as well as its ability to cater to parametric uncertainties.

3.5 Vehicle Control Using AFS- A Preliminary Study

Active front steering techniques can also be implemented to improve the handling stability of the vehicle. In this section, a preliminary study aiming to design an AFS to

stabilize the vehicle experiences a tire blowout is introduced. This AFS controller will be further enhanced and may be integrated with the DYC for a more optimal solution.

In order to build a simpler controller using the well-developed linear control theory, the system presented in chapter three can be linearized about the operating points. The linear tire model governing equations can be expressed as:

$$F_{aij} = C_a \sigma_{ij} \tag{3.40}$$

$$F_{bij} = C_b \alpha_{ij} \tag{3.41}$$

Where

$$\sigma_{ij} = \frac{R_w \omega_{ij} - v_{xij}}{\max\left(R_w \omega_{ij}, v_{xij}\right)} \tag{3.42}$$

$$\alpha_{ij} = \frac{-v_{yij}}{v_{xij}} \tag{3.43}$$

Using the linear tire model, the nonlinear model of the vehicle is linearized using Taylor series approximation around the equilibrium points $v_y^*, \dot{\psi}^*, \omega_{ij}^*$, the state space system for the linearized model is $\dot{x} = Ax + Bu$, where the Jacobian matrices *A* and *B* are represented by

A

$$= \begin{bmatrix} \frac{\partial \dot{v}_x}{\partial v_x} & \frac{\partial \dot{v}_x}{\partial v_y} & \frac{\partial \dot{v}_x}{\partial \dot{\psi}} & \frac{\partial \dot{v}_x}{\partial \omega_{fl}} & \frac{\partial \dot{v}_x}{\partial \omega_{fr}} & \frac{\partial \dot{v}_x}{\partial \omega_{rl}} & \frac{\partial \dot{v}_x}{\partial \omega_{rl}} \\ \frac{\partial \dot{v}_y}{\partial v_x} & \frac{\partial \dot{v}_y}{\partial v_y} & \frac{\partial \dot{v}_y}{\partial \dot{\psi}} & \frac{\partial \dot{v}_y}{\partial \omega_{fl}} & \frac{\partial \dot{v}_y}{\partial \omega_{fr}} & \frac{\partial \dot{v}_y}{\partial \omega_{rl}} & \frac{\partial \dot{v}_y}{\partial \omega_{rl}} \\ \frac{\partial \ddot{\psi}}{\partial v_x} & \frac{\partial \ddot{\psi}}{\partial v_y} & \frac{\partial \ddot{\psi}}{\partial \dot{\psi}} & \frac{\partial \ddot{\psi}}{\partial \omega_{fl}} & \frac{\partial \ddot{\psi}}{\partial \omega_{fr}} & \frac{\partial \ddot{\psi}}{\partial \omega_{rl}} & \frac{\partial \ddot{\psi}}{\partial \omega_{rl}} \\ \frac{\partial \dot{\omega}_{fl}}{\partial v_x} & \frac{\partial \dot{\omega}_{fl}}{\partial v_y} & \frac{\partial \dot{\omega}_{fl}}{\partial \dot{\psi}} & \frac{\partial \dot{\omega}_{fl}}{\partial \omega_{fl}} & \frac{\partial \dot{\omega}_{fl}}{\partial \omega_{fr}} & \frac{\partial \dot{\omega}_{fl}}{\partial \omega_{rl}} & \frac{\partial \dot{\omega}_{fl}}{\partial \omega_{rl}} \\ \frac{\partial \dot{\omega}_{fr}}{\partial v_x} & \frac{\partial \dot{\omega}_{fr}}{\partial v_y} & \frac{\partial \dot{\omega}_{fr}}{\partial \dot{\psi}} & \frac{\partial \dot{\omega}_{fr}}{\partial \omega_{fl}} & \frac{\partial \dot{\omega}_{fr}}{\partial \omega_{fr}} & \frac{\partial \dot{\omega}_{fr}}{\partial \omega_{rl}} & \frac{\partial \dot{\omega}_{fr}}{\partial \omega_{rl}} \\ \frac{\partial \dot{\omega}_{rl}}{\partial v_x} & \frac{\partial \dot{\omega}_{rl}}{\partial v_y} & \frac{\partial \dot{\omega}_{rl}}{\partial \dot{\psi}} & \frac{\partial \dot{\omega}_{rl}}{\partial \omega_{fl}} & \frac{\partial \dot{\omega}_{rl}}{\partial \omega_{fr}} & \frac{\partial \dot{\omega}_{rl}}{\partial \omega_{rl}} & \frac{\partial \dot{\omega}_{rl}}{\partial \omega_{rl}} \\ \frac{\partial \dot{\omega}_{rr}}{\partial v_x} & \frac{\partial \dot{\omega}_{rr}}{\partial v_y} & \frac{\partial \dot{\omega}_{rr}}{\partial \dot{\psi}} & \frac{\partial \dot{\omega}_{rr}}{\partial \omega_{fl}} & \frac{\partial \dot{\omega}_{rr}}{\partial \omega_{fr}} & \frac{\partial \dot{\omega}_{rr}}{\partial \omega_{rl}} & \frac{\partial \dot{\omega}_{rr}}{\partial \omega_{rl}} \end{bmatrix}_{v_x^*, v_y^*, \dot{\psi}^*, \omega_{fl}^*, \omega_{fr}^*, \omega_{rl}^*, \omega_{rr}^*} \tag{3.44}$$

$$B = \begin{bmatrix} \frac{\partial \dot{v}_x}{\partial T_{bfl}} & \frac{\partial \dot{v}_x}{\partial T_{bfr}} & \frac{\partial \dot{v}_x}{\partial T_{brl}} & \frac{\partial \dot{v}_x}{\partial T_{brr}} & \frac{\partial \dot{v}_x}{\partial \delta} \\ \frac{\partial \dot{v}_y}{\partial T_{bfl}} & \frac{\partial \dot{v}_y}{\partial T_{bfr}} & \frac{\partial \dot{v}_y}{\partial T_{brl}} & \frac{\partial \dot{v}_y}{\partial T_{brr}} & \frac{\partial \dot{v}_y}{\partial \delta} \\ \frac{\partial \ddot{\psi}}{\partial T_{bfl}} & \frac{\partial \ddot{\psi}}{\partial T_{bfr}} & \frac{\partial \ddot{\psi}}{\partial T_{brl}} & \frac{\partial \ddot{\psi}}{\partial T_{brr}} & \frac{\partial \ddot{\psi}}{\partial \delta} \\ \frac{\partial \dot{\omega}_{fl}}{\partial T_{bfl}} & \frac{\partial \dot{\omega}_{fl}}{\partial T_{bfr}} & \frac{\partial \dot{\omega}_{fl}}{\partial T_{brl}} & \frac{\partial \dot{\omega}_{fl}}{\partial T_{brr}} & \frac{\partial \dot{\omega}_{fl}}{\partial \delta} \\ \frac{\partial \dot{\omega}_{fr}}{\partial T_{bfl}} & \frac{\partial \dot{\omega}_{fr}}{\partial T_{bfr}} & \frac{\partial \dot{\omega}_{fr}}{\partial T_{brl}} & \frac{\partial \dot{\omega}_{fr}}{\partial T_{brr}} & \frac{\partial \dot{\omega}_{fr}}{\partial \delta} \\ \frac{\partial \dot{\omega}_{rl}}{\partial T_{bfl}} & \frac{\partial \dot{\omega}_{rl}}{\partial T_{bfr}} & \frac{\partial \dot{\omega}_{rl}}{\partial T_{brl}} & \frac{\partial \dot{\omega}_{rl}}{\partial T_{brr}} & \frac{\partial \dot{\omega}_{rl}}{\partial \delta} \\ \frac{\partial \dot{\omega}_{rr}}{\partial T_{bfl}} & \frac{\partial \dot{\omega}_{rr}}{\partial T_{bfr}} & \frac{\partial \dot{\omega}_{rr}}{\partial T_{brl}} & \frac{\partial \dot{\omega}_{rr}}{\partial T_{brr}} & \frac{\partial \dot{\omega}_{rr}}{\partial \delta} \end{bmatrix}_{v_x^*, v_y^*, \dot{\psi}^*, \omega_{fl}^*, \omega_{fr}^*, \omega_{rl}^*, \omega_{rr}^*} \tag{3.45}$$

The state vector is $\begin{bmatrix} v_x & v_y & \dot{\psi} & \omega_{fl} & \omega_{fr} & \omega_{rl} & \omega_{rr} \end{bmatrix}^T$ and the vector of inputs is $\begin{bmatrix} T_{bfl} & T_{bfr} & T_{brl} & T_{brr} & \delta \end{bmatrix}^T$.

For the given numerical values for the vehicle and tire, it is possible to find the matrices *A* and *B* around a particular equilibrium point. Equilibrium points can be determined at a specific longitudinal velocity and steering angle. For instance, at zero steering angle, zero yaw lateral velocity, zero yaw rate, and $v_x{}^* = 20\ m/s$ and $\omega_{fl}^* = \omega_{fr}^* = \omega_{rl}^* = \omega_{rr}^* = v_x/R_w$, the following *A* and *B* matrices can be obtained

$$A = \begin{bmatrix} -16.322 & 0 & 0 & 1.330 & 1.330 & 1.330 & 1.330 \\ 0 & -17.26 & -23.452 & 0 & 0 & 0 & 0 \\ 0 & -3.934 & -44.328 & -1.1824 & 1.1824 & -1.1824 & 1.1824 \\ 2018.562 & -22.086 & -1588.823 & -661.163 & 1.037 & 1.037 & 1.037 \\ 2018.562 & -22.086 & 1588.823 & 1.037 & -661.163 & 1.037 & 1.037 \\ 2018.562 & -22.086 & -1588.823 & -1.037 & -1.037 & -663.238 & -1.037 \\ 2018.562 & -22.086 & 1588.823 & -1.037 & -1.037 & -1.037 & -663.238 \end{bmatrix}$$

and

$$B = \begin{bmatrix} 0 & 0 & 0 & 0 & 0 \\ 0 & 0 & 0 & 0 & 345.2 \\ 0 & 0 & 0 & 0 & 582.19 \\ -1 & 0 & 0 & 0 & 441.72 \\ 0 & -1 & 0 & 0 & -441.72 \\ 0 & 0 & -1 & 0 & 441.72 \\ 0 & 0 & 0 & -1 & -441.72 \end{bmatrix}$$

The advantage of such representation is that it can be used to build an AFS, a DYC, or coordinated controllers through a judicious interplay between AFS and DYC. Nevertheless, in this study, an AFS controller is considered. Therefore, the B matrix is a column vector.

The derivation of the control law is according to the procedure of solving the linear quadratic tracking problem is given in [99, 100] and introduced here. The error vector is assumed to be

$$e(t) = z(t) - y(t) = z(t) - Cx(t) \tag{3.46}$$

Where $z(t)$ is the desired output vector defined in equations 3.29 and 3.30. The performance index is defined as

$$J = \frac{1}{2}\int_{t_0}^{t_f} [e(t)^T Q\, e(t) + u(t)^T R\, u(t)]dt \tag{3.47}$$

Where Q is a symmetric positive semi-definite error weighting matrix, R is a symmetric positive definite input weighting matrix, and *u* is the input. The Hamiltonian can be formulated as

$$H\big(x(t), u(t), \lambda(t)\big) = \frac{1}{2}[z - Cx]^T Q[z - Cx] + \frac{1}{2}u^T Ru + \lambda^T[Ax + Bu \tag{3.48}$$

Where λ is the costate vector. The open-loop optimal control, optimal state, and optimal costate equations are determined by

$$\begin{aligned} \frac{\partial H}{\partial u} = 0 \longrightarrow Ru + B^T\lambda = 0 \longrightarrow u^* \\ = -R^{-1}B^T\lambda^* \end{aligned} \tag{3.49}$$

$$\begin{aligned} \frac{\partial H}{\partial \lambda} = \dot{x} \longrightarrow \dot{x} = Ax + Bu \longrightarrow \dot{x}^* \\ = Ax^* - BR^{-1}B^T\lambda^* \end{aligned} \tag{3.50}$$

$$\frac{\partial H}{\partial x} = -\dot{\lambda}^* \longrightarrow -C^T QCx^* - A^T\lambda^* + C^T Qz \tag{3.51}$$

Combining the state-costate system, we get the Hamiltonian canonical system:

$$\begin{bmatrix}\dot{x}^* \\ \dot{\lambda}^*\end{bmatrix} = \begin{bmatrix}A & -BR^{-1}B^T \\ -C^TQC & -A^T\end{bmatrix}\begin{bmatrix}x^* \\ \lambda^*\end{bmatrix} + \begin{bmatrix}0 \\ C^TQ\end{bmatrix}z \tag{3.52}$$

This solution is valid for LTV and LTI systems as well as finite-time and infinite-time trackers. The term C^TQz in the right-hand side of equation 3.52 makes the ODE system nonhomogeneous. To solve this system, affine relation between the state and costate is assumed in the form

$$\lambda^* = Px^* - g \tag{3.53}$$

Where the matrix P and the vector g are to be determined. Differentiating with respect to time gives

$$\dot{\lambda}^* = \dot{P}x^* + P\dot{x}^* - \dot{g} \tag{3.54}$$

Substituting in the Hamiltonian system gives the following matrix differential Riccati equation, auxiliary vector differential equation, and the optimal state can be solved from

$$\dot{P} + PA + A^TP - PBR^{-1}B^TP + C^TQC = 0 \tag{3.55}$$

$$\dot{g}(t) = [PBR^{-1}B^T - A^T]g(t) - C^TQz(t) \tag{3.56}$$

$$\dot{x}^*(t) = [A - BR^{-1}B^TP]x^*(t) + BR^{-1}B^Tg(t) \tag{3.57}$$

The initial and final split boundary conditions for the above equations are:

$$p(t_f) = 0$$
$$g(t_f) = 0$$
$$x(t_0) = x_0$$

The solution of the boundary value optimal control problem is

$$u^*(t) = -R^{-1}B^T[Px^*(t) - g(t)] \tag{3.58}$$

Table 3.6. AFS Controller Parameters Used in Simulations

Q_{11}	1
Q_{22}	50
Q_{33}	100
Q_{44}	1
Q_{55}	1
Q_{66}	1
Q_{77}	1
Q_{ij}, $i \neq j$	0
R	1

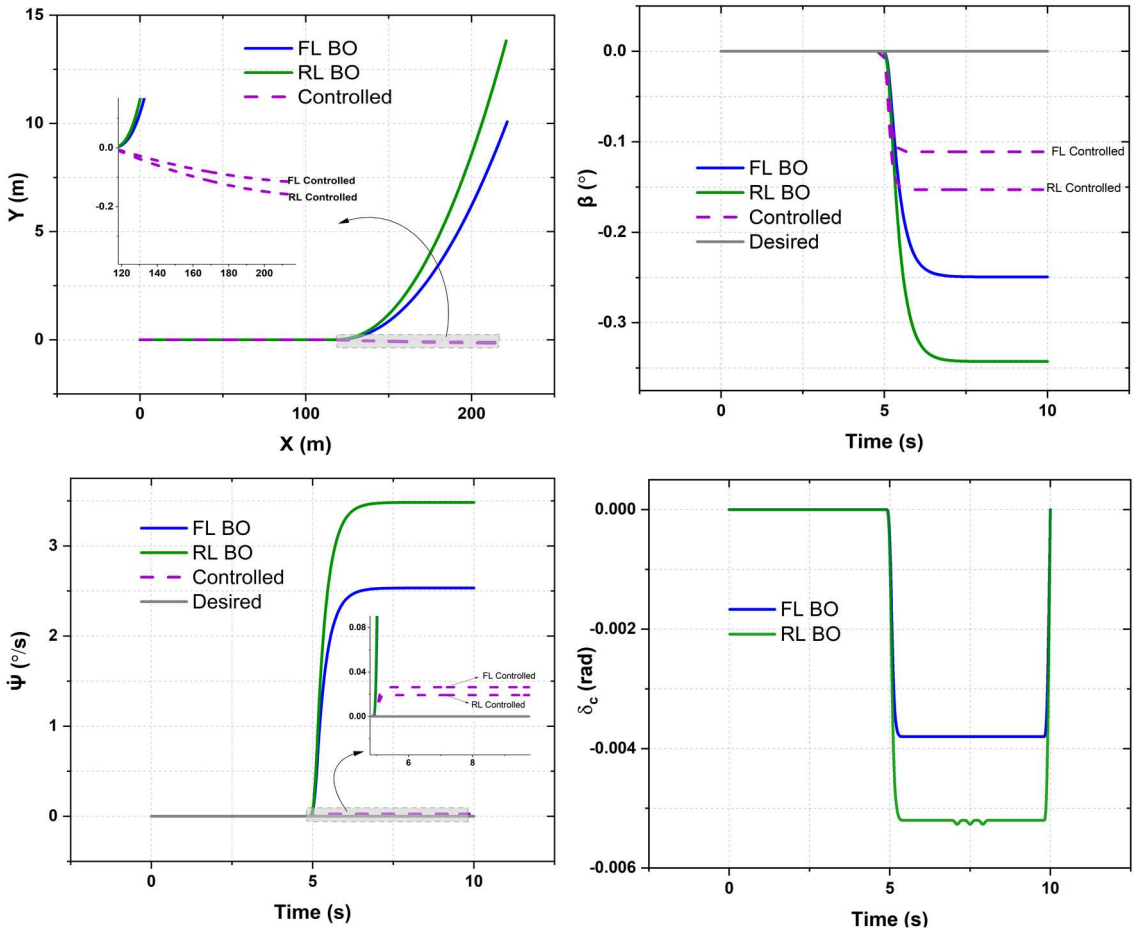

Figure 3.26. Vehicle Response With LQR Based AFS

As shown in the figure, the AFS controller can effectively reduce the profound impact of the tire blowout by manipulating the steering angle input. However, the controller is still under development to be applied for arbitrary vehicle motion.

The control system measures the input steering angle provided by the driver and adds corrections such that the vehicle follows the desired states. The total steering angle is $\delta + \delta_c$, where δ_c is the control input determined by equation 3.58.

To evaluate the proposed controller, front left and front-rear tire blowout events are conducted in straight-line motion. The controller parameters chosen in the simulation are reported in Table 3.6. Vehicle trajectory, sideslip angle, yaw rate, and control demand are recorded and presented in Figure 3.26.

CHAPTER 4

DISCUSSION, CONCLUSIONS, AND FUTURE CONSIDERATIONS

In the present study, the dynamic characteristics of a vehicle subjected to a tire blowout were investigated. Due to the high risk and high setup cost to conduct a real objective experiment, it is reasonable to carry out mathematical simulations in the early product development stage. These mathematical models and simulations are necessary prior to the actual implementation of the physical system prototype.

Along with the well-grounded nonlinear Dugoff's tire models, a three-dimensional fourteen degrees of freedom nonlinear full vehicle model was developed and validated using the high fidelity Msc Adams/car package to represent the dynamics of the vehicle. The model accounts for three-dimensional kinematic and inertial couplings between the sprung and the unsprung masses as well as the loads transmitted from the suspensions and the ground. Furthermore, the tire model accounts for the combined longitudinal and lateral slips, and the chassis model incorporates the highly-nonlinear interactions among the different degrees of freedom. A sequence of vehicle scenarios incorporating different tire blowout events was carried out. It has been found that the tire blowout affects vehicle stability dramatically and can lead to severe damages, especially at high speeds on highways. The mechanism of tire forces generation is tremendously influenced, and the most critical instability appears in the yaw direction because of the change in the tire rolling resistance. The vehicle cannot be easily controlled by the driver, especially during

cornering. Hence, the development of a safety control system to stabilize the vehicle is crucial.

The blowout was implemented using time-dependent calibrated multipliers for the tire stiffnesses and rolling resistance. The tire is integrated with a roll-handling coupled vehicle body model in a three-dimensional context. The dynamic characteristics of the vehicle subjected to a tire blowout was analyzed during both straight-line and cornering motions and for different tire blowout locations. In straight-line motion, if the vehicle is exposed to a tire blowout, it will veer in the direction of the blown tire and starts spinning. Larger deviations were observed in the case of rear tire blowouts compared with their front counterparts. On the other hand, while negotiating a turn, the vehicle experiences excessive understeer and oversteer for front and rear tire blowouts, respectively. Insignificant excitations are also observed in the bounce and pitch motions of the vehicle body as well as in the vertical motion of the unsprung mass. For a passenger car, the tire blowout does not have a significant effect on vehicle rollover. However, for sport utility vehicles (SUVs), the study showed that a rear outer tire blowout precipitates a vehicle rollover during curvilinear motion. It was also found that the vehicle is less prone to a rollover accident if the tire blowout occurs in a cross-sloped course. Furthermore, the driver can stabilize the vehicle by intervening in the motion either by steering, braking, or a combination of both. Specifically, small steering angles on the opposite side, as well as braking torque inputs, have a roll stabilizing effect. The proposed platform serves as a complete and precise picture of the three-dimensional vehicle dynamics in general and for the tire blowout as a special case. Moreover, it can be

connected to the loop as an accurate plant model to test safety control systems against the tire blowout threat. Subsequently, the study suggests that an automatic control system is needed to attenuate the blowout-induced disturbance for the in-plane motion. However, a rollover prevention control system is not required for vehicles with antiroll bars.

In order to mitigate the hazardous impacts of this phenomenon, a single front traction torque scheme has been designed and evaluated during different motion scenarios. To expand the range of applicability and exploit its inherent robustness, the controller was designed in the context of the nonlinear sliding mode controller. Instead of using the simplified single-track model, a nonlinear seven degrees of freedom vehicle model combined with the nonlinear Dugoff's tire model was utilized. The control-oriented model accounts for the longitudinal dynamics, tire and vehicle nonlinearities, large steering angle, and high lateral accelerations. In addition, the steady-state tracking performance has been enhanced by utilizing the double integral sliding mode controller. A sequence of tire blowout maneuvers has been conducted to evaluate the effectiveness of the proposed controller, both during straight-line and cornering vehicle motion. Despite the fact that this control strategy is nonoptimal in nature, the vehicle directional stability is substantially improved with insignificant slight overshoots provoked with actuator application. The proposed controller enables the vehicle to track its desired trajectories in both straight-line and cornering motions when subjected to a tire blowout. The effort from the actuators needed to stabilize the vehicle is high, especially if the tire blowout occurs in curvilinear motion. Therefore, a control allocation technique was implemented to divide the control effort among the three wheels excluding the flat tire.

The distributive controller applies a stabilizing torque to suppress the blowout-induced disturbance and robustly track the desired trajectory. The controlled torque was distributed among the three tires excluding the blown tire with prespecified contributions. Moreover, the multi- actuator technique was compared with the single actuator and showed superior performance and lower input torque demand. An additional control strategy was proposed to facilitate controller practical implementation in conventional vehicles using braking-only actuation. Furthermore, the chattering problem built in the framework of variable-structure controllers has been attenuated through the tuning of the slope of the saturation function. The proposed controller does not need additional actuators and its invariance property against external disturbances is advantageous. Finally, the performance of the proposed nonlinear controller was compared with the controllers developed with reference to the simplified model (a PID controller). The results suggested that the DISMC outperforms the conventional PID controller in terms of the convergence to the desired trajectory and the region of applicability. This emphasizes the need for such a nonlinear, fast, and robust controller to handle the consequences of the tire blowout problem.

The first step before implementing the proposed controller in a real vehicle is to build a test bench. The objective of such a test bench is to build the controller hardware and to verify its ability to exchange the dynamical information from the sensors/observers and to the actuators in real-time. In order to transmit the required vehicle state signals to the controller, the inertial measurement unit (IMU) that is equipped with accelerometers and gyros can be utilized to measure the accelerations and rotational velocities of the vehicle,

respectively. The information regarding the steering angle and the rotational speed of each wheel can also be collected using sensor measurements. However, the proposed controller needs access to the lateral and vertical tire forces as well as the vehicle sideslip angle and its derivative. Measuring the latter variables using onboard transducers is very expensive. Hence, they can be fed back to the electronic control unit (ECU) using observers. The literature contains many algorithms to estimate these vehicle parameters [3].

The electronic stability unit performs all the required calculations pertaining to the deviations from the desired values and the corrective input torque calculation and distribution, and then it transmits an output control signal to the actuators to induce the torque needed to ensure yaw stability. Such an apparatus does not require the installation of any extra sensors or actuators because all of them - apart from the tire pressure monitoring system- are already established in the ESP system. The sensor-controller and controller-actuator communications were not examined
thoroughly in this research. The existence of delays, nonlinearities, and noise during the exchange of information among these vehicle subsystems is a challenging problem in any control system, including the proposed controller.

To sum up, the contributions of the current research can be addressed as follows:

1- The design, build, and validation of an open-access, high-fidelity, comprehensive three-dimensional vehicle nonlinear dynamic model that is capable of simulating the transients associated with the tire blowout. Accordingly, a sequence of tire blowout scenarios is carried

out to analyze the handling/roll coupled dynamics. This model can be used to simulate custom vehicle events like the tire blowout easily using hand-coding. Moreover, it enables the plant-controller co-simulation to be conducted using the same platform.

2- The development and validation of a nonlinear control-oriented model that eliminates the simplifying assumptions and captures a wide range of the vehicle dynamics. The proposed control-oriented model is not limited to tire blowout control design, yet it can be used to design vehicle-handling stability controllers like electronic stability systems.

3- Introducing effective tire blowout control strategies that stabilize the vehicle and suit different vehicle platforms like conventional and electric vehicles. This was accomplished in the framework of the DISMC using the nonlinear control-oriented model. The closed-loop simulation results demonstrate the effectiveness of the developed tire-blowout control systems in both starlight line and curvilinear motion.

The results of the current work are promising and research into solving the tire blowout problem utilizing a relatively simplified linearized plant model as well as the well-developed linear control theory is already underway. Moreover, this research serves as a base for future studies which are proposed to be undertaken in the following areas:

1. Implementing and testing the proposed controller in a hardware-in-the-loop (HIL) and vehicle hardware in the loop experimentation. The hardware bench test system serves as a first step for the actual controller implementation on a real vehicle.

2. Conducting an FEA to analyze the tire forces redistribution during and after tire blowout and running an FEA-MBD-CACE 3-way cosimulation."
3. Using the proposed control-oriented model to design a nonlinear Model Predictive Control (MPC) system. MPC is a good choice for such a dynamical system because it can explicitly incorporate the system's limitations in the form of constraints (like actuator saturation for example) while minimizes the errors and the control demand by means of a cost function.
4. Integrating the proposed yaw stability control with an AFS using the same control-oriented model to reduce the control demand and improve steady-state tracking.

REFERENCES

[1] G. Mastinu and M. Plöchl, *Road and off-road vehicle system dynamics: handbook*. Boca Raton: CRC Press/Taylor & Francis Group, 2017.

[2] B. Heiring, *Chassis handbook*. Wiesbaden: Vieweg + Teubner, 2011.

[3] R. Rajamani, *Vehicle dynamics and control*. New York: Springer, 2012.

[4] H., Pacejka, I., Besselink, *Tire and Vehicle Dynamics*, Butterworth-Heinemann, Elsevier, 2006.

[5] E. Choi, "Tire-related factors in the pre-crash phase", National Highway Traffic Safety Administration, Washington DC, 2012.

[6] United States Department of Transportation. (2017). *Tires*. [online] Available at: https://www.nhtsa.gov/equipment/tires [Accessed 20 Feb. 2020].

[7] Automobile Association of the UK (2014). Tyres. [online] Available at: www.roadsafetyobservatory.com/Review/10076 [Accessed 20 Feb. 2020].

[8] J., Martin, and B., Laumon, "Tire Blow-Outs and Motorway Accidents", *Traffic Injury Prevention*, vol. 6, no. 1, pp. 53-55, 2005. Available: 10.1080/15389580490510174.

[9] G., Konghui, H., Jiang, "Analysis and Control of Vehicle Movement with Blown-out Tire", *Automotive Engineering*, vol. 29, no. 12, pp. 2014-1045, 2007.

[10] D., Franklin, "Tire Safety in the Middle East", Report published by Halliburton, 2011.

[11] S., Clark, "The *Mechanics of Pneumatic Tire*", Washington DC, US Government Printing Office, 1981.

[12] D., Thombare, "Analysis of Effect of Tire Inflation Pressure, Inflation Fluids, Load and Speed on Tire Performance," SAE Technical Paper 2019-26-0368, 2019, https://doi.org/10.4271/2019-26-0368.

[13] I. Besselink, A. Schmeitz and H. Pacejka, "An improved Magic Formula/Swift tyre model that can handle inflation pressure changes", *Vehicle System Dynamics*, vol. 48, no. 1, pp. 337-352, 2010. Available: 10.1080/00423111003748088.

[14] K. Höpping, K. Augsburg and F. Büchner, "Extending the Magic Formula Tire Model for Large Inflation Pressure Changes by Using Measurement Data from a Corner

Module Test Rig", *SAE International Journal of Passenger Cars - Mechanical Systems*, vol. 11, no. 2, pp. 103-118, 2018. Available: 10.4271/06-11-02-0009.

[15] M., Gisper, “FTire, a new fast tire model for ride comfort simulations”, *International ADAMS User’s Conference*, Berlin, Germany, 1999.

[16] M., Bäcker, V., Köttgen, and K., Dressler, “LMS CDTire model: Road load simulation on a digital test track”, *LMS Conference*, OH, US, 2002.

[17] S. Tripathi, A. K. Karwal, M. Mishra, and D. Wazir, “Effect of Tyre Inflation Pressure on Rolling Resistance: Comparing the Values of Coefficient of Rolling Resistance and Rolling Resistance at Variable Tyre Inflation Pressure,” *SAE Technical Paper Series*, 2019.

[18] A., Thiriet, F., Pujatti, and P., Araújo, “Influence of Inflation Pressure of a Tire on Rolling Resistance and Fuel Consumption,” *SAE Technical Paper Series*, 2017.

[19] A., Larocca, P., Kubo, D., Buss, D., and L., de Mello Welin, "Assessment of the Influence of Tire Inflation Pressure on the Forces Applied to a Commercial Vehicle’s Steering System," *SAE Technical Paper* 2016-36-0068, 2016, https://doi.org/10.4271/2016-36-0068.

[20] B. Shyrokau, D. Wang, L. Heidrich, and K. Hopping, “Analysis of subsystems coordination for electric vehicle during straight-line braking and brake-in-turn,” *2013 IEEE Symposium on Computational Intelligence for Engineering Solutions (CIES)*, 2013.

[21] A., Janulevicius, G., Pupinis, “Influence of uneven tire inflation pressure on vehicle dynamics during braking”, *19th Intern Scient Conf Engineering for Rural Development*, Jelgava, 2020.

[22] D. Savitski, K. Hoepping, V. Ivanov, and K. Augsburg, “Influence of the Tire Inflation Pressure Variation on Braking Efficiency and Driving Comfort of Full Electric Vehicle with Continuous Anti-Lock Braking System,” *SAE International Journal of Passenger Cars - Mechanical Systems*, vol. 8, no. 2, pp. 460–467, 2015.

[23] S. Arrigoni, F. Cheli, P. Gavardi and E. Sabbioni, "Influence of Tire Parameters on ABS Performance", *Tire Science and Technology*, vol. 45, no. 2, pp. 121-143, 2017. Available: 10.2346/tire.17.450203.

[24] M., Toma, C., Andreescu, and C., Stan, “Influence of tire inflation pressure on the results of diagnosing brakes and suspension,” *Procedia Manufacturing*, vol. 22, pp. 121–128, 2018.

[25] M., Hamed, B., Tesfa, M., Aliwan, G., Li, F., Gu and A.,Ball, "The influence of vehicle tyres pressure on the suspension system response by applying the time-frequency approach," *2013 19th International Conference on Automation and Computing*, London, 2013, pp. 1-6.

[26] S., Sassi, and A., Sassi, “Destabilising effect of tyre burst on vehicles dynamics,” *International Journal of Vehicle Systems Modelling and Testing*, vol. 10, no. 2, p. 185, 2015.

[27] M., Reiter, and J., Wagner, “Automated Automotive Tire Inflation System – Effect of Tire Pressure on Vehicle Handling,” *IFAC Proceedings Volumes*, vol. 43, no. 7, pp. 638–643, 2010.

[28] J., Wo, Z., Wang., and J., Wang, “Influence of Tire Inflation Pressure on Vehicle Dynamics and Handling Performance”, *Proceedings of the ASME 2019 Dynamic Systems and Control Conference. Volume 2: Modeling and Control of Engine and Aftertreatment Systems; Modeling and Control of IC Engines and Aftertreatment Systems; Modeling and Validation; Motion Planning and Tracking Control; Multi-Agent and Networked Systems; Renewable and Smart Energy Systems; Thermal Energy Systems; Uncertain Systems and Robustness; Unmanned Ground and Aerial Vehicles; Vehicle Dynamics and Stability; Vibrations: Modeling, Analysis, and Control*. Park City, Utah, USA. October 8–11, 2019. V002T26A003. ASME. https://doi.org/10.1115/DSCC2019-9055.

[29] J., Wu, Z. Wang, and Z. Zhao, “Influence of Tire Inflation Pressure on Vehicle Dynamics and Compensation Control on FWID Electric Vehicles,” *Journal of Dynamic Systems, Measurement, and Control*, vol. 142, no. 7, 2020.

[30] V., Cossalter, V., Favaron, E., Giolo, and T., Jomaa, "The effect of the inflation pressure of tyres on motorcycle weave stability: experiments and simulation", *Vehicle System Dynamics*, vol. 54, no. 10, pp. 1474-1490, 2016. Available: 10.1080/00423114.2016.1213863.

[31] M., Massaro, V., Cossalter and G., Cusimano, "The effect of the inflation pressure on the tyre properties and the motorcycle stability", *Proceedings of the Institution of Mechanical Engineers, Part D: Journal of Automobile Engineering*, vol. 227, no. 10, pp. 1480-1488, 2013. Available: 10.1177/0954407013496231.

[32] M., Al-Solihat, S., Rakheja and A., Ahmed, "Influence of tyre pressure on an urban bus transient and steady state handling performance", *Proceedings of the Institution of Mechanical Engineers, Part D: Journal of Automobile Engineering*, vol. 224, no. 7, pp. 893-908, 2010. Available: 10.1243/09544070jauto1402.

[33] H., Shraim, A., Rabhi, M., Ouladsine, N., Msirdi, and L., Fridman, “Estimation and Analysis of the Tire Pressure Effects on the Comportment of the Vehicle Center of Gravity,” *International Workshop on Variable Structure Systems, 2006. VSS06.*

[34] A., Brown, S., Lapapong, K., Swanson, S., Brennan, ”Modeling of planar vehicle dynamics during gradual tire deflation”, *22nd International symposium on Dynamics of Vehicles on Roads and Tracks*, Manchester, UK, 2011.

[35] K., Parczewski, “Effect of tyre inflation pressure on the vehicle dynamics during braking maneuver”, *Journal Maintenance and Reliability*, vol 15 (2), pp. 134–139, 2013.

[36] P., Stryjek, G., Motrycz, and W., Pieniążek, “Impact Of Pressure Loss In Steerable Tyre Wheel On Steerability Of Four-Axle Special Purpose Vehicle,” *Journal of Science of the Gen. Tadeusz Kosciuszko Military Academy of Land Forces*, vol. 170, no. 4, pp. 92–100, 2013.

[37] W., Blythe, T., Day, and W., Grimes, “3-Dimensional simulation of vehicle response to tire blow-outs,” SAE Publication No. 980221, 1998.

[38] R., Robinette, D., Deering, and R., Fay, “Drag and Steering Effects of Under Inflated and Deflated Tires*”, SAE Publication No. 970954*, 1997.

[39] R., Fay, R., Robinette, J., Smith, J., etc., “Drag and Steering Effects from Tire Tread Belt Separation and Loss”, *SAE Technical Paper No. 1999-01-0447*, 1999.

[40] R., Robinette, R., Fay, “Drag and Steering Effects from Disablements of Run Flat Tires”, *SAE Technical Paper No. 2000-01-1316*, 2000.

[41] Z. Lozia, “Simulation tests of biaxial vehicle motion after a ‘tire blow-out,’” *SAE Tech. Pap.*, no. April 2005, 2005, doi: 10.4271/2005-01-0410.

[42] Y. Wang and K. Guo, “Analysis of vehicle’s kinetic characteristic after tire blow-out,” *Adv. Mater. Res.*, vol. 455–456, pp. 1115–1121, 2012, doi: 10.4028/www.scientific.net/AMR.455-456.1115.

[43] K., Guo, “Analysis and control of vehicle movement with blownout tire”, *automotive engineering*, vol. 29, no. 12, pp. 1041 – 1045, 2007.

[44] A. Cornetto, F. Bayan, A. Dunn, C. Tanner, R. Wahba, J. Suway, G. J. Heydinger, K. Chakravarthy, and D. A. Guenther, “Tractor-Semitrailer Stability Following a Steer Axle Tire Blowout at Speed and Comparison to Computer Simulation Models,” *SAE Technical Paper Series*, 2013.

[45] I., Han, "Modeling the tire forces for a simulation analysis of a vehicle accident reconstruction", Automobile Engineering, vol. 231(1), pp. 16-26, 2017.

[46] C., Vichare, and S., Palanivelu, “Simulation of Heavy Commercial Vehicle Response to Rear Super Single Tire Blow Out,” *SAE Technical Paper Series*, 2017.

[47] K., Tagesson, B., Jacobson, and L., Laine, “Driver response at tyre blow-out in heavy vehicles & the importance of scrub radius,” *2014 IEEE Intelligent Vehicles Symposium Proceedings*, 2014.

[48] R., Larson, J, Cuadrado, “Heavy truck stability with a trailing axle tire blowout. SAE Technical Paper Series 2012-01-0238” *SAE International Journal of Commercial Vehicles,* 2012, doi:10.4271/2012-01-0238.

[49] D., Tandy, B., Ault, J., Colborn, and R., Pascarella, " Objective Measurement of Vehicle Steering and Handling Performance When a Tire Loses Its Air", *SAE International Journal of Passenger Cars - Mechanical Systems,* 2013.

[50] F., Orengo, M., Ray, and C., Plaxico, "Modeling tire blow-out in roadside hardware simulations using LS-DYNA", *ASME International Mechanical Engineering Congress & Exposition*. Washington DC. 2003.

[51] US Department of Transportation. Report to Congress: *National Motor Vehicle Crash Causation Survey*, No.DOT HS 811 059, 2008.

[52] D., Horak, and S., Lack, "Dynamics of Tire Blowout Events and Driver Assist System for Controlling Them", *Volume 1: Adaptive and Intelligent Systems Control; Advances in Control Design Methods; Advances in Non-Linear and Optimal Control; Advances in Robotics; Advances in Wind Energy Systems; Aerospace Applications; Aerospace Power Optimization; Assistive Robotics; Automotive 2: Hybrid Electric Vehicles; Automotive 3: Internal Combustion Engines; Automotive Engine Control; Battery Management; Bio Engineering Applications; Biomed and Neural Systems; Connected Vehicles; Control of Robotic Systems*, 2015.

[53] L., Yu, Z., Wang, N., Pan, L., Zhang, and J., Song, "Stability Control for Tire Blowout Vehicle Based on Brake by Wire System Considering Driver Operation", *Volume 3: 16th International Conference on Advanced Vehicle Technologies; 11th International Conference on Design Education; 7th Frontiers in Biomedical Devices*, 2014.

[54] E., Bolarinwa, and O., Olatunbosun, "Finite element simulation of the tyre burst test," *Proceedings of the Institution of Mechanical Engineers, Part D: Journal of Automobile Engineering*, vol. 218, no. 11, pp. 1251–1258, 2004.

[55] K., Jeong, " Prediction of Burst Pressure of a Radial Truck Tire Using Finite Element Analysis", *World Journal of Engineering and Technology*, Vol. 4, pp. 228-237, 2016.

[56] L., Vadean, R., Benoit, and L., Michel, "Tire burst phenomenon and rupture of a typical truck tire bead design", *Tire Science and Technology*, 2011.

[57] D., Barbani, M., Pierini, and N., Baldanzini, "FE modelling of a motorcycle tyre for full-scale crash Simulations", *International Journal of Crashworthiness*, 17(3), 309-318, 2012.

[58] Y., Cai, M., Zang, Y., Chen, and W., Liu, "Experiments and finite element simulations of a tyre blow-out process", *Automobile Engineering*, Vol. 228(9) 1116–1124, 2014.

[59] Y., Cai, M., Zang, and F., Duan, "Modeling and Simulation of Vehicle Responses to Tire Blowout", *Tire Science and Technology*, Vol. 43, No. 3, pp. 242-258, 2015.

[60] S., Patwardhan, H., Tan, M., and Tomizuka, M., "Experimental results of a tire-burst controller for AHS", *Control Eng. Pract*., vol. 5, no. 11, pp. 1615–1622, 1997.

[61] D., Andreatta, R., Bixel, and D., Guenther, "An Analysis of the Time Deflate a Ruptured Tire, *Accident Reconstruction Journal*, Volume 17, 29-30, 2006.

[62] S., Savaresi, M., Tanelli, P., Langthaler, P., and L., del Re, " New regressors for the direct identification of tire deformation in road vehicles via 'in-tire' accelerometers", IEEE Trans. Control Syst. Technol., vol. 16, no. 4, pp. 769–780, 2008.

[63] E., Choi, "Tire-related factors in the pre-crash phase, Nat. Highway Traffic Safety Administration", Washington, DC, USA, Tech. Rep. DOT HS 811 617, Apr. 2012.

[64] G., Tavazza, "The Prevention of Bead Dislodgement of Tires and the Importance of Limited Run Flat Capability on Safety", *Tenth Int. Technical Conf on Experimental Safety Vehicles*, Oxford, England, pp243-248,1985.

[65] R., Megalingam, C., Jayakrishnan, S., Nambiar, R., Mathews, V., Das., and P., Rao, " Automatic Pressure Maintenance System for Tyres in Automobiles to Reduce Accidents", *International Conference on VLSI Systems, Architectures, Technology and Applications*, Bangalore, India, 2016.

[66] S., Patwardhan, M., Tomizuka, W., Zhang, et al., "Theory and experiments of tire blow-out effects and hazard reduction control", *American Control Conference*, pp:1207-1209, 1994.

[67] H., Guo, F., Wang, H., Chen, D., and D., Guo, " Stability Control of Vehicle With Tire Blowout Using Differential Flatness based MPC Method", *World Congress on Intelligent Control and Automation*, pp. 2066–2071, 2012.

[68] F., Wang, H., Guo, and H., Chen, "Nonlinear Model Predictive Control of Blowout Tire Vehicles and Its Map-based Implementation", *Proceedings of the 34th Chinese Control Conference*, Hangzhou, China, 2015.

[69] Z., Hong-yu, Z., Chang-fu, and L., Hai-zhen, "Tire Blow-out Modelling and Active Braking Control Algorithm of Vehicle", *China Journal of Highway and Transport*, 25(4), pp. 147-152, 2012.

[70] H., Liu, W., Deng, C., Zong, and J., Wu, "Development of Active Control Strategy for Flat Tire Vehicles", *SAE Technical Paper 2014-01-0859*, 2014, doi:10.4271/2014-01-0859.

[71] F., Wang, H., Chen, H., Guo, and D., Cao, "Constrained H∞ control for road vehicles after a tire blow-out," *Mechatronics*, vol. 30, pp. 371–382, 2015.

[72] F., Wang, N., Hao, L., Song, and H., Chen, "Triple-step nonlinear control design for road vehicles after a tire blow-out on the highway," *2016 12th World Congress on Intelligent Control and Automation (WCICA)*, 2016.

[73] F., Wang, H., Chen, and D., Cao, "Nonlinear Coordinated Motion Control of Road Vehicles After a Tire Blowout," in *IEEE Transactions on Control Systems Technology*, vol. 24, no. 3, pp. 956-970, May 2016.

[74] F., Wang, H., Chen, K., Guo, and D., Cao, "A novel integrated approach for path following and directional stability control of road vehicles after a tire blow-out", *Mechanical Systems and Signal Processing*, vol. 93, pp. 431-444, 2017.

[75] Xulina, Xuejianfeng, and Sunjinhao, "the tire burst of automotive early-warning system design", *International Conference on Networks Security*, 2009.

[76] Q., Chen, Y., Liu, and X., Li, "Stability Control of Vehicle Emergency Braking with Tire Blowout," *International Journal of Vehicular Technology*, vol. 2014, 2014.

[77] Q., Chen, J., Weaver, J., Xu, "Research on Real-time Identification for Tire Failure", *American Journal of Mechanical Engineering*, Vol. 2, No. 3, pp. 54-57, 2014.

[78] S., Li, C., Zong, G., Chen, and L., He, " A Control Algorithm for Electric Power Steering of Tire Blowout Vehicle to Reduce the Impact Torque on Steering Wheel", *SAE Technical Paper 2013-01-1239*, https://doi.org/10.4271/2013-01-1239, 2013.

[79] Q., Chen, J., Weaver, W., Wang, "Development of Test Set for Tire Failure Emergency Braking System", *Vehicle Engineering (VE),* Volume 3, 2015.

[80] L., Yang, M., Yue, J., Wang, and W., Hou, "RMPC-Based Directional Stability Control for Electric Vehicles Subject to Tire Blowout on Curved Expressway", *Journal of Dynamic Systems, Measurement, and Control*, vol. 141, no. 4, 2018.

[81] H., Jing and Z., Liu, "Gain-scheduling robust control for a tire-blow-out road vehicle", *Proceedings of the Institution of Mechanical Engineers, Part D: Journal of Automobile Engineering*, vol. 233, no. 2, pp. 344-362, 2018.

[82] Q., Meng, C., Qian, and Z., Sun, "Finite-time stability control of an electric vehicle under tyre blowout", *Transactions of the Institute of Measurement and Control*, vol. 41, no. 5, pp. 1395-1404, 2018.

[83] Q. Meng, C. Qian, and Z. Y. Sun, "Finite-time stability control of an electric vehicle under tyre blowout," *Trans. Inst. Meas. Control*, vol. 41, no. 5, pp. 1395–1404, 2019, doi: 10.1177/0142331218780967.

[84] D., Schramm, M., Hiller, and R., Bardini, *Vehicle Dynamics: Modeling and Simulation*, Berlin, Springer, 2018.

[85] G. Genta and L. Morello, *The Automotive Chassis*. Cham: Springer International Publishing AG, 2020.

[86] J., Wagner, and J., Keane, "A strategy to verify chassis controller software-dynamics, hardware, and automation", *IEEE Transactions on Systems, Man, and*

Cybernetics - Part A: Systems and Humans, vol. 27, no. 4, pp. 480-493, 1997. Available: 10.1109/3468.594914.

[87] T., Shim, and C., Ghike, "Understanding the limitations of different vehicle models for roll dynamics studies", *Vehicle System Dynamics*, vol. 45, no. 3, pp. 191-216, 2007. Available: 10.1080/00423110600882449.

[88] A., Jahromi, R., Bhat, and W., Xie, "Integrated ride and handling vehicle model using Lagrangian quasi-coordinates", *International Journal of Automotive Technology*, vol. 16, no. 2, pp. 239-251, 2015. Available: 10.1007/s12239-015-0026-1.

[89] E., Kutluay, "Development and Demonstration of a Validation Methodology for Vehicle Lateral Dynamics Simulation Models", Ph.D. dissertation, Technischen Universität Darmstadt, 2013.

[90] *Passenger cars — Test track for a severe lane-change manoeuvre,* ISO 3888-1:2018, 2018.

[91] *Road vehicles - Lateral transient response test methods - Open-loop test methods*, ISO 7401:2003, 2003.

[92] H., Khalil, *Nonlinear control*. Boston: Pearson, 2015.

[93] J., Slotine and W. Li, *Applied nonlinear control: an introduction*. Englewood Cliffs, NJ: Prentice-Hall, 1991.

[94] T., Mo, X., Zhang, K., Fan, W., Mo, and Y., Qiu, "Design and simulation of the sliding mode controller for the vehicle blow-out process control", *International Journal of Vehicle Safety*, vol. 6, no. 4, p. 333-346, *2013. Available: 10.1504/ijvs.2013.056967.*

[95] E., Kutluay, and H., Winner, "Assessment methodology for validation of vehicle dynamics simulations using double lane change maneuver," *Proceedings Title: Proceedings of the 2012 Winter Simulation Conference (WSC)*, 2012.

[96] B., Subudhi, and S., Ge, "Sliding-Mode-Observer-Based Adaptive Slip Ratio Control for Electric and Hybrid Vehicles," in *IEEE Transactions on Intelligent Transportation Systems*, vol. 13, no. 4, pp. 1617-1626, Dec. 2012.

[97] M., Guiggiani, *The Science of Vehicle Dynamics: Handling, Braking, and Ride of Road and Race Cars*, Netherlands, Springer, 2014.

[98] M., Abe, *Vehicle handling dynamics*. Amsterdam: Elsevier, Butterworth-Heinemann, 2015.

[99] D., Naidu, Optimal control systems. Boca Raton: CRC Press, 2003.

[100] F., Lewis, V. L. Syrmos, and D. L. Vrabie, *Optimal control*. Hoboken, NJ: Wiley, 2012.

[101] H., Pacejka, and E., Bakker, "THE MAGIC FORMULA TYRE MODEL", *Vehicle System Dynamics*, vol. 21, no. 001, pp. 1-18, 1992. Available: 10.1080/00423119208969994.

[102] S., Velupillai, and L., Guvenc, "Tire Pressure Monitoring [Applications of Control]," in *IEEE Control Systems Magazine*, vol. 27, no. 6, pp. 22-25, Dec. 2007, doi: 10.1109/MCS.2007.909477.

[103] F., Wang, H., Chen, L., Guo, Y., Hu, "Predictive safety control for road vehicles after a tire blowout", Science China Information Sciences, 61(7), 2018.

[104] M., Yue, L., Yang, H., Zhang, and G., Xu, "Automated hazard escaping trajectory planning/tracking control framework for vehicles subject to tire blowout on expressway," *Nonlinear Dynamics*, vol. 98, no. 1, pp. 61–74, 2019.

[105] Y., Wand, et. al., "Path-following control of autonomous ground vehicles using triple-step model predictive control", Science China Information Sciences, 63(10), 2020.

[106] M., Aki, "Investigation of Vehicle and Driver Behaviour During Tyre Burst Using Driving Simulator," *Lecture Notes in Mechanical Engineering Advances in Dynamics of Vehicles on Roads and Tracks*, pp. 1062–1070, 2020.

[107] L. Yang, M. Yue, H. Tian, and B. Yao, "Tire blow-out control for direct drive electric vehicles using reconfiguration of torque distribution and vertical load," no. 2, 2020, doi: 10.1177/0142331219892114.

[108] A. Li, Y. Chen, X. Du and W. Lin, "Enhanced Tire Blowout Modeling Using Vertical Load Redistribution and Self-Alignment Torque", ASME Letters in Dynamic Systems and Control, vol. 1, no. 1, 2020. Available: 10.1115/1.4046314.

[109] A. Li, Y. Chen, W. Lin and X. Du, "Shared Steering Control of Tire Blowout for Ground Vehicles," *2020 American Control Conference (ACC)*, Denver, CO, USA, 2020, pp. 4862-4867, doi: 10.23919/ACC45564.2020.9147390.

[110] T., Gillespie, Fundamentals of Vehicle Dynamics, SAE International, 1992. doi: 10.4271/r-114.

[111] R. Pradhan and B. Subudhi, "Double Integral Sliding Mode MPPT Control of a Photovoltaic System," in IEEE Transactions on Control Systems Technology, vol. 24, no. 1, pp. 285-292, Jan. 2016, doi: 10.1109/TCST.2015.2420674.

[112] M. Doumiati, A. Charara, and Victorino Alessandro Corrêa, *Vehicle dynamics estimation using Kalman filtering: experimental validation*. London: ISTE, 2013.

[113] M. K. Aripin, Y. Md Sam, K. A. Danapalasingam, K. Peng, N. Hamzah, and M. F. Ismail, "A Review of Active Yaw Control System for Vehicle Handling and Stability Enhancement," *International Journal of Vehicular Technology*, vol. 2014, pp. 1–15, 2014.

[114] N. Chatrenour, H. Razmi, and H. Doagou-Mojarrad, "Improved double integral sliding mode MPPT controller based parameter estimation for a stand-alone photovoltaic system," *Energy Conversion and Management*, vol. 139, pp. 97–109, 2017.

APPENDIX A

CHATTERING ATTENUATION

Figures A1-A12 demonstrate how changing the parameter η in the saturation function term affects the chattering. Three values for η are simulated: 0.5 (which is the one chosen for the simulations in chapter 3), 1, and 1.5. The responses of the sideslip angle, yaw rate, lateral acceleration, and the input torque are shown. It can be observed that increasing η increases the chattering problem.

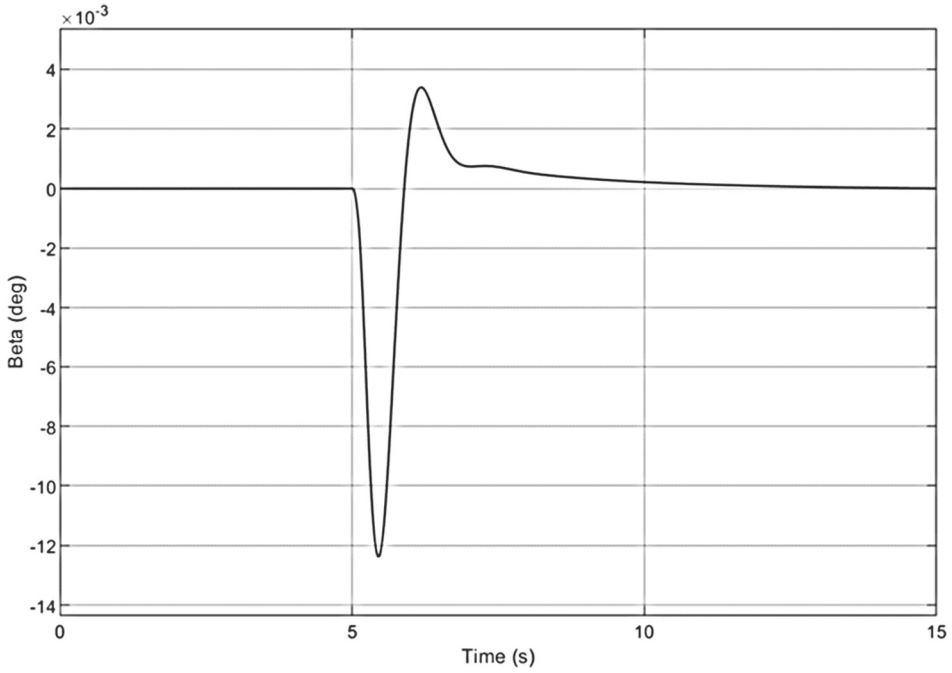

Figure A1: Sideslip Angle Response for $\eta = 0.5$

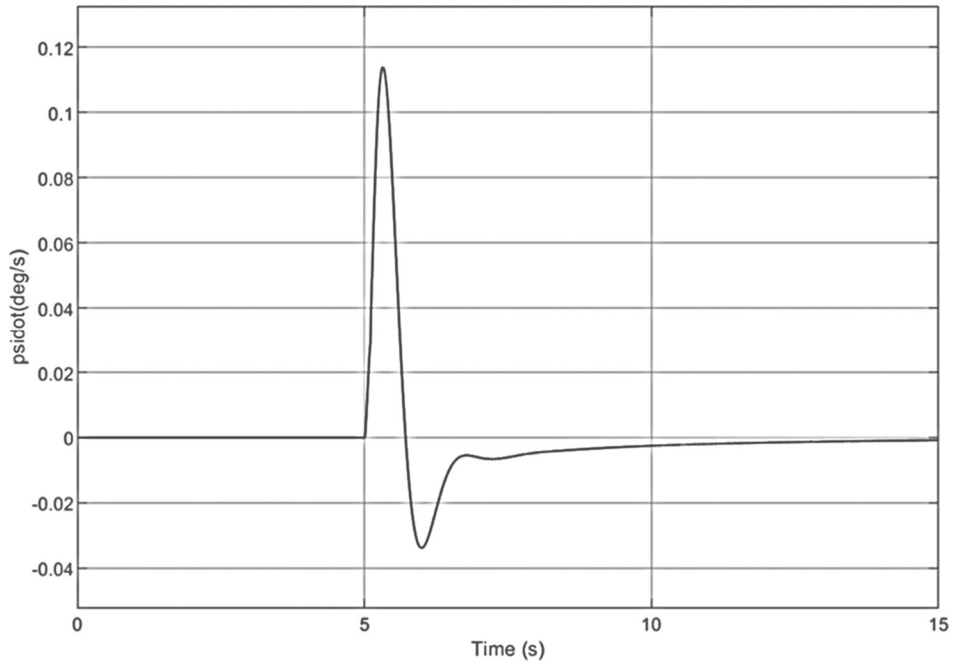

Figure A2: Yaw Rate Response for $\eta = 0.5$

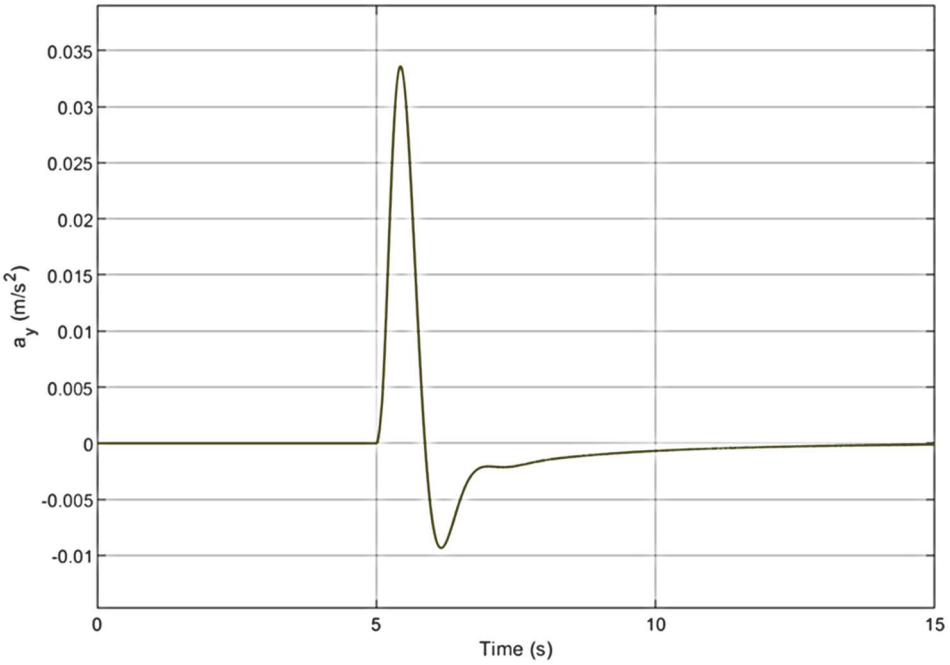

Figure A3: Lateral Acceleration Response for $\eta = 0.5$

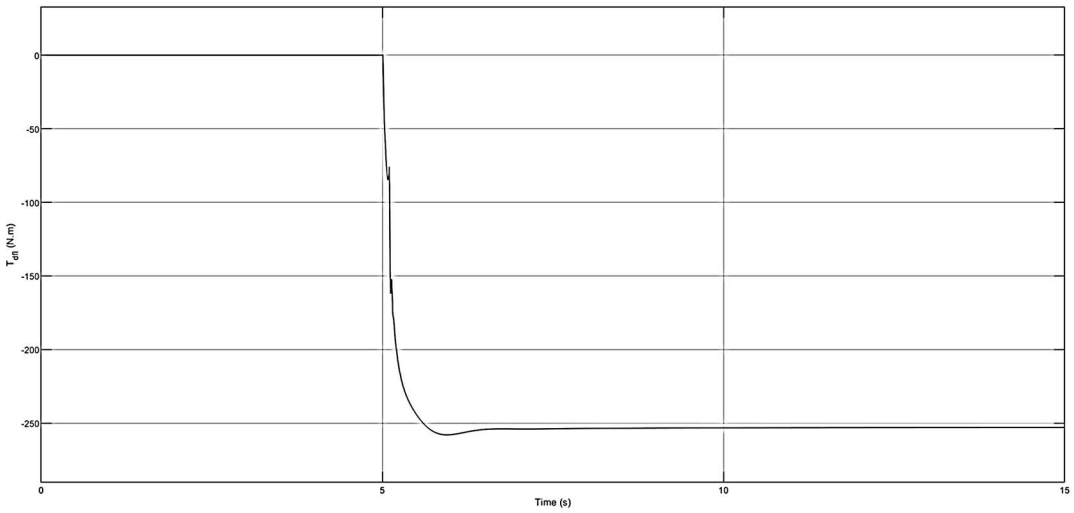

Figure A4: Torque Input Response for $\eta = 0.5$

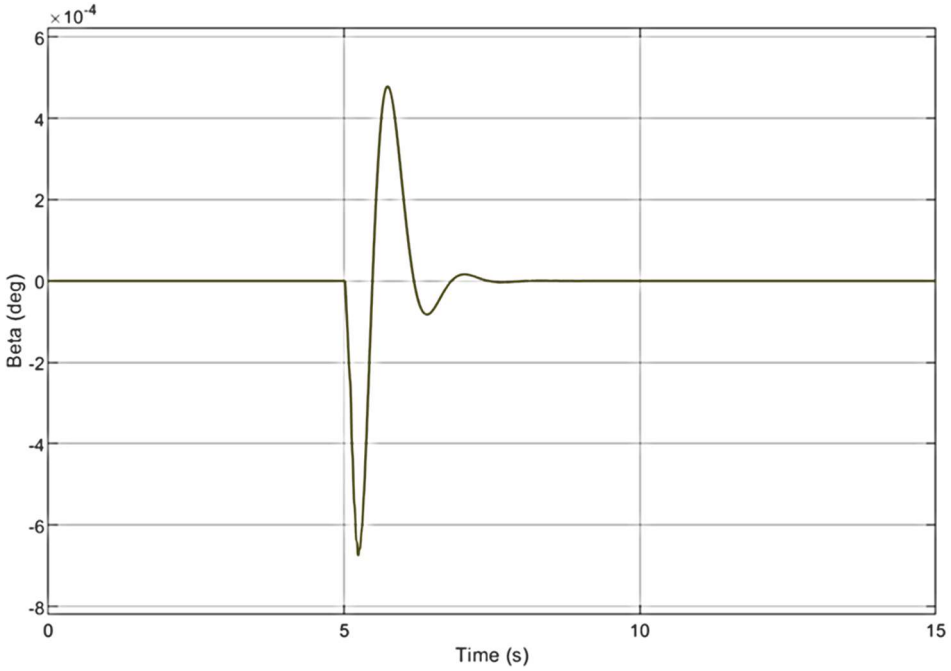

Figure A5: Sideslip Angle Response for $\eta = 1$

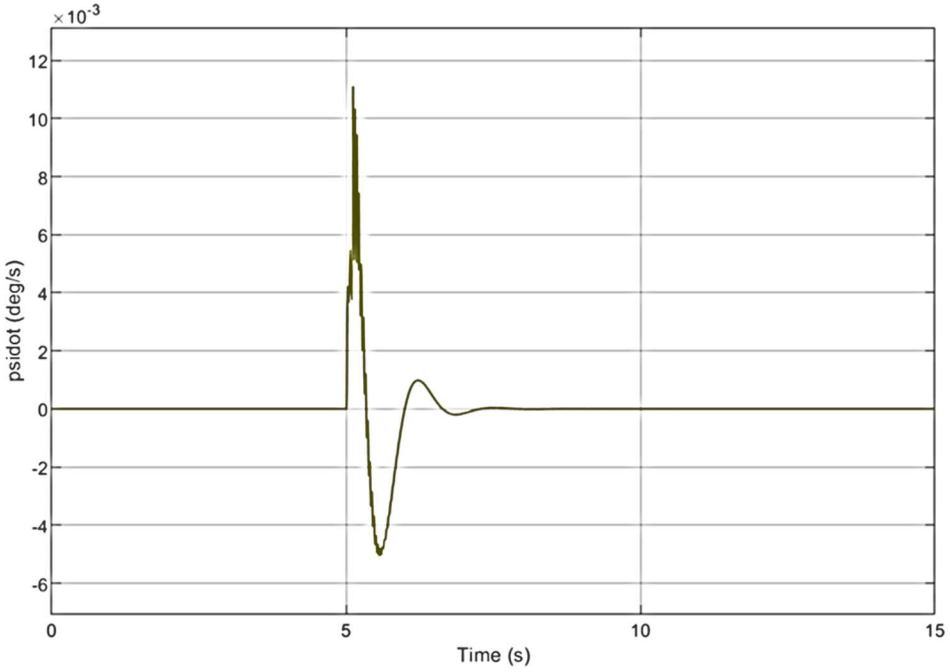

Figure A6: Yaw Rate Response for $\eta = 1$

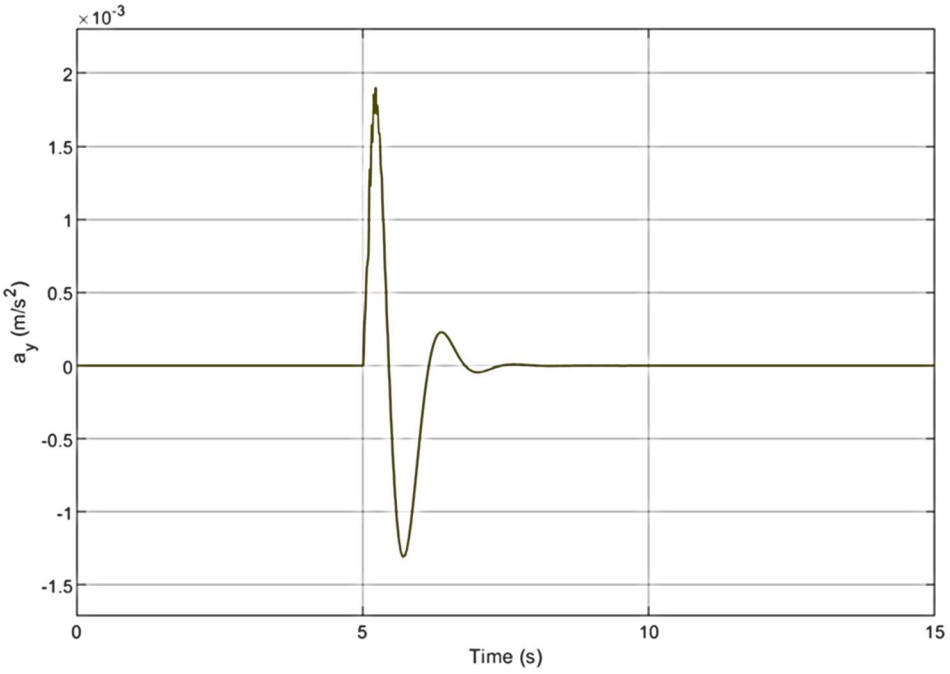

Figure A7: Lateral Acceleration Response for $\eta = 1$

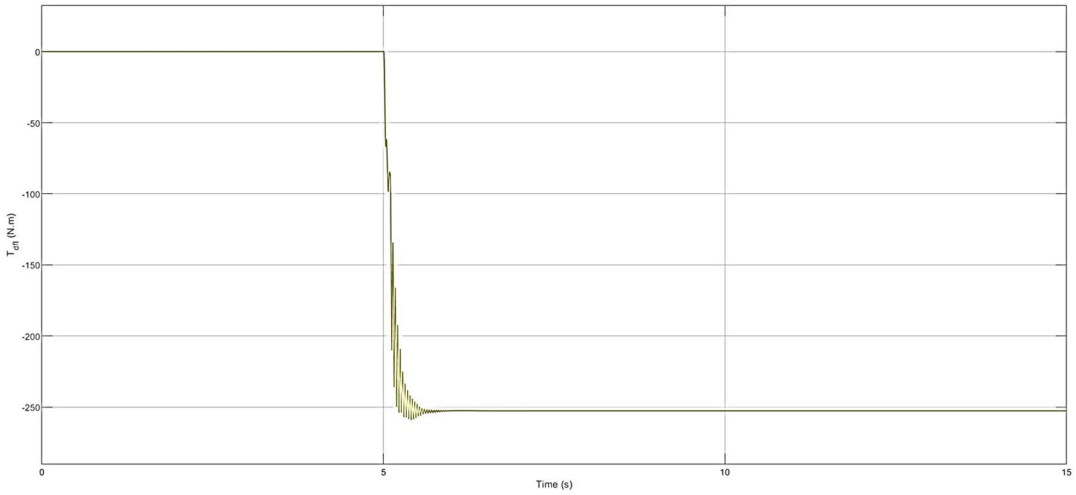

Figure A8: Torque Input Response for $\eta = 1$

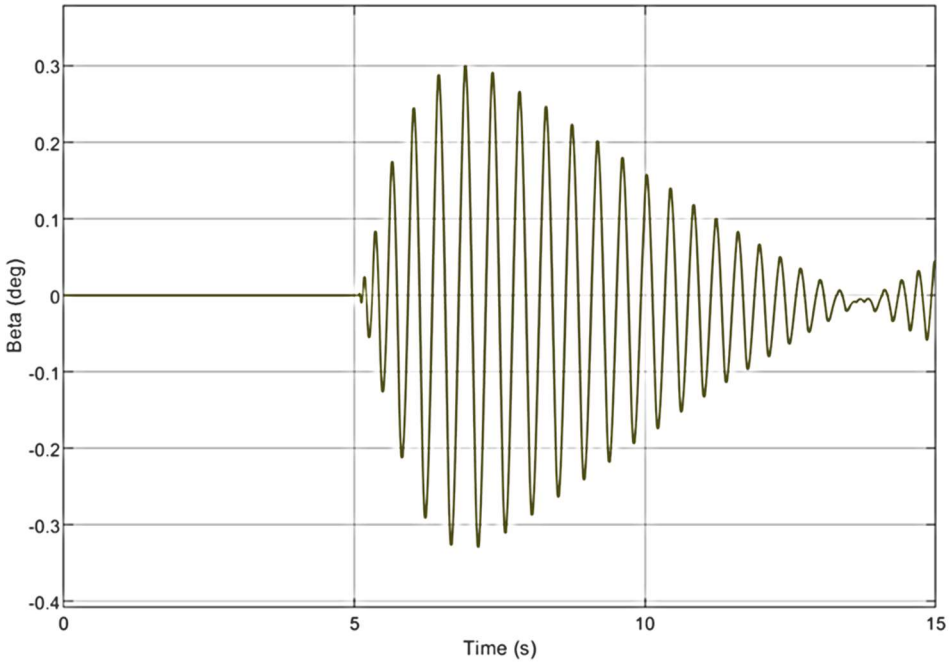

Figure A9: Sideslip Angle Response for $\eta = 1.5$

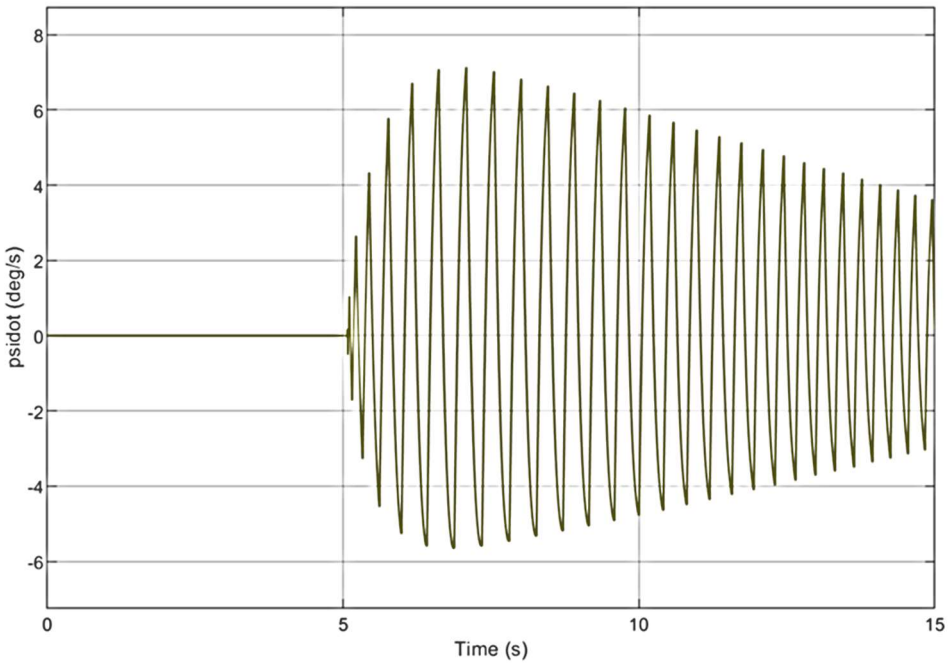

Figure A10: Yaw Rate Response for $\eta = 1.5$

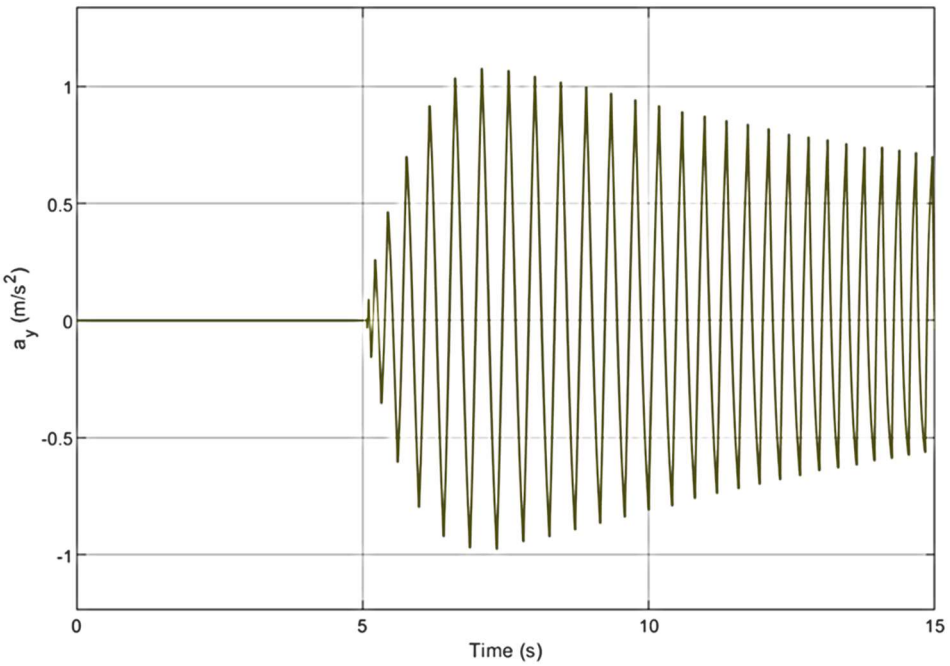

Figure A11: Lateral Acceleration Response for $\eta = 1.5$

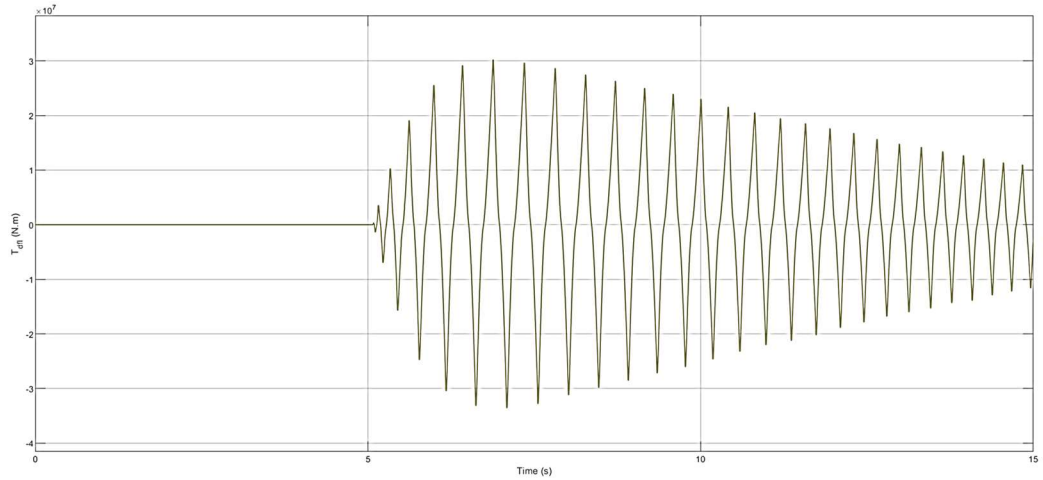

Figure A12: Sideslip Angle Response for $\eta = 1.5$

APPENDIX B

DISTRIBUTIVE-TORQUE CLOSED LOOP RESPONSE

Figures B1-B9 illustrate the closed-loop system dynamic response for the vehicle using the distributive torque control technique.

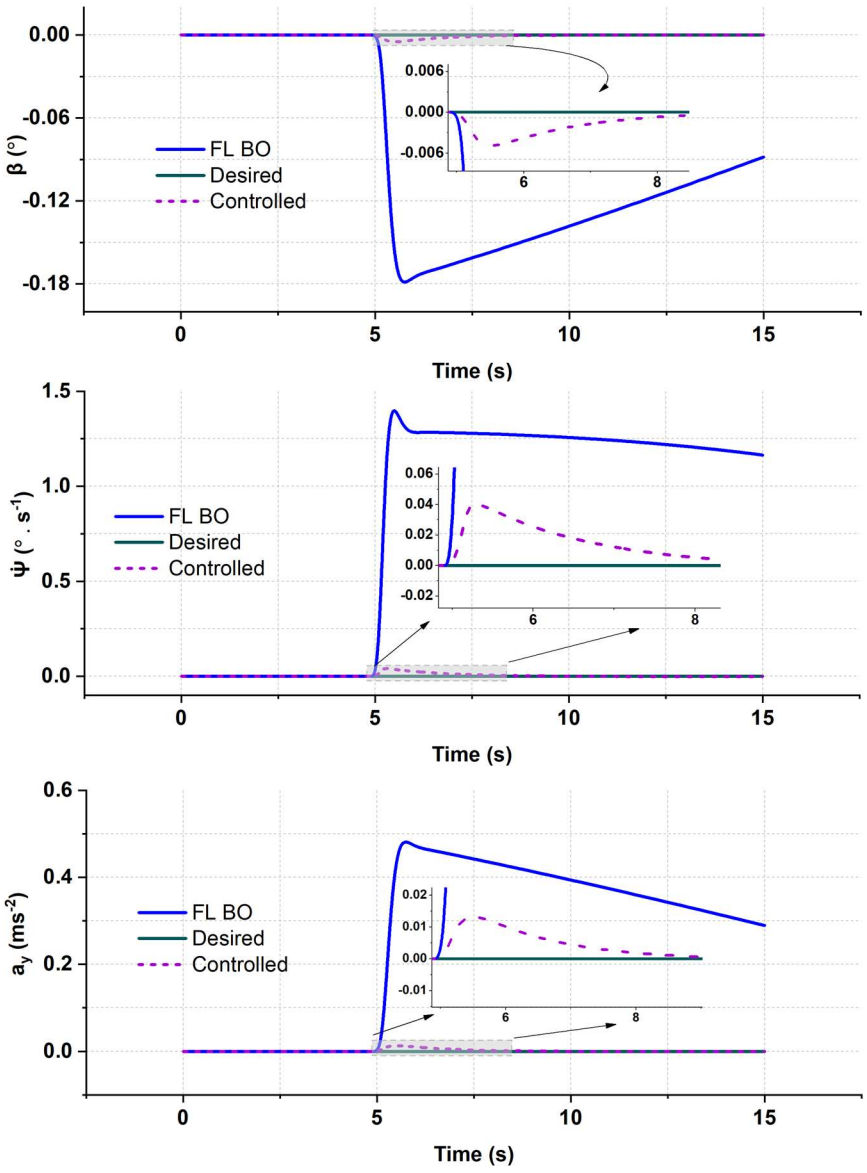

Figure B.1. FL TBO in Straight-Line (Distributive)

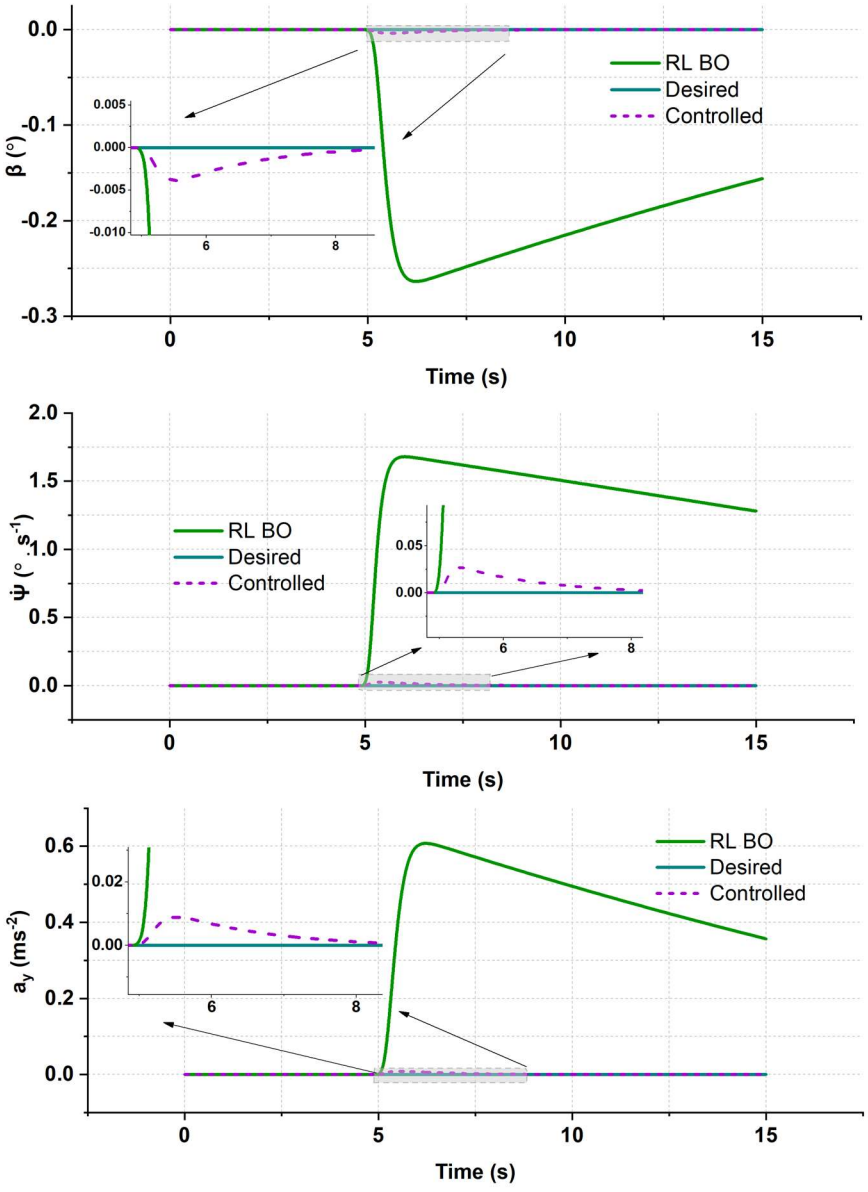

Figure B.2. RL TBO in Straight-Line (Distributive)

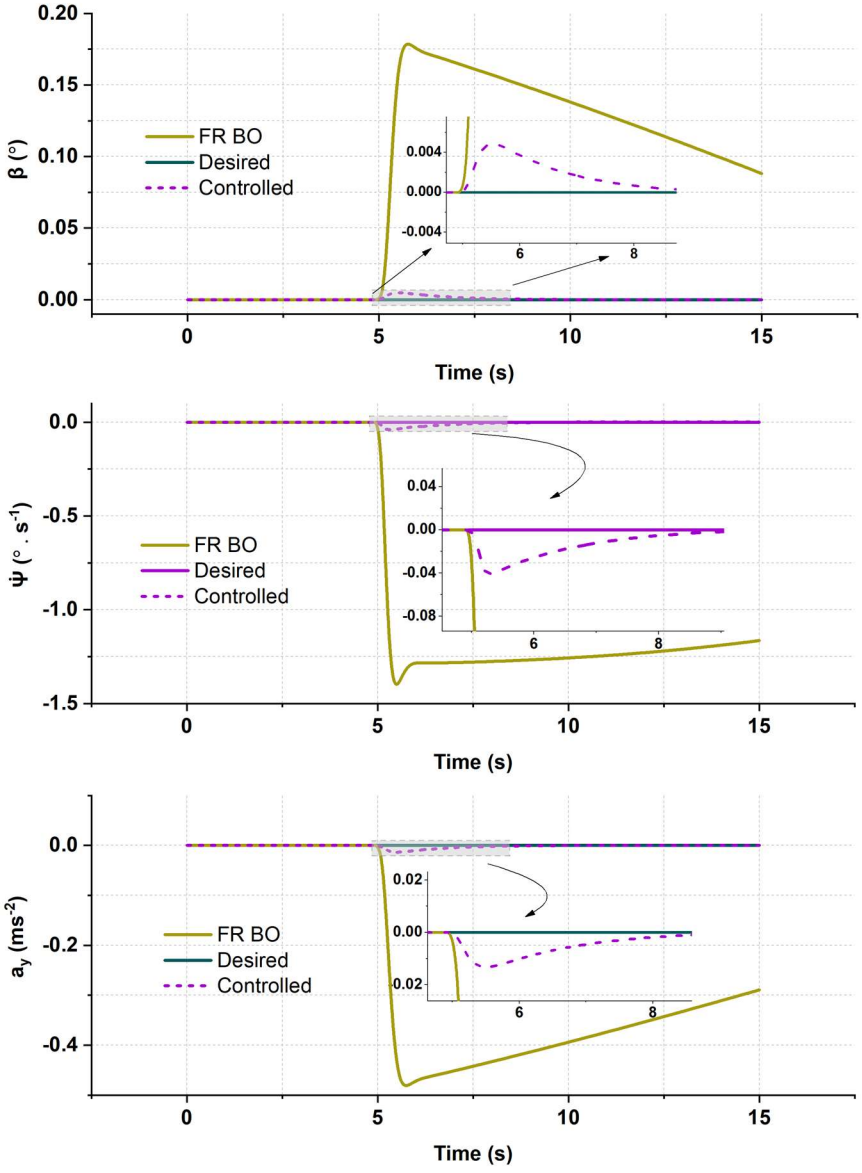

Figure B.3. FR TBO in Straight-Line (Distributive)

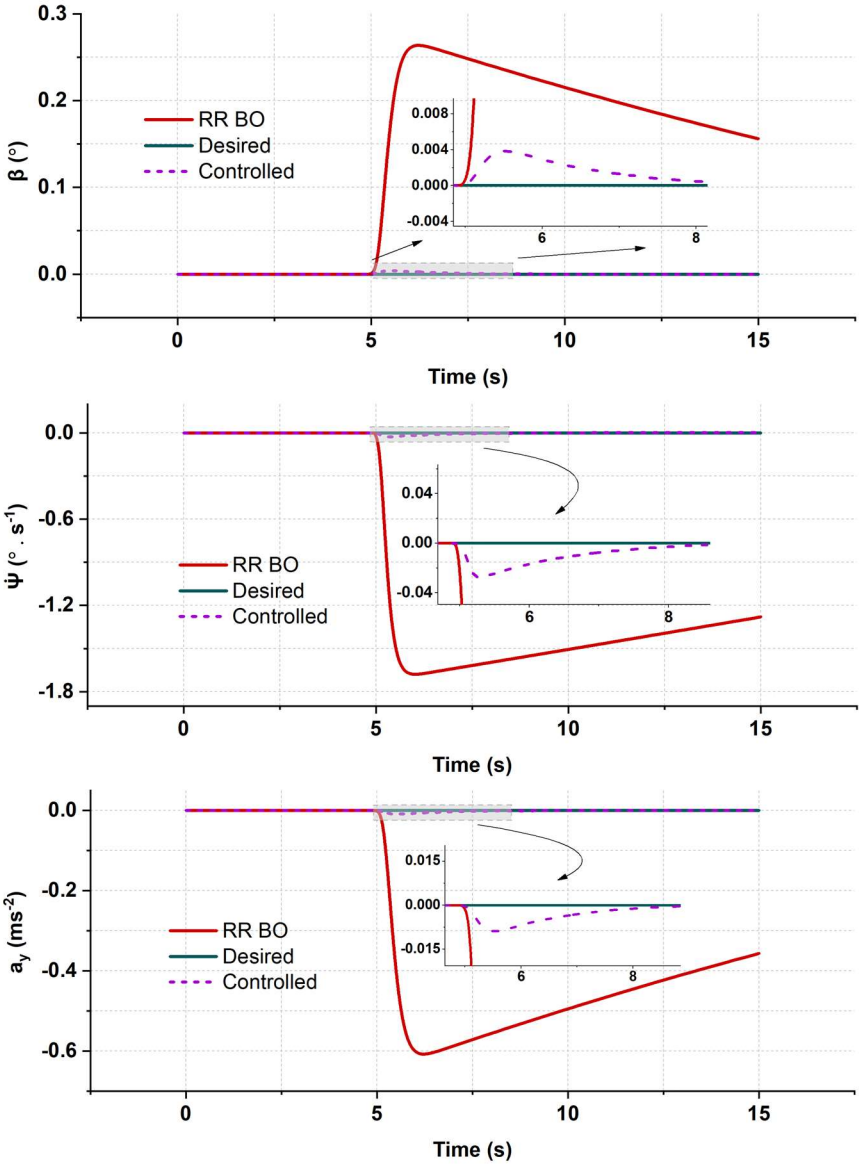

Figure B.4. RR TBO in Straight-Line (Distributive)

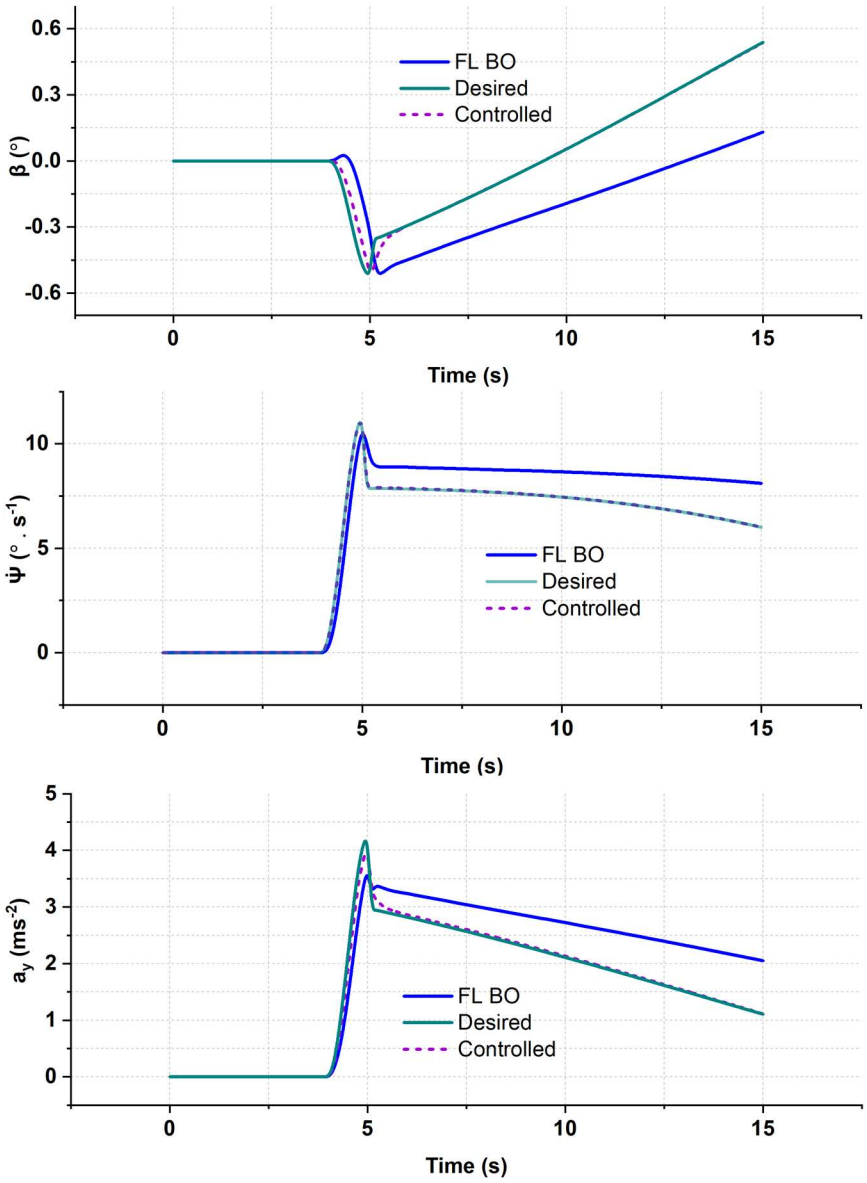

Figure B.5. FL TBO in Cornering (Distributive)

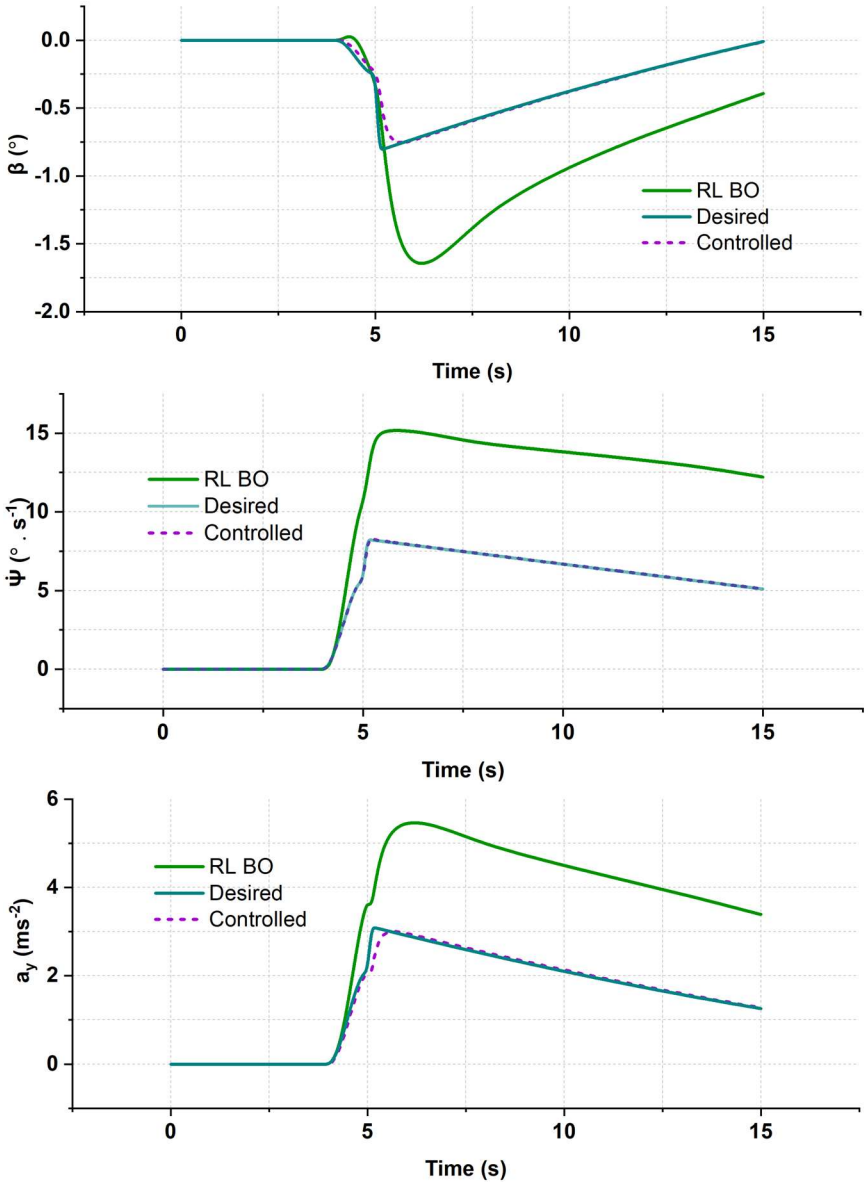

Figure B.6. RL TBO in Cornering (Distributive)

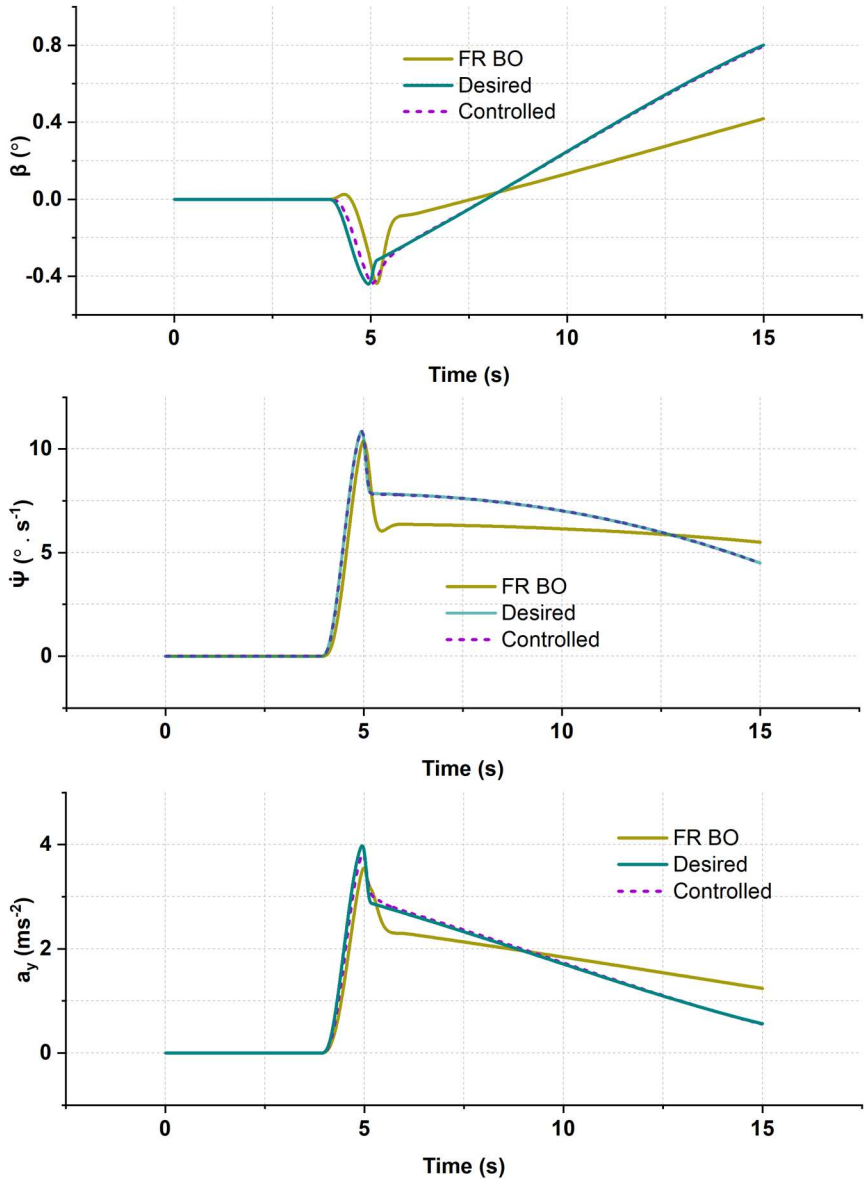

Figure B.7. FR TBO in Cornering (Distributive)

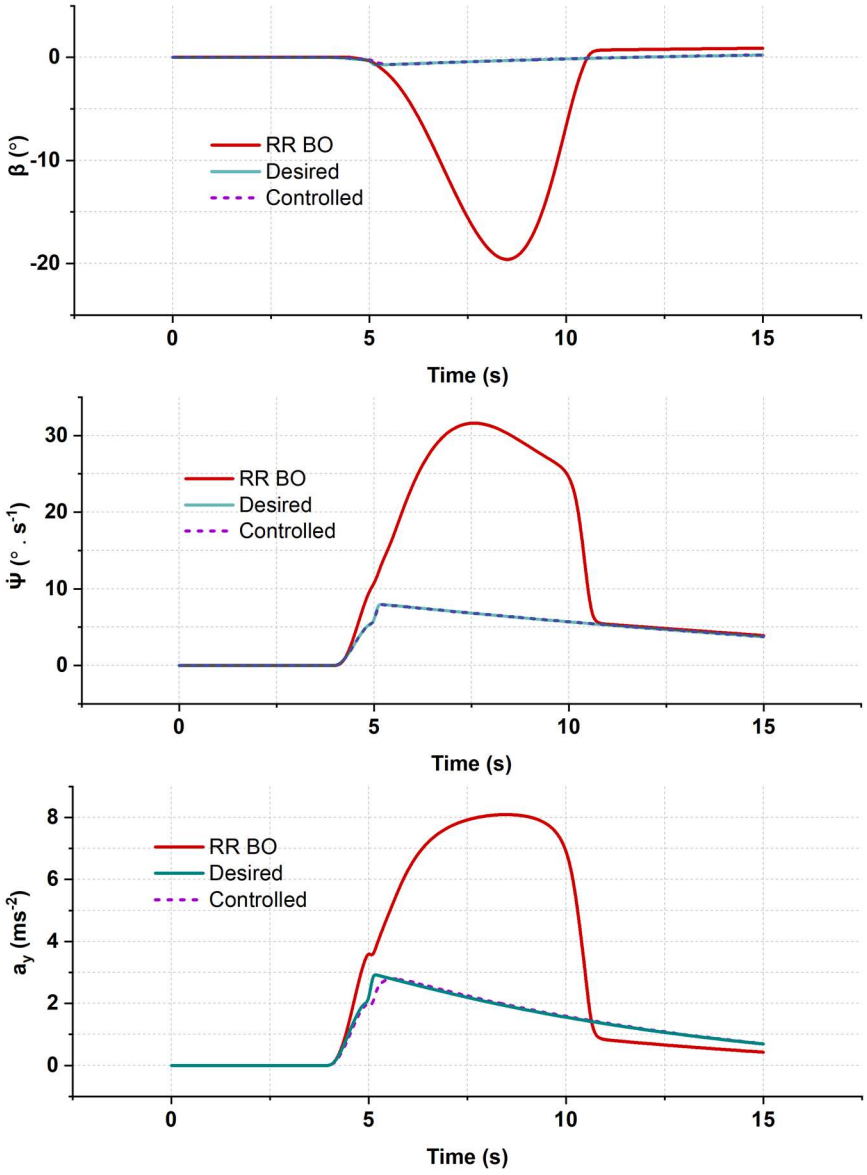

Figure B.8. RR TBO in Cornering (Distributive)

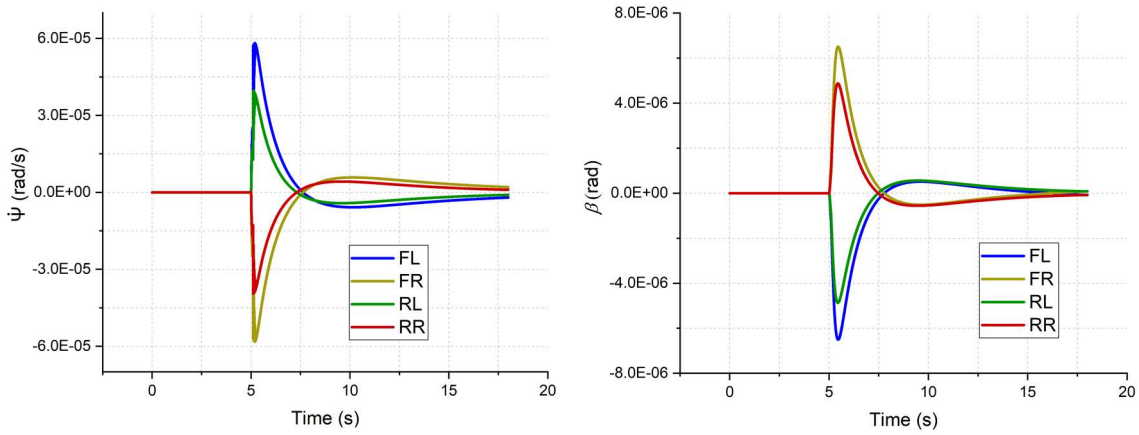

(a) Straight-line

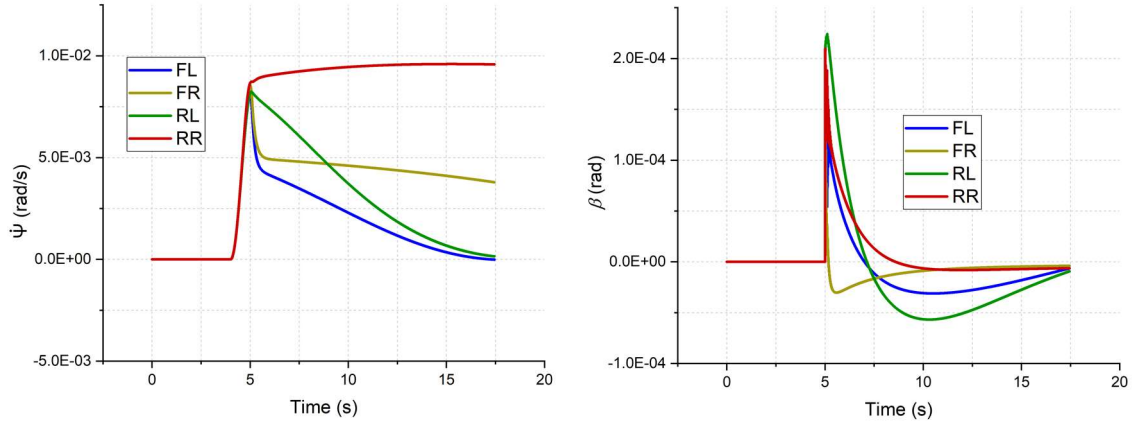

(b) Cornering

Figure B.9. Error Dynamics (Distributive) (A) Straight-Line (B) Cornering

It can be observed that the error converges to zero during both straight-line and cornering motions.